INVESTIGATION OF THE EFFECT OF TORSIONAL NATURAL FREQUENCY ON STALL-INDUCED DYNAMIC LOADING

F. J. Tarzanin, et al

Boeing Vertol Company

Prepared for:

Army Air Mobility Research and Development Laboratory

February 1974

Unclassified

Security Classification

AD776 415

DOCUMENT CONTROL DATA - R & D

(Security classification of title, body of abstract and indexing annotation must be entered when the overall report is classified)

1 ORIGINATING ACTIVITY (Corporate author)	2a. REPORT SECURITY CLASSIFICATION
Boeing Vertol Company (A Division of the Boeing Company) Philadelphia, Pennsylvania	Unclassified 2b. GROUP

3 REPORT TITLE

INVESTIGATION OF THE EFFECT OF TORSIONAL NATURAL FREQUENCY ON STALL-INDUCED DYNAMIC LOADING

4 DESCRIPTIVE NOTES (Type of report and inclusive dates)

Final Technical Report

5 AUTHOR(S) (First name, middle initial, last name)

Frank J. Tarzanin
Joseph Ranieri

6 REPORT DATE	7a. TOTAL NO OF PAGES	7b. NO OF REFS
February 1974	161	11

8a. CONTRACT OR GRANT NO	9a. ORIGINATOR'S REPORT NUMBER(S)
DAAJ02-72-C-0093 b. PROJECT NO. 1F162208AA82 c.	USAAMRDL Technical Report 73-94 9b. OTHER REPORT NO(S) (Any other numbers that may be assigned this report)
d.	D210-10678-1

10. DISTRIBUTION STATEMENT

Approved for public release; distribution unlimited.

11. SUPPLEMENTARY NOTES	12 SPONSORING MILITARY ACTIVITY
	Eustis Directorate U.S. Army Air Mobility R&D Laboratory Fort Eustis, Virginia

13 ABSTRACT

For flight conditions at high blade loadings or airspeeds, the rotor control system experiences a rapid load growth resulting from stall-induced blade torsional moments. These loads frequently grow so large that the aircraft flight envelope is restricted. This report describes an analytical study that determined the effect of changing blade torsional properties on control loads for a wide range of flight conditions. The results showed that reducing the blade torsional stiffness could significantly reduce the large stall loads. However, too large a stiffness reduction results in a large nosedown advancing blade load, which eventually leads to a blade torsional divergence.

DD FORM 1 NOV 1473 REPLACES DD FORM 1473, 1 JAN 64, WHICH IS OBSOLETE FOR ARMY USE.

Unclassified

Security Classification

14 KEY WORDS	LINK A		LINK B		LINK C	
	ROLE	WT	ROLE	WT	ROLE	WT
Control Loads						
Control Stiffness						
Dynamic Stall						
Live Twist						
Pitch Inertia						
Pitch Link Load						
Stall						
Torsional Frequency						
Torsional Load						
Torsional Stiffness						

DEPARTMENT OF THE ARMY
U S ARMY AIR MOBILITY RESEARCH & DEVELOPMENT LABORATORY
EUSTIS DIRECTORATE
FORT EUSTIS, VIRGINIA 23604

This report has been reviewed by the Eustis Directorate, U.S. Army Air Mobility Research and Development Laboratory and is considered to be technically sound. The purpose of this program was to analytically investigate the effect of blade first torsional natural frequency on stall-induced dynamic loading. The report is published for the exchange of information and appropriate application. The technical monitor for this contract was Paul H. Mirick, Aeromechanics, Technology Applications Division.

Project 1F162208AA82
Contract DAAJ02-72-C-0093
USAAVLABS Technical Report 73-94
February 1974

INVESTIGATION OF THE EFFECT OF TORSIONAL NATURAL FREQUENCY ON STALL-INDUCED DYNAMIC LOADING

Final Report

Boeing Document Number D210-10678-1

by

F. J. Tarzanin
J. Ranieri

Prepared by

Boeing Vertol Company
(A Division of The Boeing Company)
Philadelphia, Pennsylvania

for

EUSTIS DIRECTORATE
U.S. ARMY AIR MOBILITY RESEARCH AND DEVELOPMENT LABORATORY
FORT EUSTIS, VIRGINIA

SUMMARY

This report documents the results of a study to find the effect of rotor blade torsional natural frequency on stall-induced torsional loads. The primary objective was to analytically determine the effects of blade torsional natural frequency on control loads for a wide range of airspeeds and rotor loadings. Secondary objectives were: (1) to expand the correlative base of the unsteady aerodynamic theory through comparison with stalled model rotor data and (2) to determine the parameters that influence large stall-induced control loads.

For the rotor studied, the analysis showed that stall-induced control loads can be reduced by lowering the rotor blade torsional stiffness so that the first torsional natural frequency is about 4/rev. Larger reductions in torsional frequency (to about 3/rev) reduce control loads for moderate advance ratios (μ = 0.3), but result in a large load increase and poor rotor stability at high advance ratios (μ = 0.4). Higher frequency blades (about 7/rev) generate large stall loads at moderate advance ratios (μ = 0.3 to 0.35), but may provide lower loads at high advance ratios (μ = 0.4 and beyond). The figure below summarizes these results as control load flight envelopes for four blades with different torsional natural frequencies. Flight conditions (C_T/σ and μ) that fall above the boundary line have pitch-link loads in excess of 2500 pounds (which is approximately the endurance limit for the pitch links of a CH-47C size aircraft); flight conditions below the boundary line have pitch-link loads below 2500 pounds. The figure shows that the overall best blade, as far as control loads are concerned, has a torsional natural frequency of 4/rev.

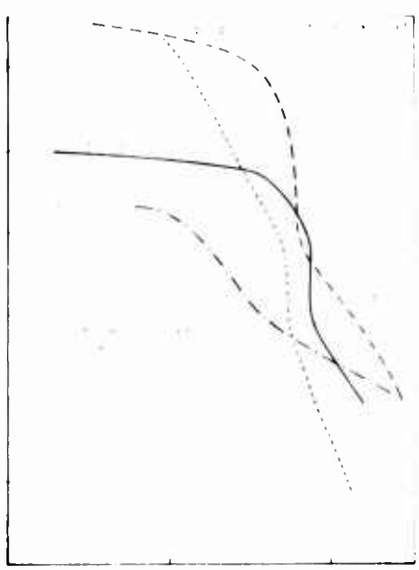

FOREWORD

This report presents the results of an analytical study conducted under Contract DAAJ02-72-C-0093, INVESTIGATION OF THE EFFECTS OF TORSIONAL NATURAL FREQUENCY ON STALL-INDUCED DYNAMIC LOADING. The work was performed by the Boeing Vertol Company, funded by the Eustis Directorate, U.S. Army Air Mobility Research and Development Laboratory (USAAMRDL), and covered the period July 1972 through July 1973. Frank J. Tarzanin Jr. was the Vertol Project Engineer; Paul H. Mirick and William E. Nettles monitored the contract for the Eustis Directorate.

The authors gratefully acknowledge the assistance of C. Hutchinson for his dedicated effort and needed assistance.

TABLE OF CONTENTS

LIST OF ILLUSTRATIONS

LIST OF SYMBOLS

b	length of pitch arm, in.
bl	number of blades per rotor
C	blade chord, in.
C_D	aerodynamic drag coefficient
C_L	aerodynamic lift coefficient
C_M	aerodynamic moment coefficient
C_T/σ	blade loading
D	rotor diameter, ft
e_o	hub offset, in.
f	plunging frequency, cycles/sec
GJ	blade torsional stiffness, lb-in.
H	blade vertical position, in.
ΔH	plunging amplitude, in.
$\dot{H}$	relative vertical velocity between blade and air, in./sec
$\ddot{H}$	relative vertical acceleration between blade and air, in./sec^2
I_o	blade pitch inertia, lb-sec^2-in.
K_z	control system stiffness at pitch link, lb/in.
q	dynamic pressure, lb/ft^2
R	blade radius, ft
T.P.	test point number
V	velocity of free stream, kt
X	rotor propulsive force, lb
$\bar{X}$ $(=X/qD^2\sigma)$	nondimensional propulsive force
α	total blade angle of attack, deg

α_s	rotor shaft angle of attack, deg
β	blade flapping angle, deg
β_{1c}	blade longitudinal flapping, deg
β_{1s}	blade lateral flapping, deg
Γ	stall delay function
θ	blade mechanical angle of attack, deg
$\dot{\theta}$, $\frac{d\theta}{dt}$	time rate of change of blade angle of attack, deg/sec
θ_o	blade collective angle of 0.75 R, deg
θ_{1c}	lateral cyclic pitch angle, deg
θ_{1s}	longitudinal cyclic pitch angle, deg
μ	advance ratio
σ	rotor solidity = bl C/πR
ϕ	blade-induced angle of attack, deg
$\dot{\phi}$, $\frac{d\phi}{dt}$	time rate of change of blade-induced angle of attack, deg/sec
ψ	blade azimuth position, deg
ω_θ	blade torsional natural frequency/rev
Ω	rotor rpm, rev/min

INTRODUCTION

A prime limitation to the operational boundaries of helicopters has been the large stall-induced control loads that occur during maneuvers or level flight at high airspeeds, gross weight or altitude. A systematic study[1] with analysis and model tests showed that proper selection of the rotor blade torsional natural frequency* can reduce the large stall-induced control loads, making flight envelope growth possible.

Helicopter structural envelopes are established from component life calculations. For any practical design, the level-flight steady-state component loads should be below the endurance limit (infinite life load) so that sufficient component life will be available to absorb the larger maneuver loads. A major design objective is to produce an aircraft with a flight envelope limited by aircraft power and not by structural limits. Frequently, however, the operational flight envelope is limited by a rapid growth of stall-induced control loads that exceed the endurance limit. Therefore, the flight envelope is limited by control loads, and the available power cannot be fully utilized.

The rapid control load growth is attributed to "stall flutter," which is a consequence of high angles of attack and the resulting retreating blade stall. Visual confirmation of the large stall loads can be found in pitch link or blade torsional load waveforms on which characteristic stall spikes appear in the fourth quadrant of the blade azimuth. These high loads result from an aeroelastic self-excited pitch motion in conjunction with repeated submersion of a large portion of the rotor blade into and out of stall.

Analytical investigations, tests of oscillating airfoils, reviews of existing flight test data and extensive wind tunnel testing of model rotors have led to the development of semi-empirical aeroelastic theory[2] that predicts control magnitudes and waveforms for all flight conditions, including the stall flutter regime.

This theory includes compressible, unsteady aerodynamics with linear shed wake, three-dimensional flow and stall hysteresis for lift, drag and pitching moment. The basis for this approach is Theodorsen's unsteady linear aerodynamic airplane

*The term "torsional natural frequency" as used in the report refers to the classical definition of an uncoupled torsional natural frequency as obtained in a vacuum. There is no torsional airspring in the calculation.

theory for small angles of attack[3]. By using airfoil section test results to include compressibility, stall, dynamic stall hysteresis and three-dimensional flow in the cited theory, an approach suitable for the analysis of helicopter rotors was developed. This aerodynamic theory was then incorporated in an aeroelastic rotor analysis (Boeing program C-60) that can now be used to predict the high pitch-link loads associated with blade stall.

Analytical studies, using this theory (program C-60) and another theory developed by Sikorsky Aircraft[2,4], indicate that reducing the blade torsional frequency from the 7-8/rev region to the 4-5/rev region, through reduced control system stiffness, significantly reduces the stall-induced control loads. Recently, a more extensive analytical study was performed[1] to evaluate the effects of torsional stiffness, control system stiffness and pitch inertia on the stall-induced loads of a highly loaded (C_T/σ = 0.114) full-scale rotor at an advance ratio of 0.29.

The analytical results showed that large reductions in stall-induced loads can be achieved by changing the blade torsional natural frequency. Since the torsional natural frequency variation was obtained by varying blade torsional stiffness (GJ), control system stiffness and blade pitch inertia, independently, the results indicate that pitch-link loads are a direct function of torsional natural frequency.

These encouraging theoretical results led to a 6-foot-diameter model test to initially verify the control load-torsional frequency trend. Three sets of blades were tested; each set had a different torsional stiffness with torsional natural frequencies of 3/rev, 4.25/rev and 5.65/rev at full-scale tip speeds. The test results showed that the model stall flutter torsion spike was reduced by 73 percent when the torsional natural frequency was reduced from 5.65/rev to 3/rev, giving a first verification of the analytical trend.

This report documents further investigation into the influence of torsional frequency on stall-induced control loads. The investigation has been divided into four main tasks:

Comparison of the aeroelastic rotor analysis program results (see Appendix I) with the 6-foot-diameter model stall test data for blades with different torsional natural frequencies.

Expansion of the previous study[1] (which was performed at one flight condition) to evaluate the effects of torsional natural frequency on stall-induced loads for a wide range of airspeeds (0 to 175 knots) and rotor loads (C_T/σ =

0.05 to 0.12) for blades with different torsional stiffnesses.

Investigation of the effects of propulsive force, cyclic pitch and blade twist on the stall-induced loads.

Performance of a limited correlation with the model rotor data using a fully coupled flap-lag-pitch rotor analysis (Boeing program C-70).

DISCUSSION

CORRELATION WITH MODEL DATA

The initial effort under this contract was to determine the aeroelastic rotor analysis capability for predicting model rotor stall-induced blade torsion loads. The aeroelastic rotor analysis (designated by the Boeing Vertol Company as program C-60) is fully described in Appendix I. The analysis has been successfully correlated with full-scale CH-47C flight data[2] for both stalled and unstalled flight conditions.

Model test data[1] was recently obtained for blades with torsional natural frequencies of 3.1/rev, 4.25/rev, and 5.65/rev over a wide range of rotor loadings at an advance ratio of 0.3. A complete discussion of the test and determination of the model blade physical properties are given in Appendix II.

Comparing the C-60 program results with the model data is an essential step in establishing the ability to properly account for:

The large stall-induced control loads

The effect of varying blade physical properties (primarily torsional natural frequency)

The effect of varying rotor thrust

Rotor propulsive force.

It is this comparison that will determine the validity of the torsional frequency, rotor loading, and airspeed study that comprise the bulk of this report.

Three test runs were selected for correlation from the model test data, one run for each blade torsional frequency. A minimum of five test points (at least two points in deep stall) for each test run were analyzed, using the aeroelastic rotor analysis (program C-60), and a theory/test comparison was made. The comparison was evaluated and judged inadequate, and the aeroelastic rotor analysis program was modified. The theory/test comparison was repeated for the modified analysis to verify improved results. The torsional frequency theoretical investigation, reported under the section entitled ANALYTICAL INVESTIGATION OF STALL-INDUCED DYNAMIC LOADING, utilized the resulting improved analysis.

Basic Analysis

Comparisons of the blade torsional amplitudes, obtained from the model test, with results of the basic rotor analysis

(program C-60) are presented in Figures 1, 2 and 3. These figures show the load variation with rotor C_T/σ for the low-frequency (3.1/rev), standard reference (4.25/rev) and morganite blades (5.65/rev), respectively. The analysis predicts the sub-stall low-load growth, the large-load growth associated with stall and the inception of the large stall loads near the proper C_T/σ. However, the analysis generally overpredicts the magnitude of these loads.

The overprediction is least for the low-stiffness blade and greatest for the morganite blade. In addition, the analysis shows a drop in blade torsion amplitude at high C_T/σ (near 0.12) which is not evident in the test data. This inability to predict the torsional load trend at the high rotor loading condition represents a serious deficiency, since the major objective of this study is to determine the variation of torsional load with blade natural frequency for rotor flight conditions experiencing significant stall (i.e., high C_T/σ conditions).

Modified Analysis

In order to improve the theory/test correlation presented in the previous section, a number of analytical modifications were made to the C-60 program. These included three modifications which generally improved the analytical load predictions:

1) Incorporated steady and vibratory inplane loads in the blade torsion calculation, replacing the steady only inplane loads used previously.

2) Modified the lift stall delay for a Mach number of 0.6 to agree with an earlier value (used in Reference 2), replacing the value recommended in Reference 6.

3) Included an aerodynamic center of pressure shift to account for dynamic overshoot of the static C_M.

There were three other modifications that yielded significantly poorer correlation and were abandoned:

1) Reduced the lift curve slope to account for the theoretically lower model Reynolds number (full-scale C_L, C_D and C_M provided significantly better correlation).

2) Forced the analysis to match the measured model 1/rev flap angle.

3) Transferred the blade shear center from 25 percent to 30 percent, as indicated by questionable static test results (see Appendix II).

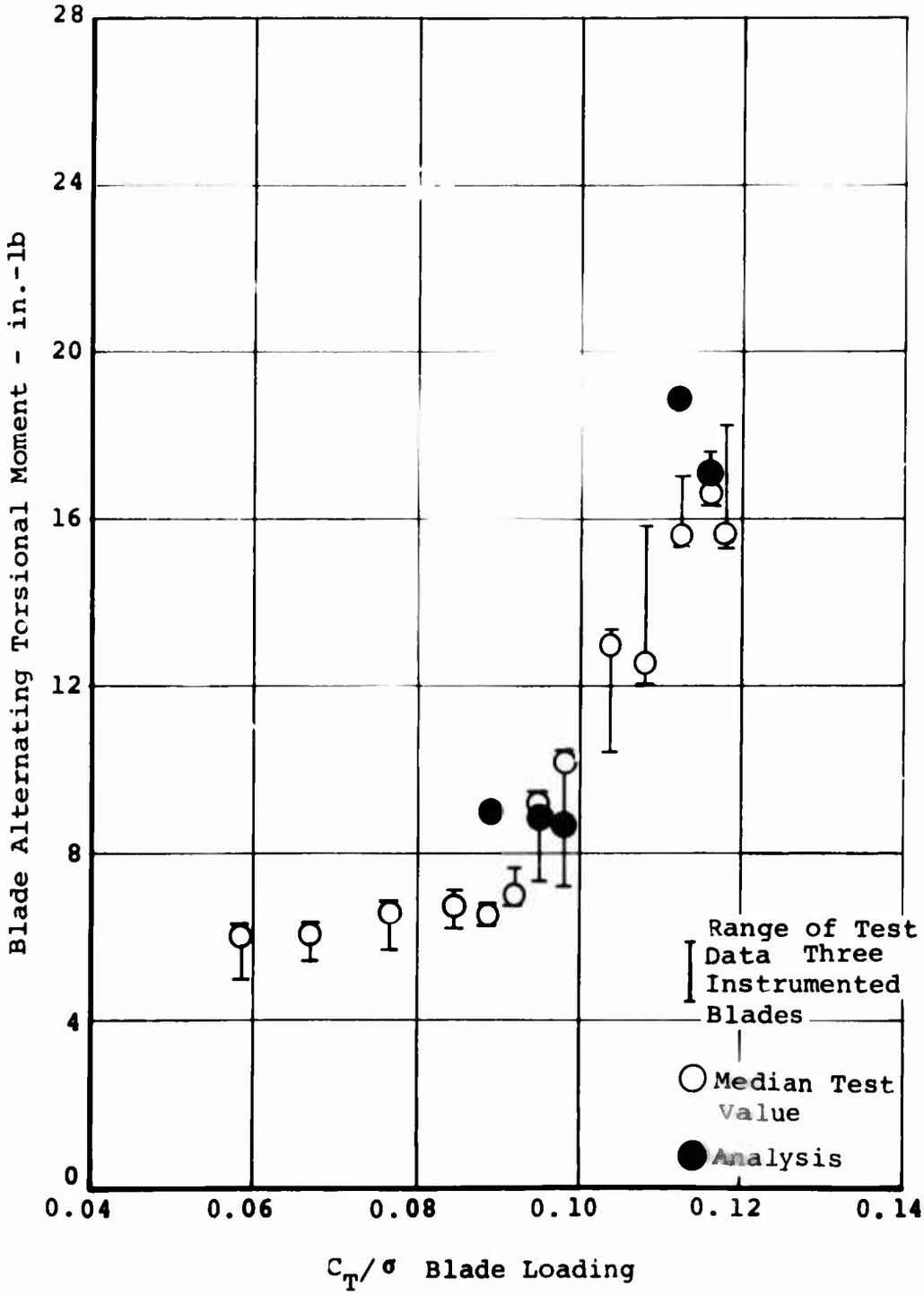

Figure 1. Comparison of Measured and Calculated Blade Torsional Moment for Low GJ Blade (Basic Analysis). Torsional Natural Frequency = 3.1/Rev.

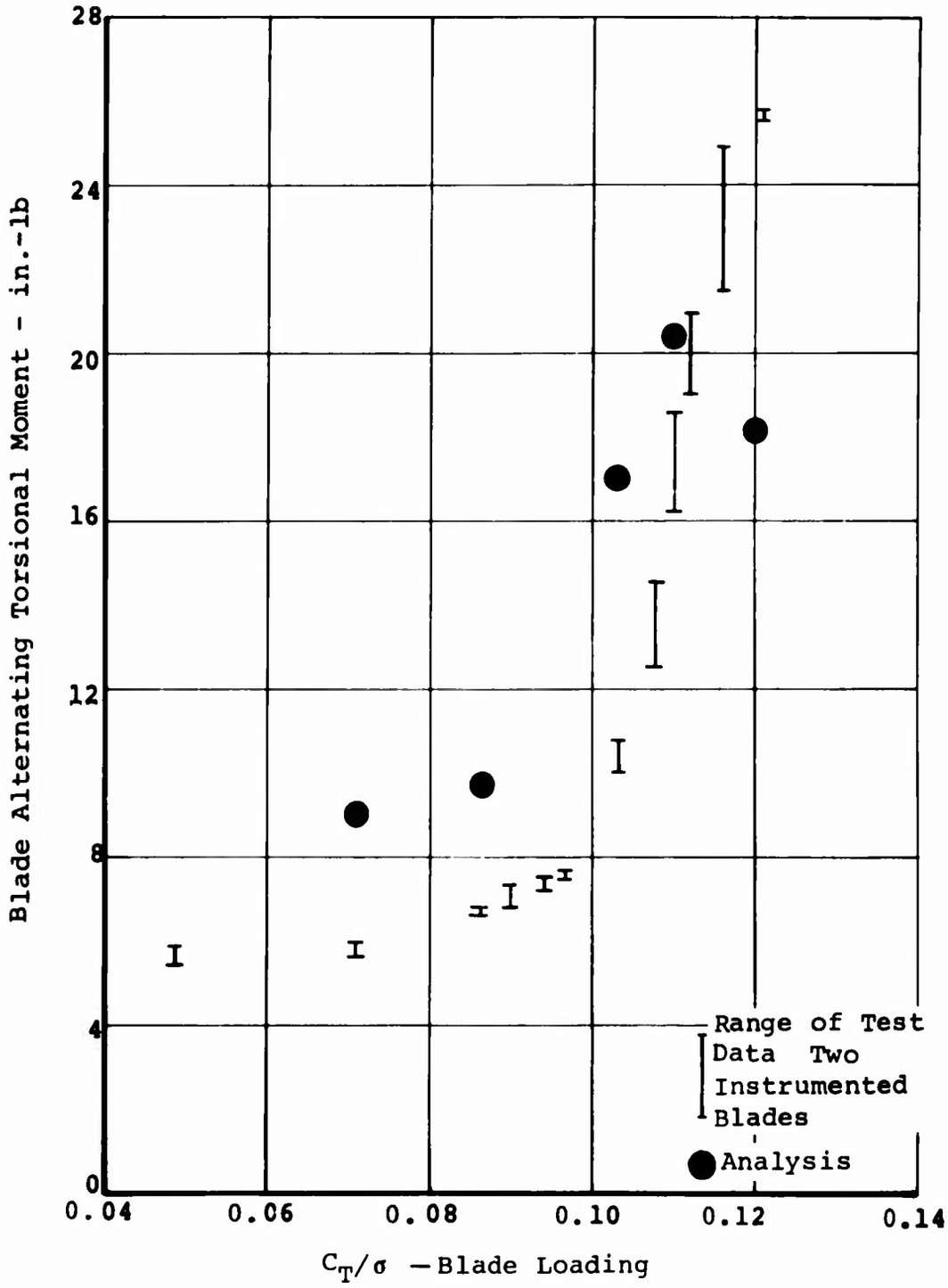

Figure 2. Comparison of Measured and Calculated Blade Torsional Moment for the Standard Reference Blade (Basic Analysis). Torsional Natural Frequency = 4.25/Rev.

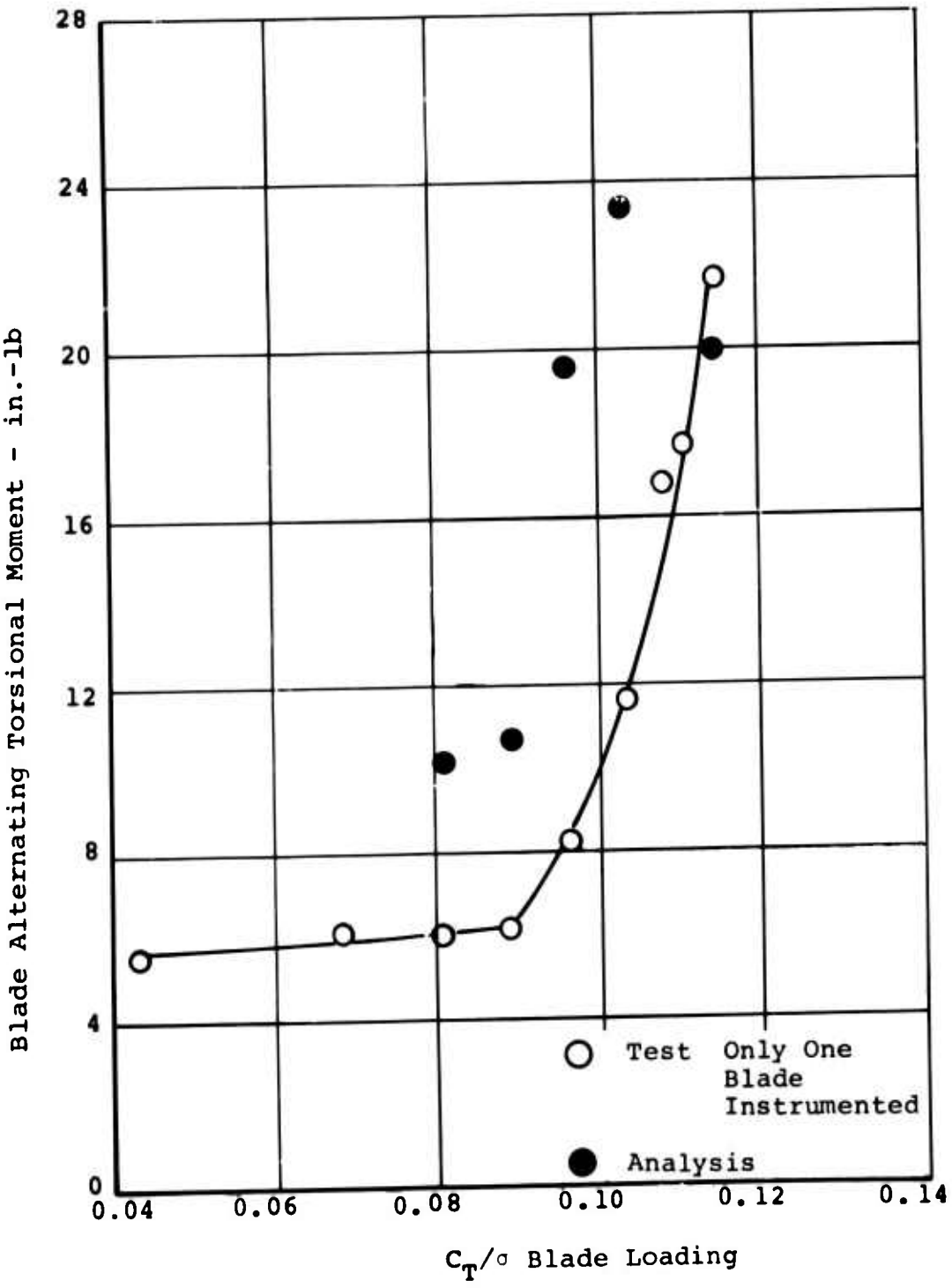

Figure 3. Comparison of Measured and Calculated Blade Torsional Moment for the Morganite Blade (Basic Analysis). Torsional Natural Frequency = 5.65/Rev.

The analysis was rerun using each of these modifications and some combinations of these modifications for the standard reference blade. The most promising improvement was then used to analyze the other blades. The program improvements are summarized below:

-Effects of Analyses Improvements

- Vibratory Inplane Loads - The C-60 program utilizes an iterative technique between blade airloads and a coupled flap-pitch response to calculate blade torsion loads (see Appendix I for details). Inplane loads are calculated only once at the conclusion of airload-coupled flap-pitch response iterations, and only the steady inplane loads are considered in the blade torsion calculation. In order to improve the correlation, the analysis was modified to include the vibratory inplane loads in the blade torsion calculation for the last iteration only. With this modification, the analysis improves the below-stall theory/test correlation by reducing the predicted loads to very near the test results. Above stall, the analysis shows no significant change.

- Modified Lift/Stall Delay - The unsteady aerodynamic theory of the C-60 program requires a parameter, called the lift gamma function (γ_L), which is used to determine the airfoil dynamic stall delay. While investigating the source of the poor deep-stall correlation, a discrepancy was discovered between the original value for the lift gamma function at a Mach number of 0.6 and the value recently published in Reference 6. The original values were used in the earlier correlation work (References 1 and 2). The published trend represented the most recent work and, therefore, was used in the above theory/test comparison.

  Figure 4 illustrates the lift gamma function variation with Mach number for both the original and the published trends. The square symbol points were obtained from two-dimensional oscillating airfoil test data. The major difference between the two gamma function trends is that the original value at a Mach number of 0.6 is zero while the published value is 0.45. Close examination of this discrepancy revealed that the recently published gamma function (γ_L) was based upon a semi-empirical formulation which was developed to define γ_L as a function of Mach number for a wide range of airfoil sections. The original γ_L was based upon the actual two-dimensional test data. Both sets of γ_L essentially agree at low Mach numbers where leading-edge stall is present, and the stall occurrence is

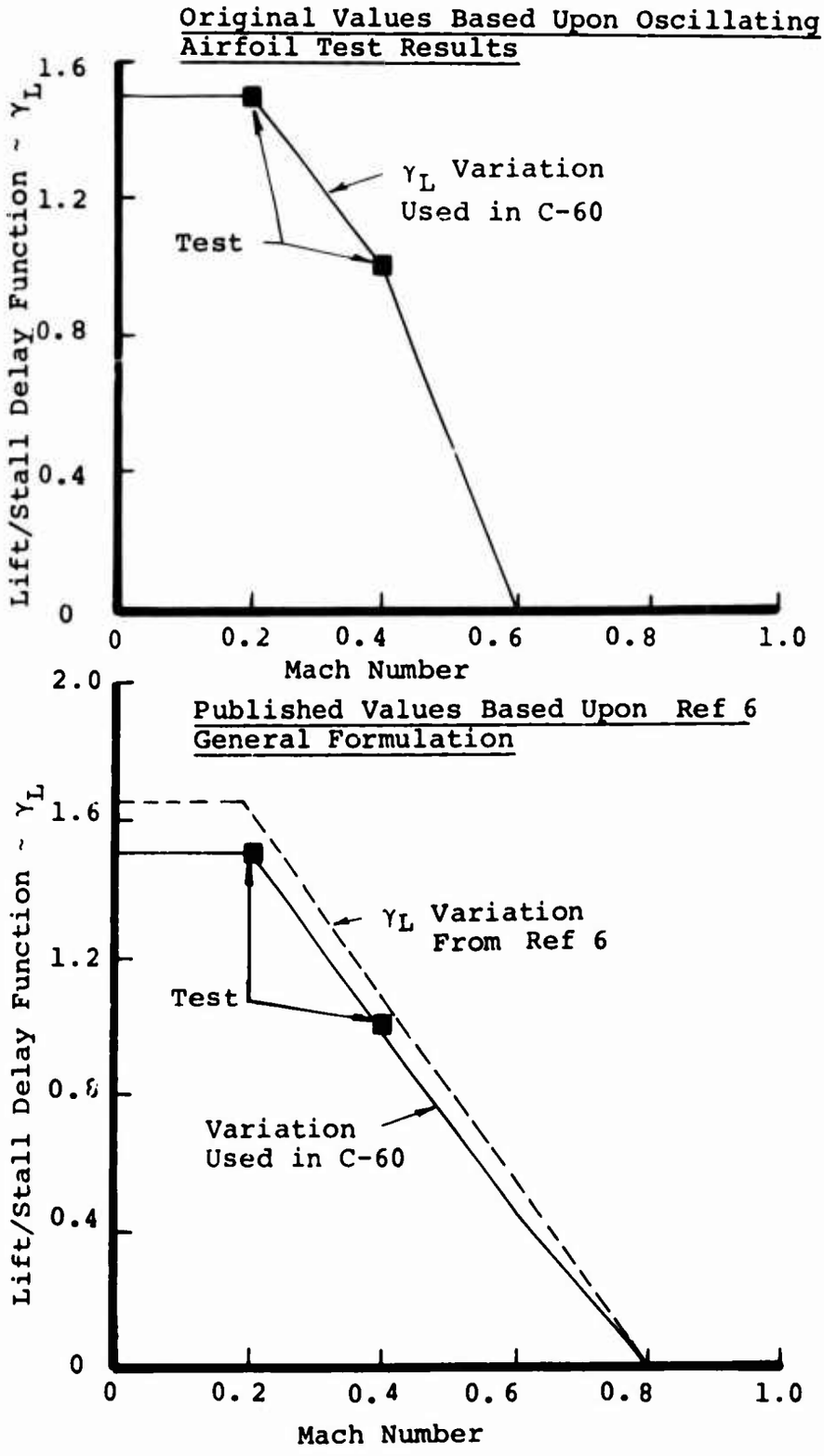

Figure 4. Comparison of γ_L Used in C-60.

clearly defined. At a Mach number of 0.6, trailing edge stall is present, and a gradual transition from unstalled to stalled flow results. Through observation of the static and dynamic data, it is easily observed that the stall delay at a Mach number of 0.6 is only a small fraction of stall delay at a Mach number of 0.4 (see Figure 5). In fact, a value of zero stall delay is a rational approximation. The published value of γ_L at 0.6 Mach number represents almost half that at 0.4 Mach number. This discrepancy arose from the generality of the published formulation which could not properly account for the airflow changes with Mach number.

Using the original value of γ_L (i.e., zero for Mach number equals 0.6) eliminated the load drop-off at $C_T/\sigma = 0.12$ and resulted in a stall torsional load trend in better agreement with the model test load growth.

- Dynamic C_M Overshoot - The combined program modifications of dynamic C_M overshoot, together with the inclusion of the vibratory inplane loads, shows promise for improving the theory/test comparison, as shown in Appendix III. However, since the dynamic C_M overshoot represents a major change in the theory and since adequate theory/test comparisons have been obtained without this capability, it will not be included in the modified analysis to be used for the rest of this report. When more diverse correlation substantiates the improved theory/test comparison, this capability will be added permanently to the C-60 rotor analysis program.

-Correlation Results

The inclusion of vibratory inplane loads in the blade torsion calculations significantly improves the correlation. When, in addition, the lift stall delay (gamma function) was modified for a Mach number of 0.6, the best overall correlation was obtained. These combined improvements were included in calculations of the torsional loads for the low stiffness blade, the standard reference blade and morganite blades so that an overall theory/test comparison using the improved analysis was obtained.

- Blade Torsion Amplitude

  Variation With Blade Loading - The variation of test and analytical blade torsional amplitude with blade loading (C_T/σ) is shown in Figures 6, 7, and 8 for the low stiffness, standard reference, and morganite blades, respectively. In general, the analysis correctly predicts the trend of blade torsional load amplitude with

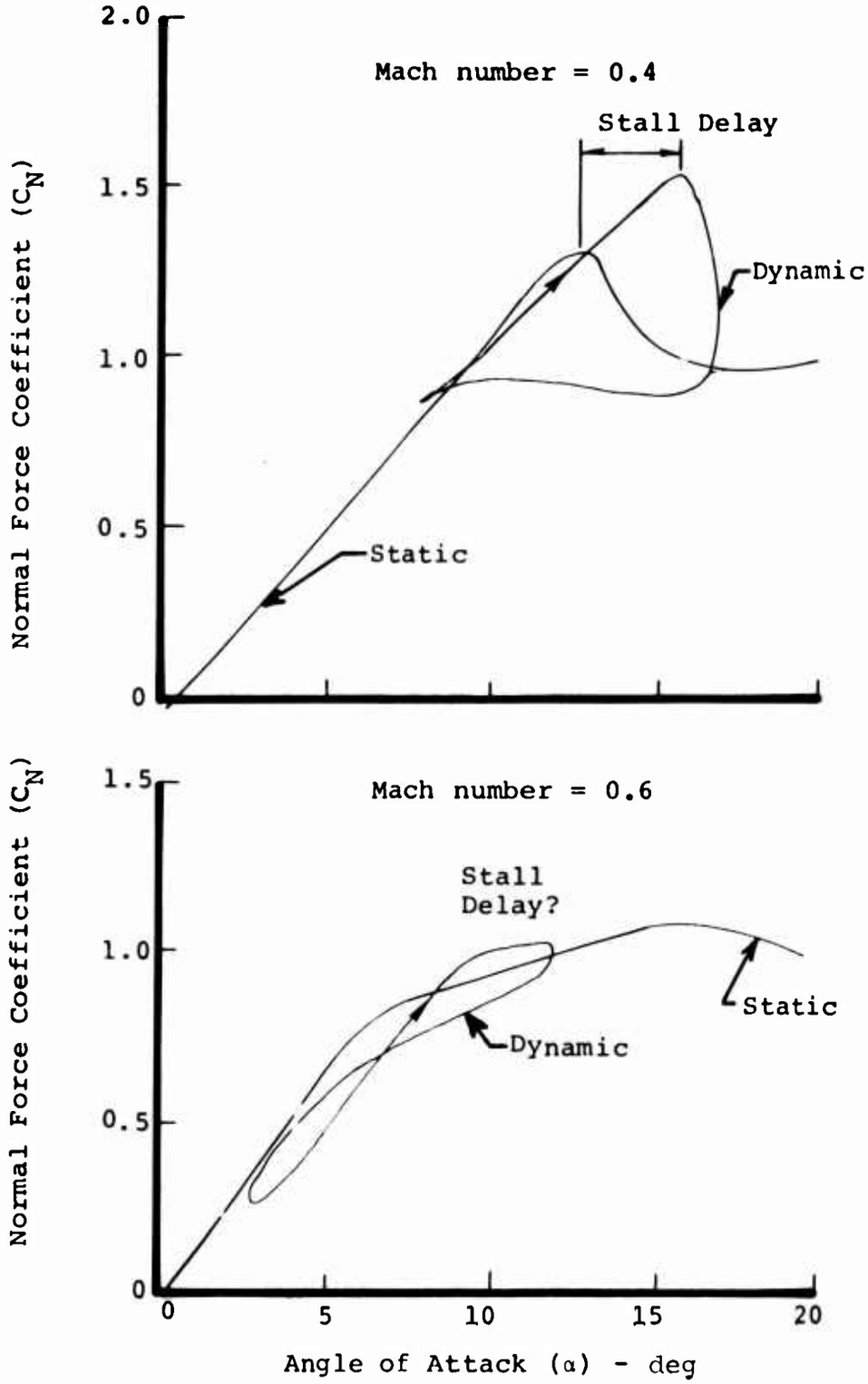

Figure 5. Typical Dynamic Stall for Mach Numbers of 0.4 and 0.6.

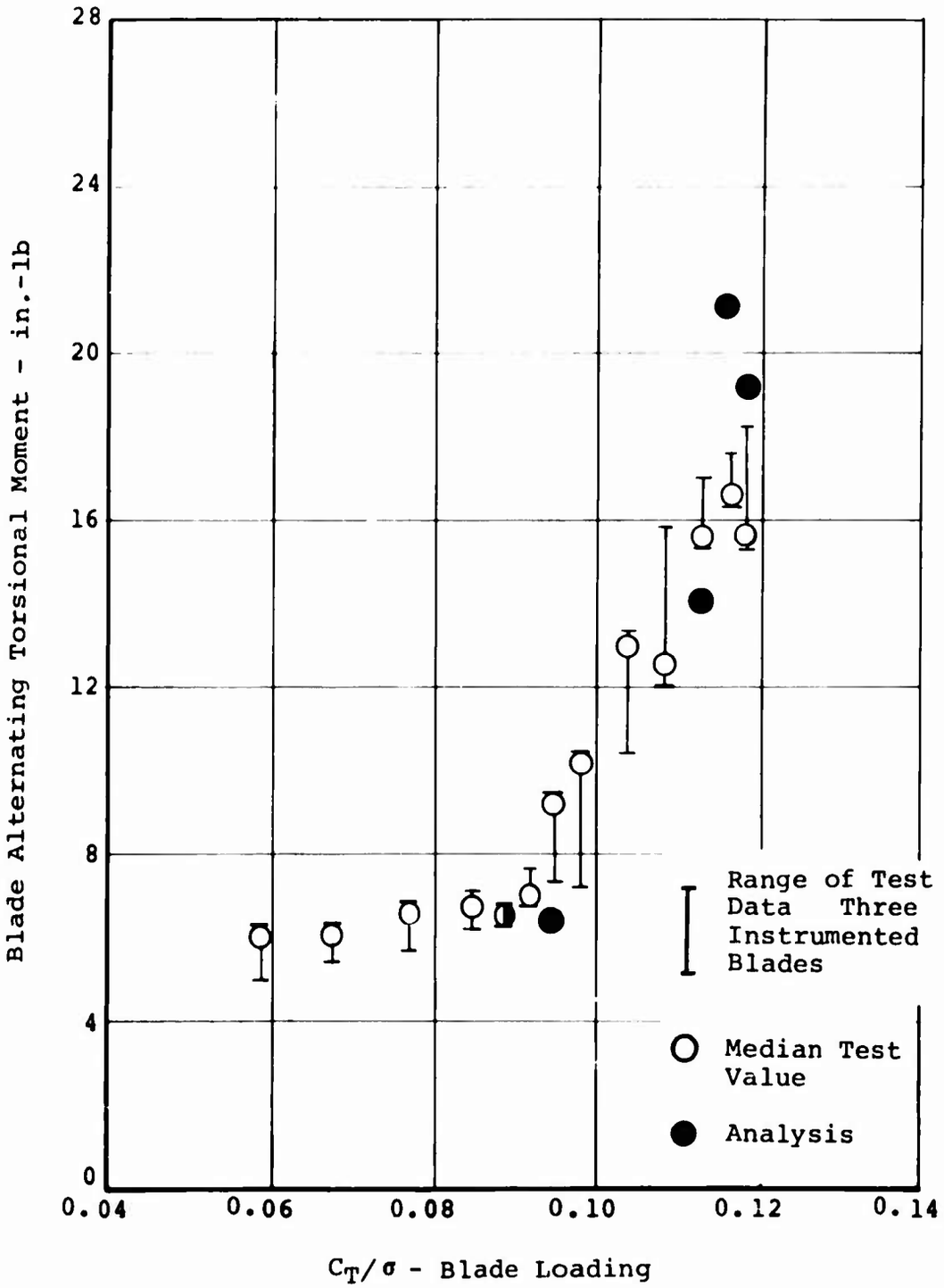

Figure 6. Comparison of Measured and Calculated Blade Torsional Moment for the Low GJ Blade (Improved Analysis).

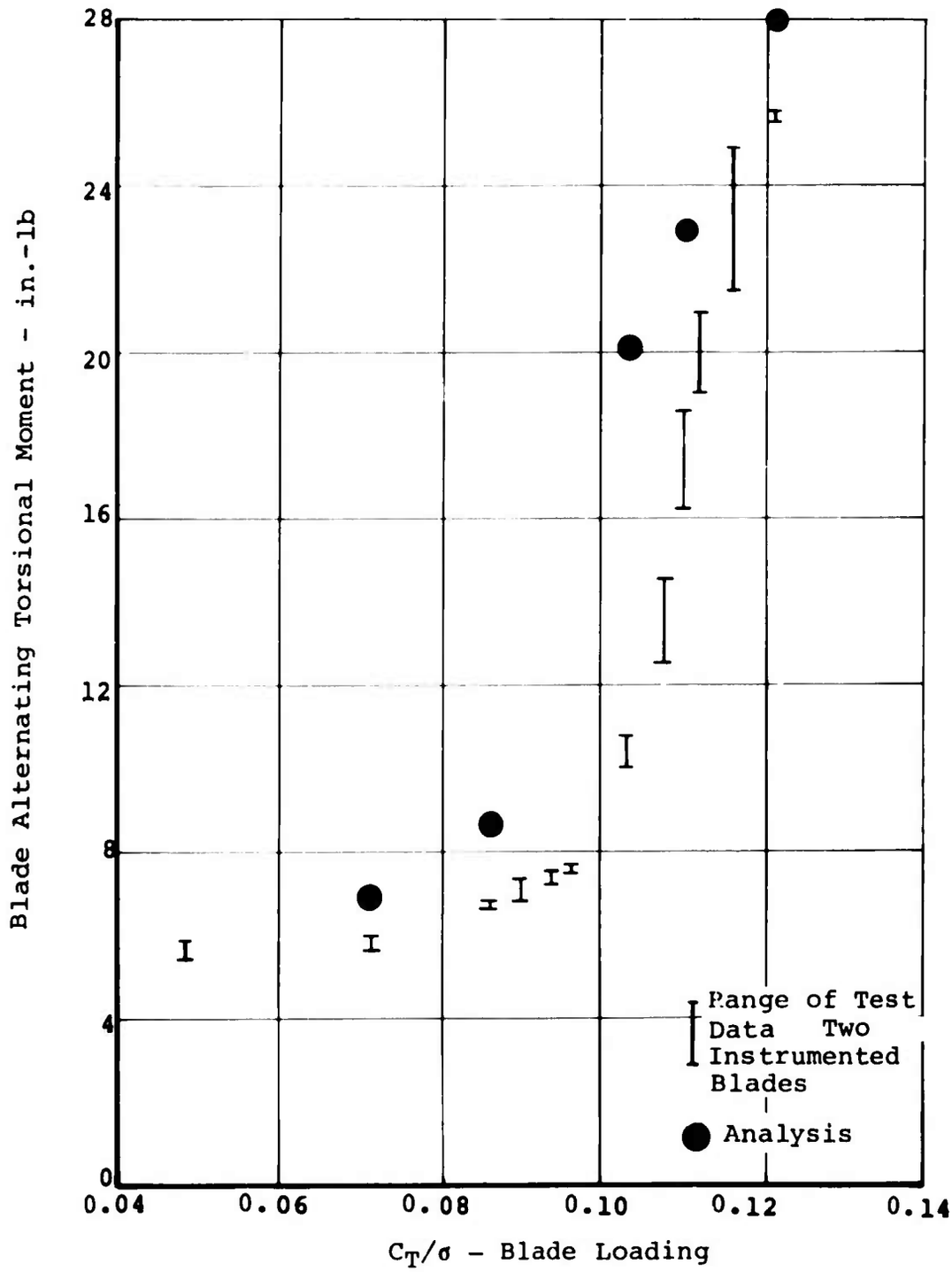

Figure 7. Comparison of Measured and Calculated Blade Torsional Moment for the Standard Reference Blade (Improved Analysis).

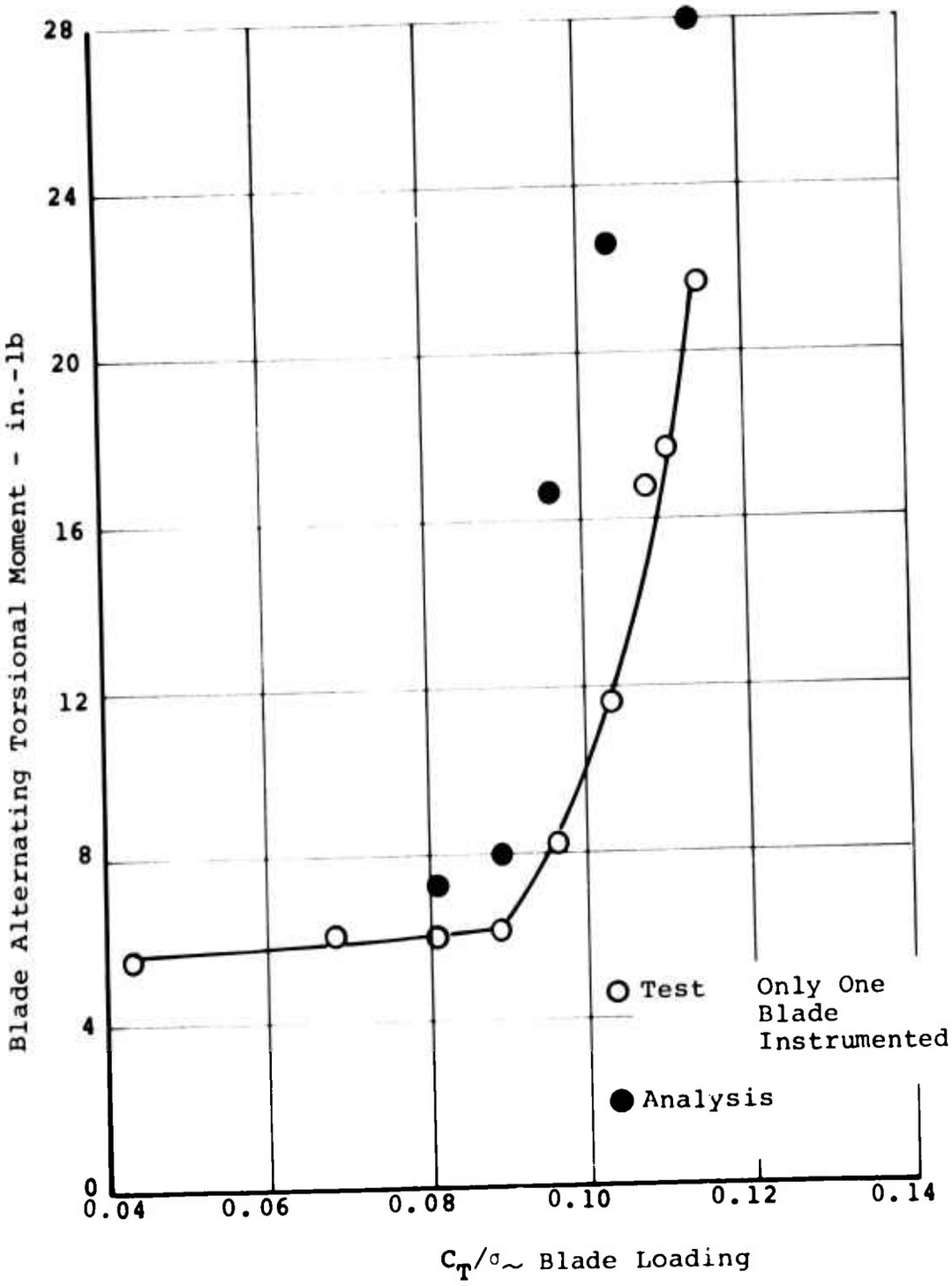

Figure 8. Comparison of Measured and Calculated Blade Torsional Moment for the Morganite Blade (Improved Analysis).

C_T/σ for both stalled and unstalled flight conditions. The predicted stall inception agrees well with test for the low-stiffness blade. For the standard reference blade and the morganite blade, stall inception is predicted about 0.01 C_T/σ too early (see Figures 7 and 8). The analysis predicts approximately the correct torsional load growth rate in stall; but, because the stall inception is predicted early, the stall loads are overpredicted for the two stiffer blades. The torsional load overprediction is largest for the morganite blade and smallest for the low-stiffness blade.

Both theory and test for the standard reference blade and the morganite blade show a continually increasing load trend with increasing blade loading (C_T/σ). For the low-stiffness blade, both theory and test results show a load reduction at a C_T/σ of 0.1179. Similar load reversal has been observed at other rotor test conditions in this test and in other model rotor tests.

Despite the inability of the analysis to numerically predict the torsional loads, it has been demonstrated that the analysis agrees fairly well qualitatively with the test results. Therefore, the analysis may be used with reasonable confidence as a tool for investigating the effects of blade torsional properties on stall-induced dynamic loads.

To further qualify the program's ability, the following theory/test comparisons will be made:

Torsional load trend with frequency

Torsional load waveform

Propulsive force variation with C_T/σ

Required collective pitch

Variation With Torsional Natural Frequency - Figures 9 and 10 illustrate the variation of blade torsional amplitude with natural frequency at various C_T/σ for both test and analysis. (These figures were drawn by fairing Figures 6, 7 and 8 against blade C_T/σ and then cross plotting versus torsional natural frequency at constant C_T/σ.)

In general, both test and analysis exhibit the same trend with natural frequency. At a C_T/σ of 0.09, the analytical results show a flat trend with natural frequency and agree well with the measured data. At a C_T/σ of 0.11, however, the analysis predicts a

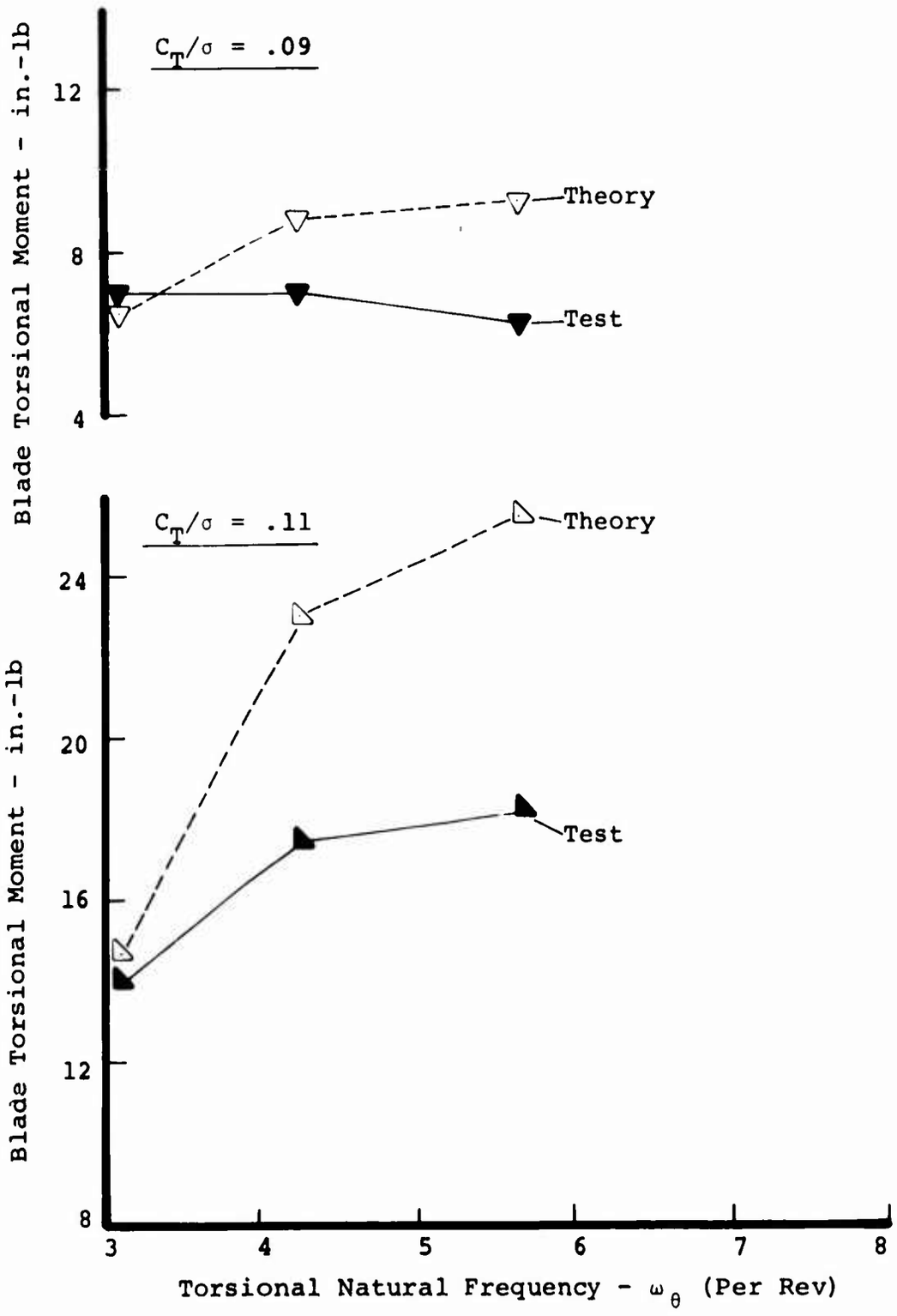

Figure 9. Variation of Torsional Load With First Torsional Natural Frequency.

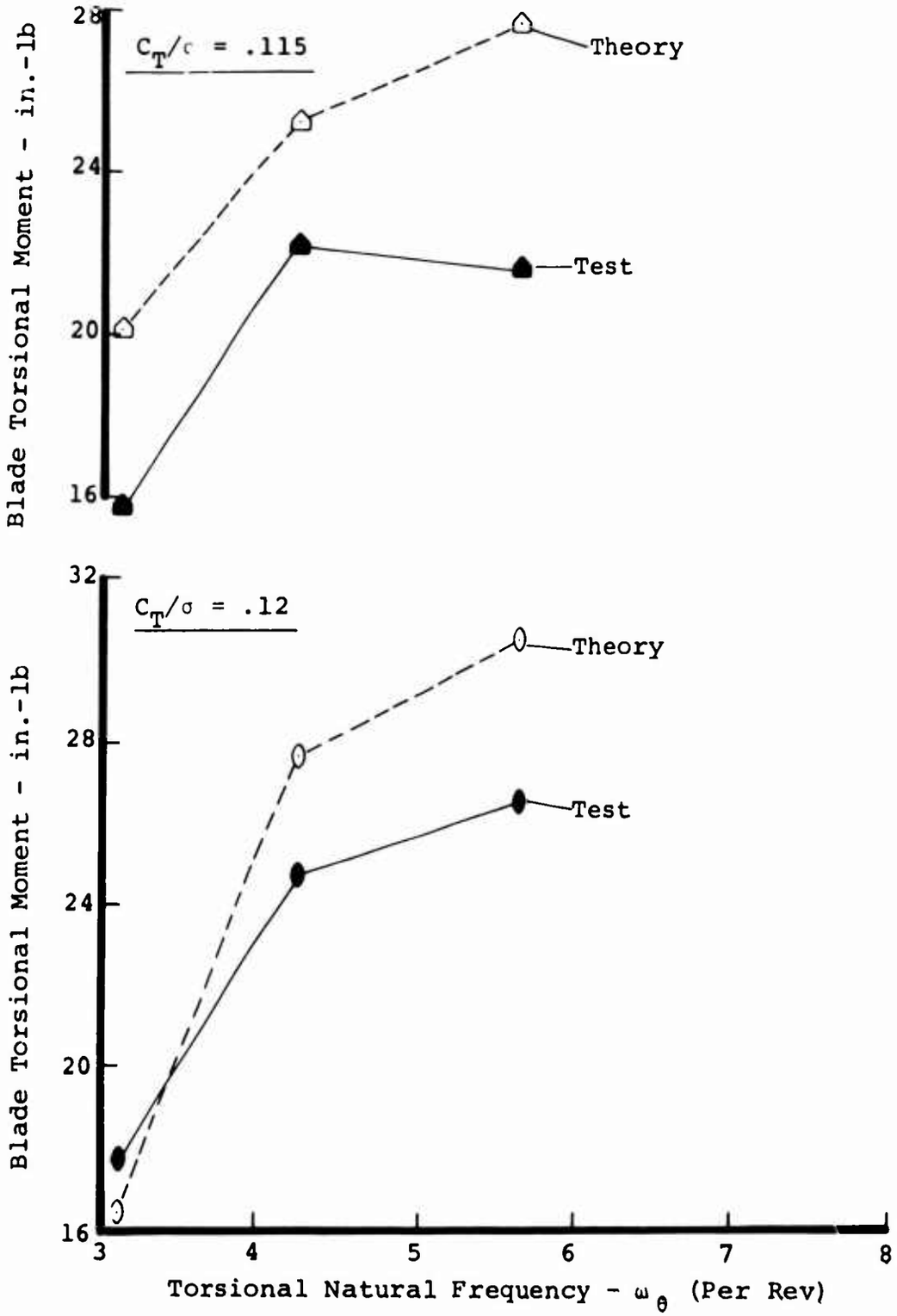

Figure 10. Variation of Torsional Load With First Torsional Natural Frequency.

significant torsional load growth with natural frequency which is not observed in the test data. This is due to the analysis' premature prediction of stall inception for the standard reference and morganite blades. At the high C_T/σ, the analytical trend compares favorably with the measured data.

- Torsional Waveform - Generally, correlation between test and analytical waveform predictions of blade torsion was fair despite the analysis' tendency to overpredict the amplitude. For both test and analysis, the amplitude of the waveform at low C_T/σ (below C_T/σ = 0.095) was controlled by the 1/rev component; whereas, at the high C_T/σ, the amplitude was controlled by the torsion spike.

  The upper half of Figures 11, 12, and 13 illustrate typical correlation for an unstalled condition for each of the blades. The waveforms are predominately 1/rev and exhibit good theory/test agreement. However, the theory appears to lead the test waveform by about 30 degrees for both the low-stiffness and standard reference blades.

  Typical waveform correlations for stalled conditions are illustrated in the lower half of Figures 11, 12, and 13. The analysis consistently predicts the test stall spike azimuth positions but overpredicts the spike amplitude. Further, the analysis overpredicts the higher harmonic components throughout the waveform. The best waveform correlation is obtained for the high-stiffness morganite blade and the worst correlation for the low-stiffness blade.

  However, even though the theoretical model waveforms are deficient, the theory does predict the load trend correctly with C_T/σ and blade torsional frequency.

- Propulsive Force - Test and analytical propulsive force predictions are compared in Figure 14 for the low-stiffness, standard reference, and morganite blades, respectively. In all cases, the analysis overpredicts the test results but does obtain the same trend with blade loading (C_T/σ) as the test data. The upper half of Figure 15 compares the measured propulsive force for each model blade and shows that low-stiffness and morganite blades produced nearly identical propulsive force, while the standard reference blade produced a slightly higher propulsive force. A similar comparison is made in the lower half of Figure 15 for the analytical propulsive force predictions. The relative positions of the calculated results remain

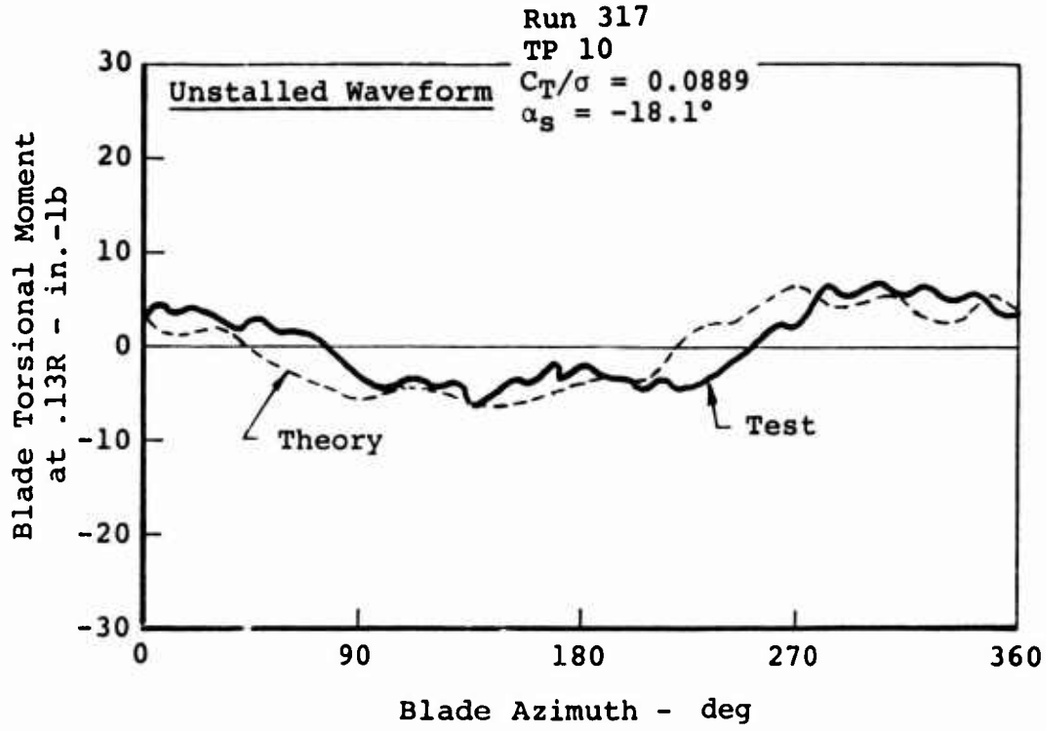

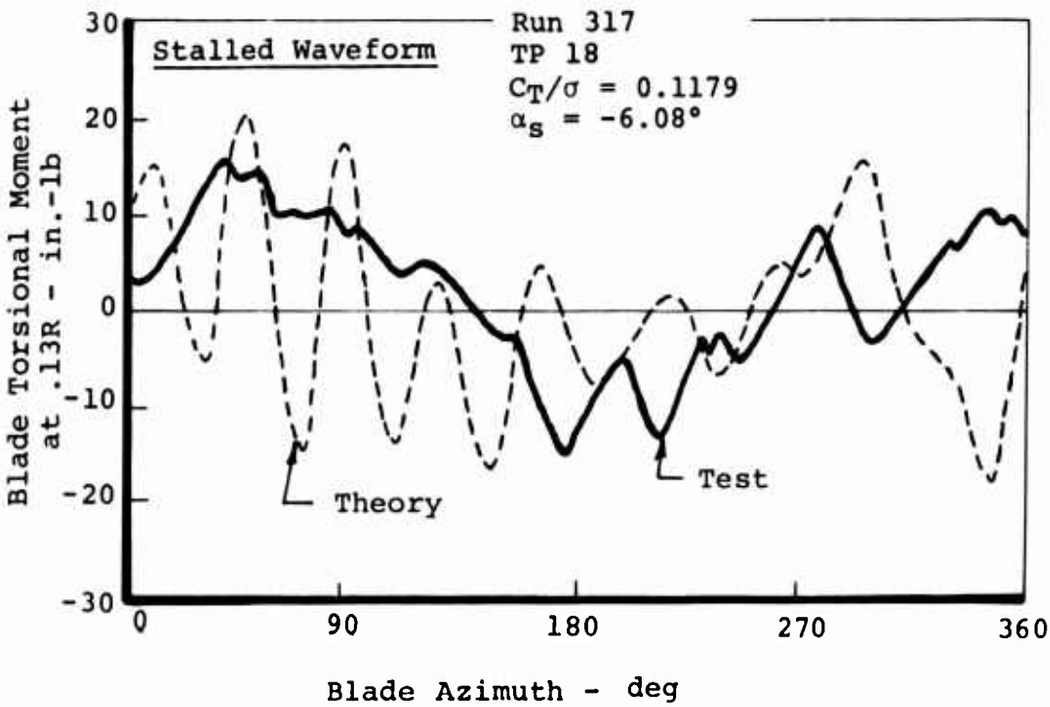

Figure 11. Test/Theory Torsional Waveform Comparison for the Low-Stiffness Blade.

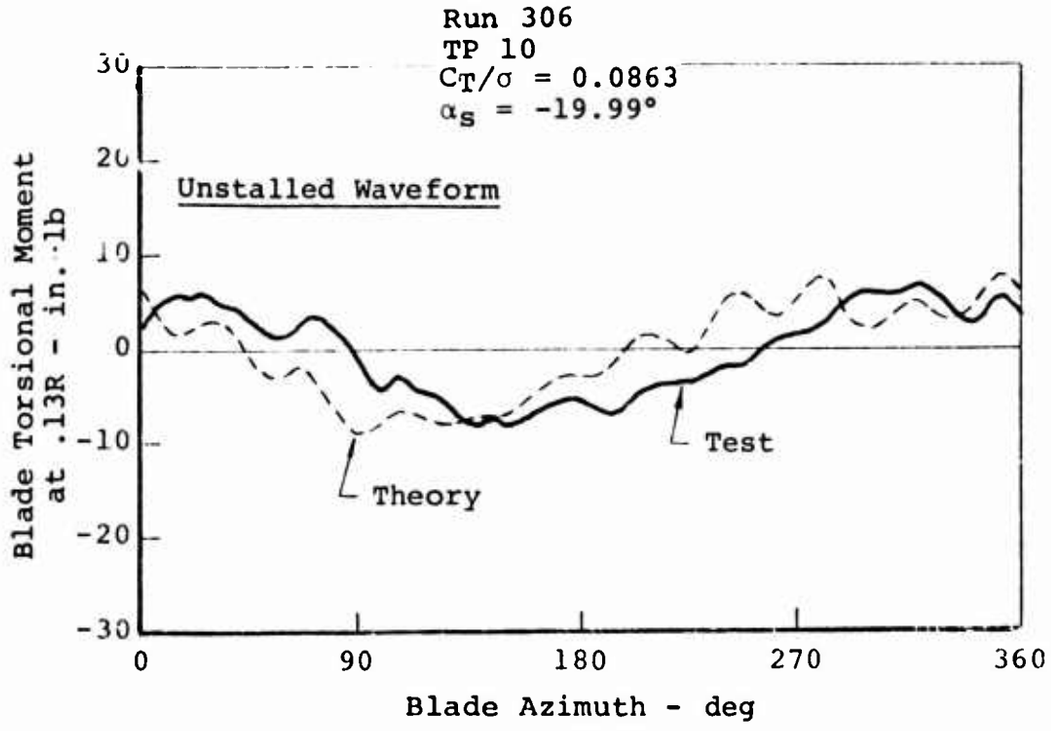

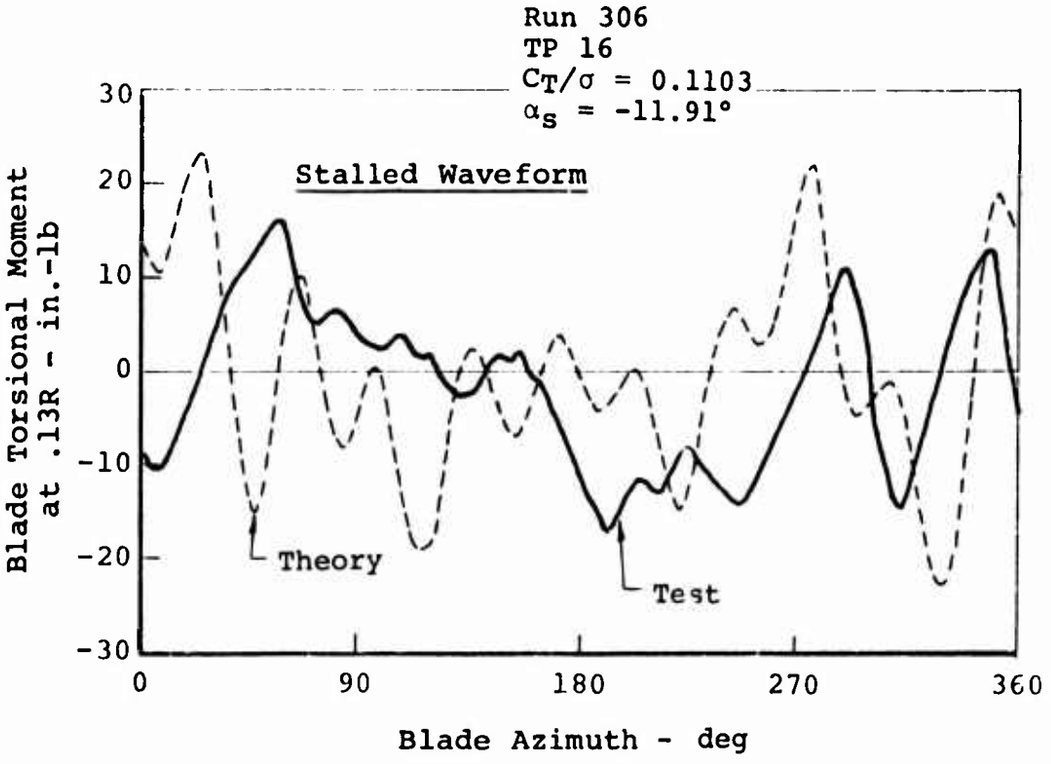

Figure 12. Theory/Test Torsional Waveform Comparison for the Standard Reference Blade.

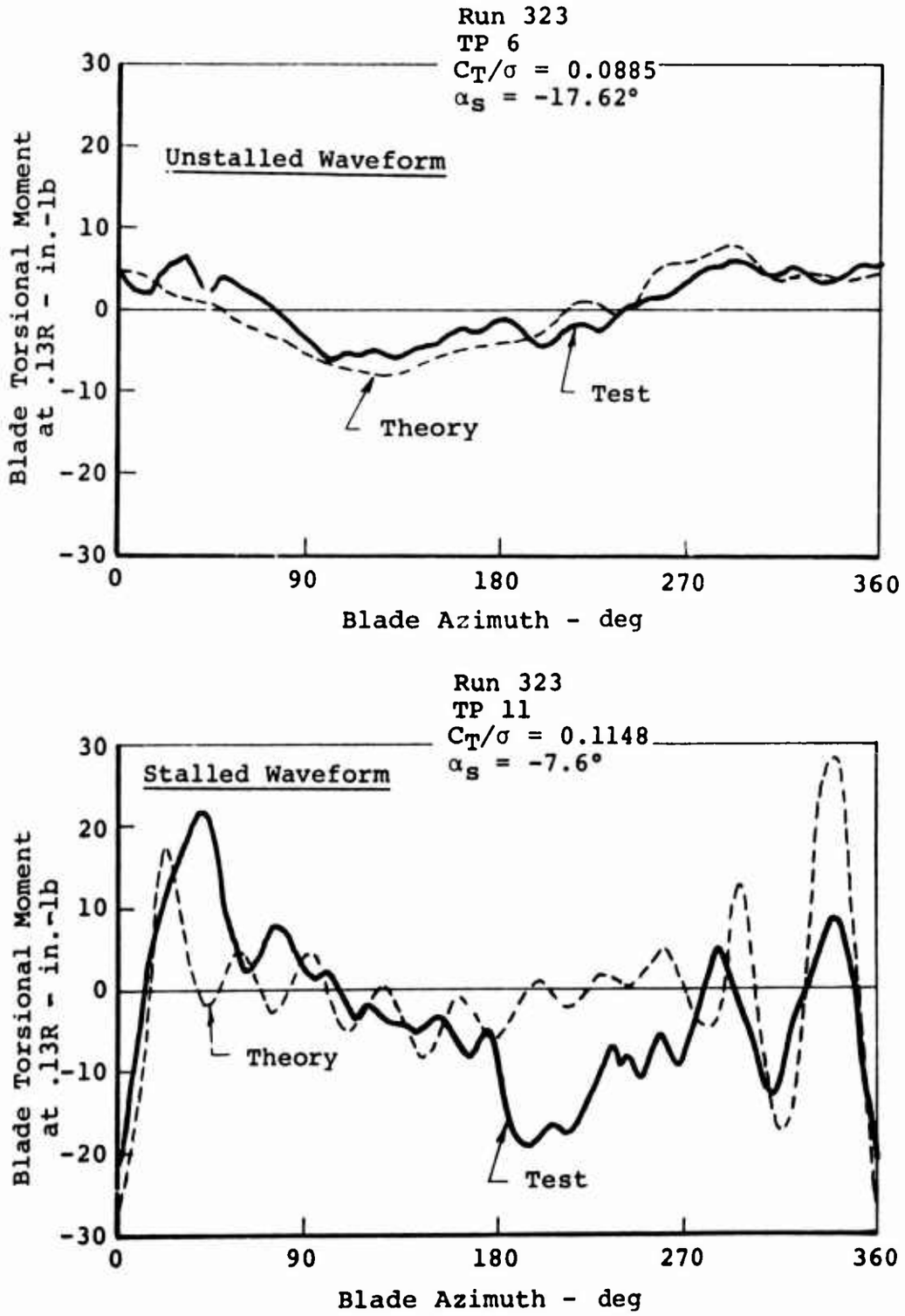

Figure 13. Theory/Test Torsional Waveform Comparison for the Morganite Blade.

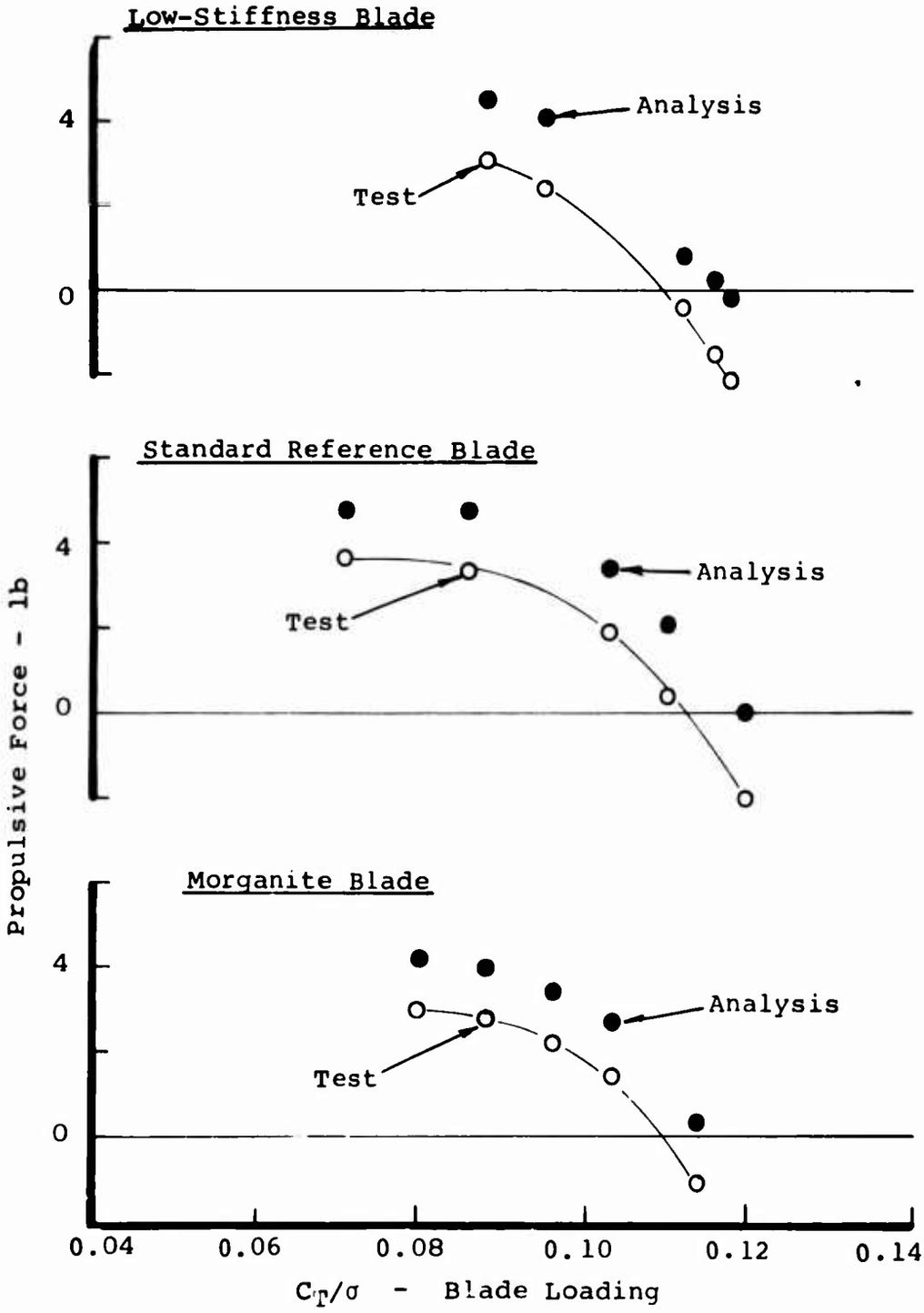

Figure 14. Theory/Test Propulsive Force Comparison.

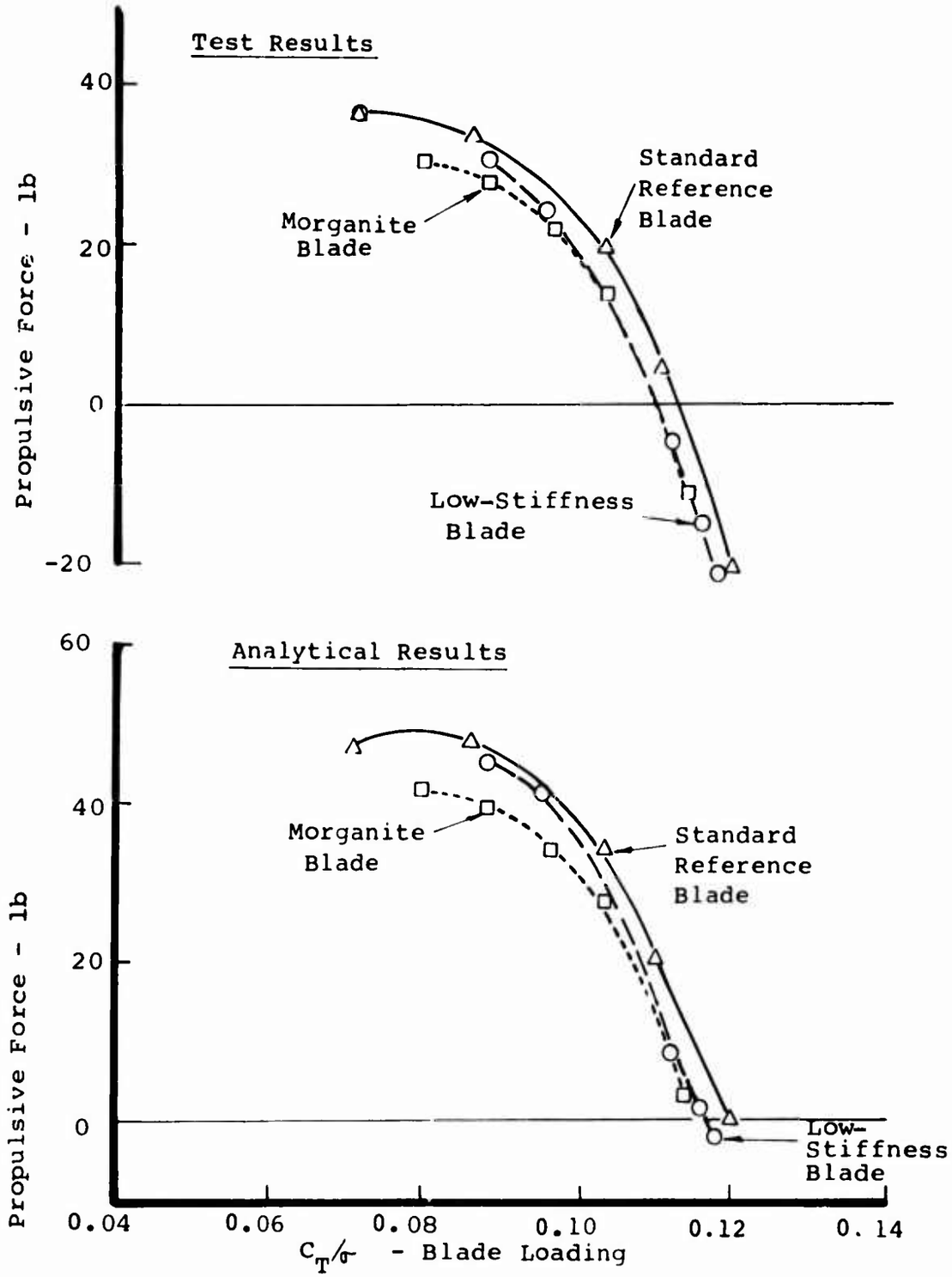

Figure 15. Rotor-to-Rotor Propulsive Force Comparison.

the same, indicating that the relative values are valid and that the propulsive force error is approximately the same for each of the blade sets.

The inability of the analysis to properly predict the rotor propulsive force can be traced to the inability to predict blade flapping. Figure 16 compares theory and test cyclic flapping angle versus rotor blade loading. The figure shows that the analysis does not predict the large tip-path-plane blow-back experienced by the model. This explains the overprediction of propulsive force, since the theoretical tip-path plane is tilted further forward than the model, giving a larger propulsive force.

- Collective Angle and Thrust - The relationship between rotor thrust and collective angle is illustrated in Figure 17 for each model blade for both test and analysis. Since the wind tunnel test procedure was to hold the collective constant and to vary the shaft incidence angle, the measured data is constant and appears as a vertical line. The analytical results, in general, agree very well with the measured data but tend to underpredict the collective angle at the higher thrusts.

A possible explanation for this trend may be proposed by reviewing the model test procedure. The rotor is set at a constant collective pitch angle, the rotor shaft is pointed approximately 20 degrees into the wind, and the shaft is tilted toward the vertical in discrete increments. Changing the shaft tilt toward the vertical decreases the inflow, which results in increased rotor thrust. The upper portion of Figure 18 shows the flow field through a rotor operating in free space and set at a 20-degree shaft tilt. The free-stream velocity field is altered in the vicinity of the rotor due to the rotor induced inflow. From momentum considerations, the larger the rotor thrust, the larger the induced mass flow rate through the rotor disc.

The lower portion of Figure 18 illustrates the flow field around the same rotor operating in a wind tunnel. In order to produce the same thrust, the same induced mass flow rate through the rotor disc is required. The presence of the tunnel roof, however, restricts the area available for the airstream. As a result, the inflow velocity must increase. The increased inflow velocity increases the negative induced angle of attack, which reduces the effective rotor angle of attack, reducing the rotor thrust. The analysis does not take this phenomenon into account; it simply

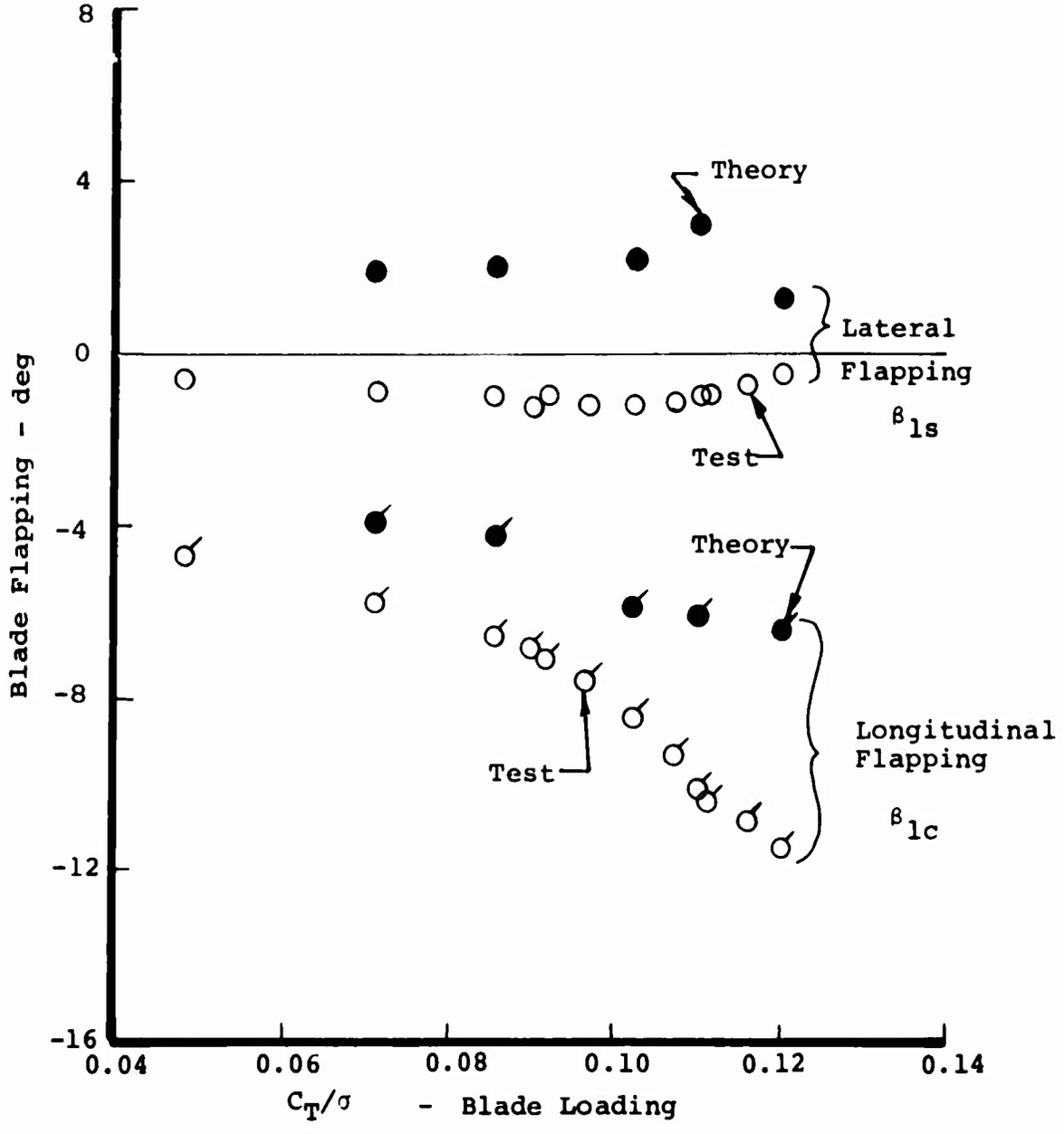

Figure 16. Comparison of Test and Theory 1/Rev Flapping for the Standard Reference Blade.

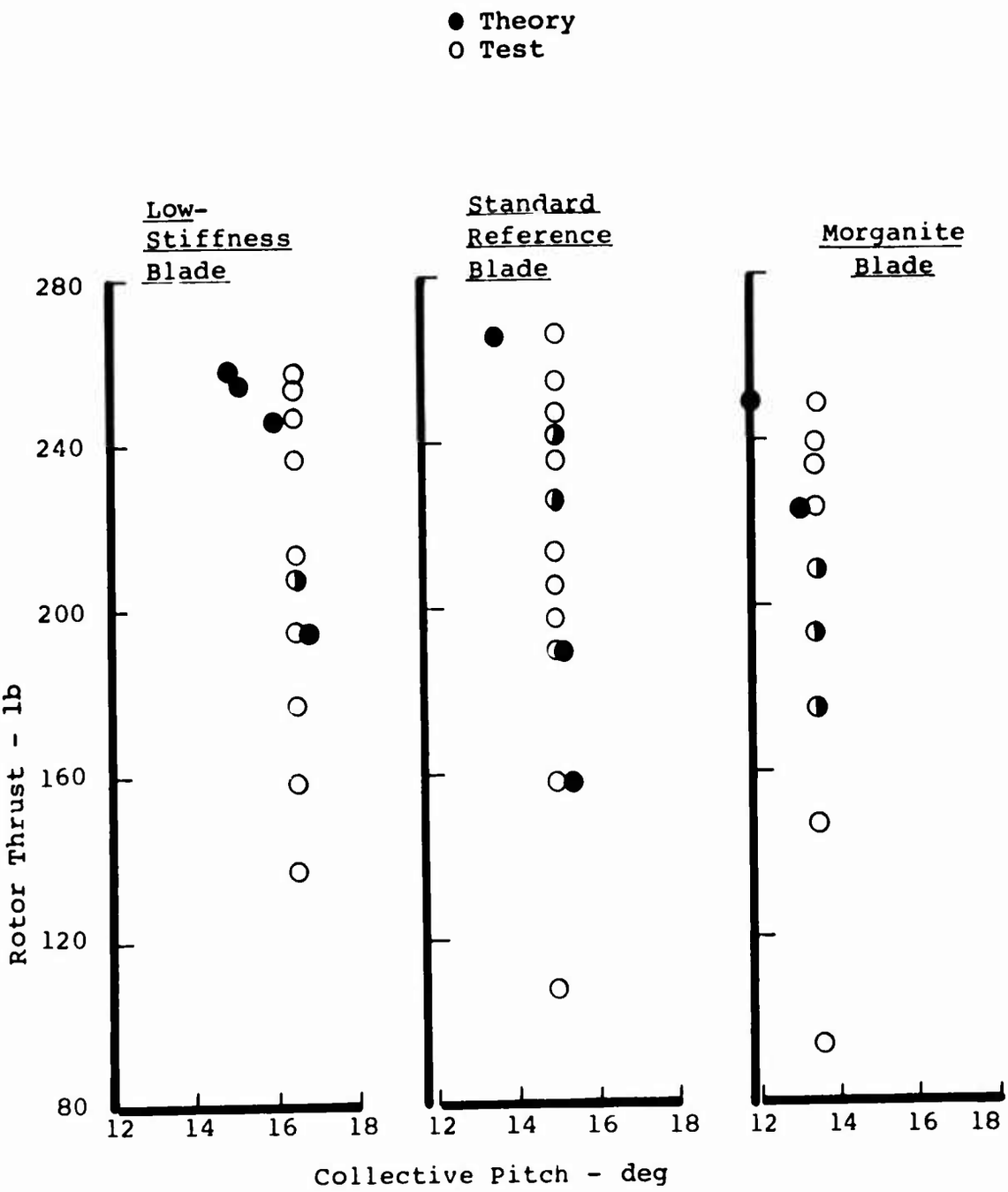

Figure 17. Test/Theory Comparison of Rotor Thrust and Collective Pitch.

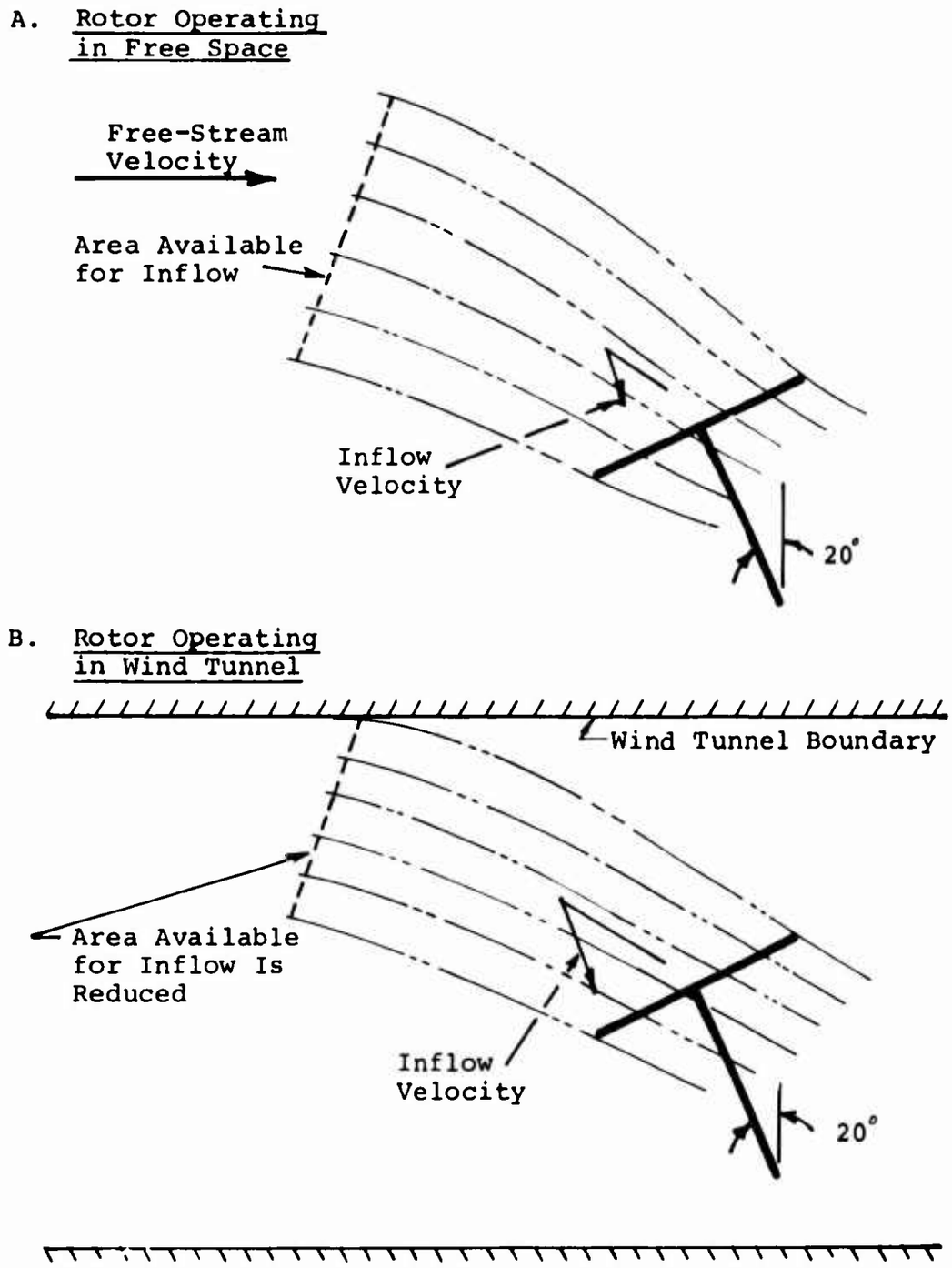

Figure 18. Effect of Wind Tunnel Boundary on Induced Velocity.

predicts a smaller collective angle to obtain the given reduced model rotor thrust. At higher rotor thrusts and near vertical shaft incidence angles, this effect becomes more pronounced, causing the analytical thrust versus collective line to bend toward smaller collective angles at the higher thrust conditions.

- Discussion of Analytical Deficiencies - Although the unsteady aeroelastic analysis correctly predicts the torsional load trend with variations of C_T/σ and torsional natural frequency, a number of deficiencies have been observed in the theory/test comparison. These deficiencies include:

  Early stall inception and the resulting overprediction of the stall-induced control loads

  Large higher harmonic components in the torsional load waveform

  Poor 1/rev flap angle prediction

Full-scale correlation with flight data has been shown (Reference 2) to be significantly better than the model correlation indicated here. The model full-scale discrepancy is so surprising that an investigation into the problem was undertaken by comparing these model results with full-scale predictions. The second part of this report calculates torsional loads for full-scale blades with torsional natural frequencies from 3/rev to 7/rev. It is possible to find a full-scale flight condition near a model test condition, with approximately the same torsional natural frequency, to scale down the torsional loads, and to compare the waveforms. This is exactly what has been done in Figure 19. The upper portion of the figure compares theory and test torsional load waveforms for the low-stiffness model blade. This figure shows the same waveform comparison as the lower half of Figure 11, and probably represents the worst correlation obtained, due to the large theoretical higher harmonic component in the waveform. The lower portion of this figure compares the same model test data with a waveform calculated for a CH-47C rotor blade with its torsional stiffness (GJ) reduced to 0.25 of its original value and the torsional load scaled down to the model size. The model and full-scale rotors have approximately the same C_T/σ (0.1179 and 0.115) and torsional natural frequency (3.1/rev and 3.0/rev); however, the cyclic pitch, rotor shaft tilt, and blade flapping are significantly different (see the parameters noted on the figure). Even though the flight conditions are

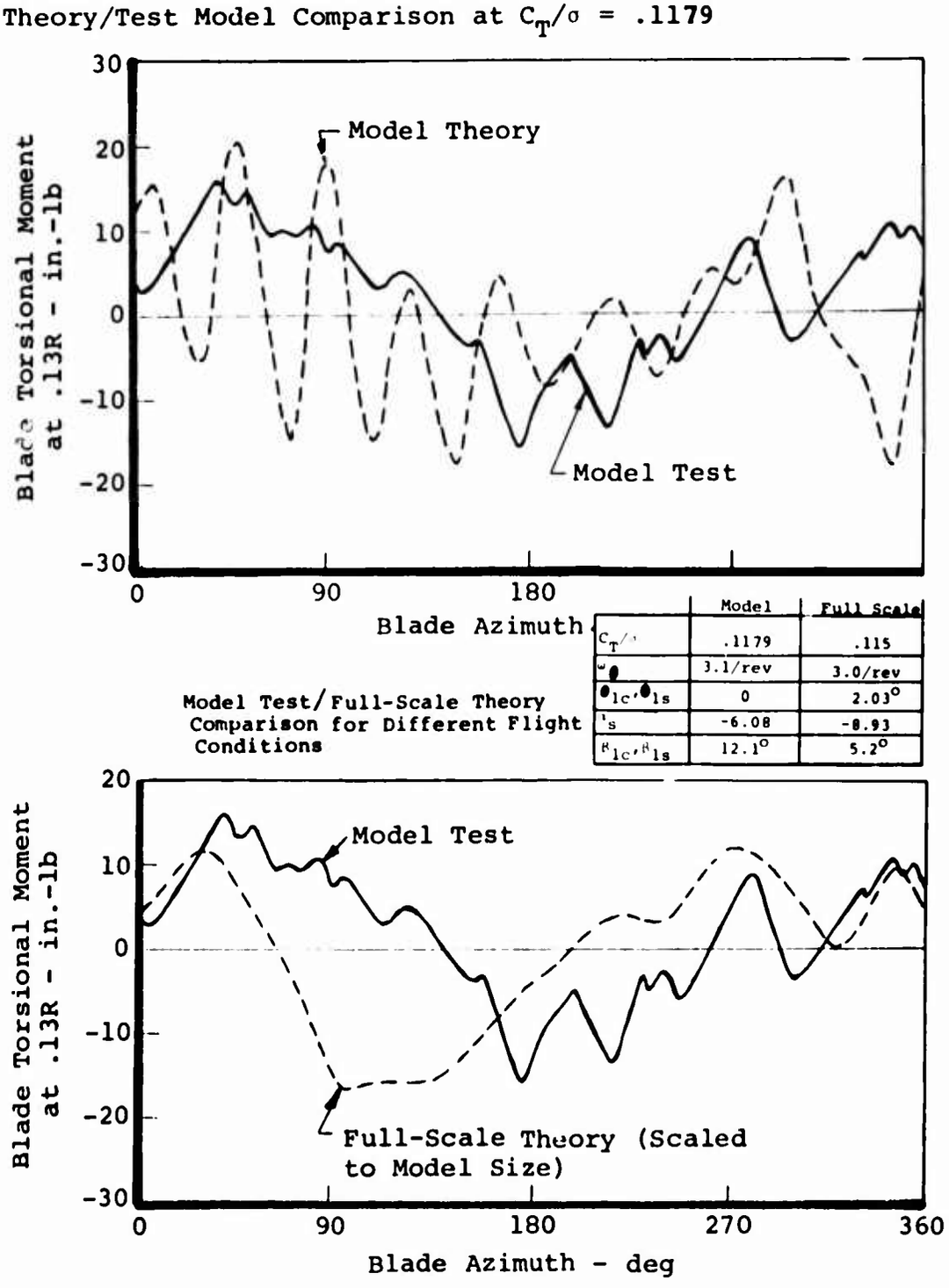

Figure 19. Theory/Test Correlation for Low-Stiffness Blade.

significantly different, there are many similarities in the waveform, including:

Peak-to-peak amplitudes are about the same.

Both waveforms are predominantly 1/rev.

Stall-induced spikes between 270 and 360 degrees azimuth are about the same magnitude and in phase.

The same can be observed in Figure 20, where the standard reference blade (torsional natural frequency equals 4.25/rev) is compared with a CH-47C blade with one-half the torsional stiffness (torsional natural frequency equals 4.0/rev). Again, in this case, the full-scale and model waveforms agree fairly well. The stall spikes agree well (though slightly phase shifted), the amplitudes are equivalent, and the large high-harmonic load evident in the calculated model waveform is not present.

In general, it is clear that the calculated full-scale waveform compares better with the model waveform than do the calculated model results, especially as far as the large high-harmonic load components are concerned. The essential difference between the model and full-scale flight conditions is the lack of cyclic pitch and the large flapping of the model rotor (i.e., 12.1 degrees flapping for the model blade compared to 5.2 degrees for the full-scale blade). The large model flapping is probably the significant difference. The unsteady aerodynamic theory was formulated solely from unsteady pitching data. A stall delay parameter (see Reference 2) was formulated from the pitch oscillating data, and correlation was performed only with the pitching data. The plunging effects (i.e., the induced angle, ϕ) were assumed to act in a manner similar to the mechanical pitch angle (θ), in that constant mechanical pitch angle (θ) and the induced angle (ϕ) due to constant plunging motion are equivalent (see Figure 21). However, as Figure 21 shows, time varying θ and time varying ϕ are not equivalent, since they do not lead to the same chordwise velocity distribution. Though Theodorsen's equations (Reference 3) account for this below stall, it has not been taken into account in the determination of stall delay. For stall delay, it has been assumed that $d\theta/dt$ and $d\phi/dt$ have the same effect, but this clearly may not be true.

To determine whether plunging may be the problem, a two point theory/test comparison was performed with two-dimensional vibratory plunging airfoil test data.

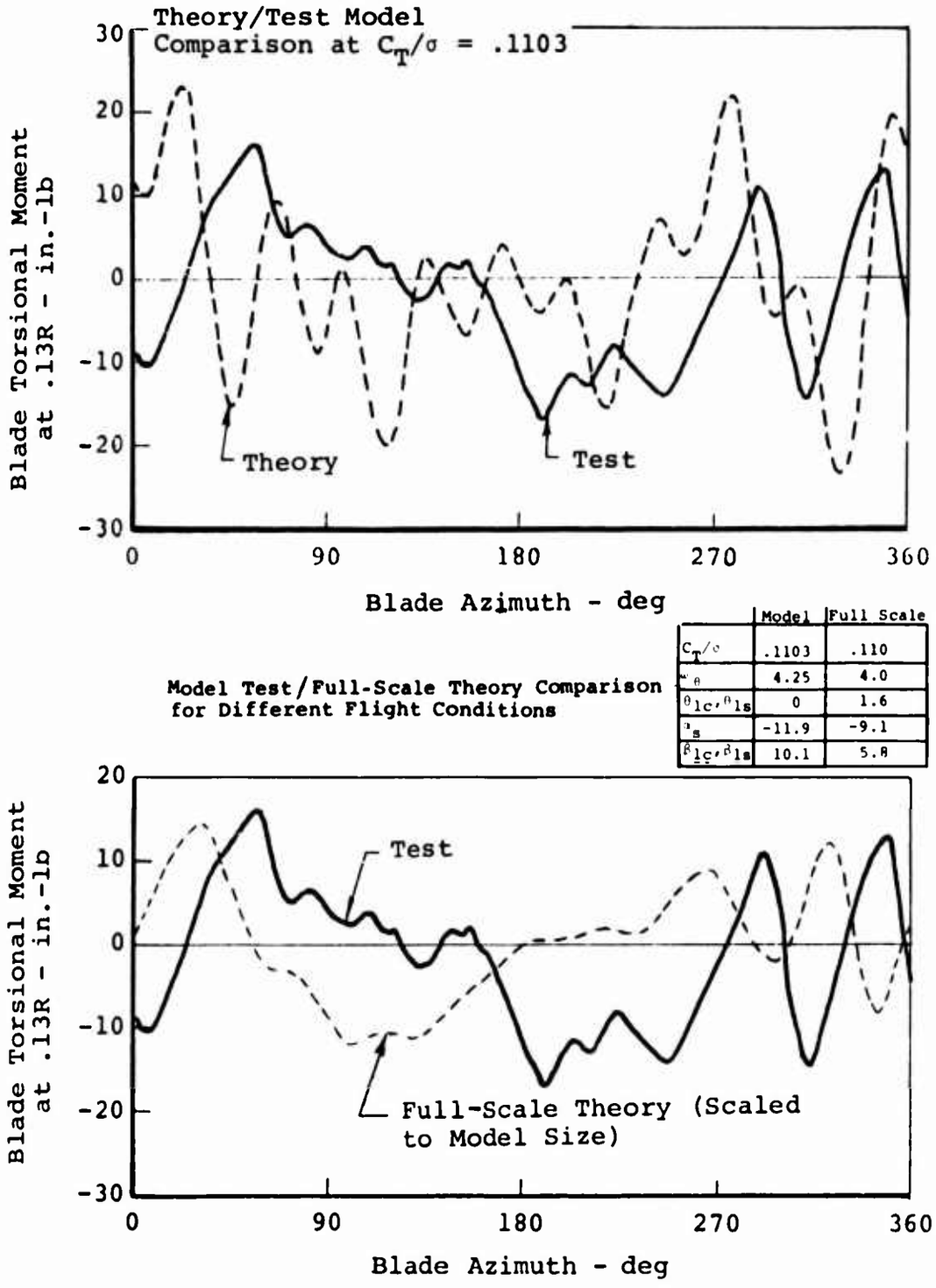

Figure 20. Theory/Test Correlation for Standard Reference Blade.

Statically, Pitch Deflection and Constant Vertical Motion Are Equivalent.

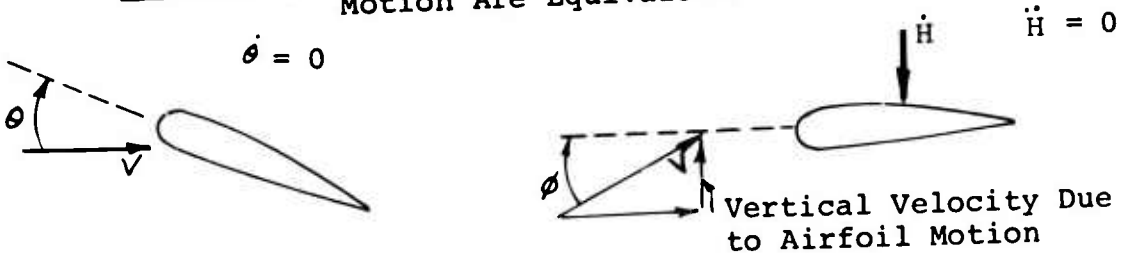

- Constant Angle of Attack

- Constant Down Motion

θ and ϕ Are Equivalent

(a) Induced Angle for a Constant Vertical Velocity is Equivalent to a Constant Angle of Attack

Dynamically, Vibratory Pitching and Vibratory Vertical Motion (Flapping or Plunging) Are Not Equivalent. They Lead to Different Chordwise Velocity Distributions.

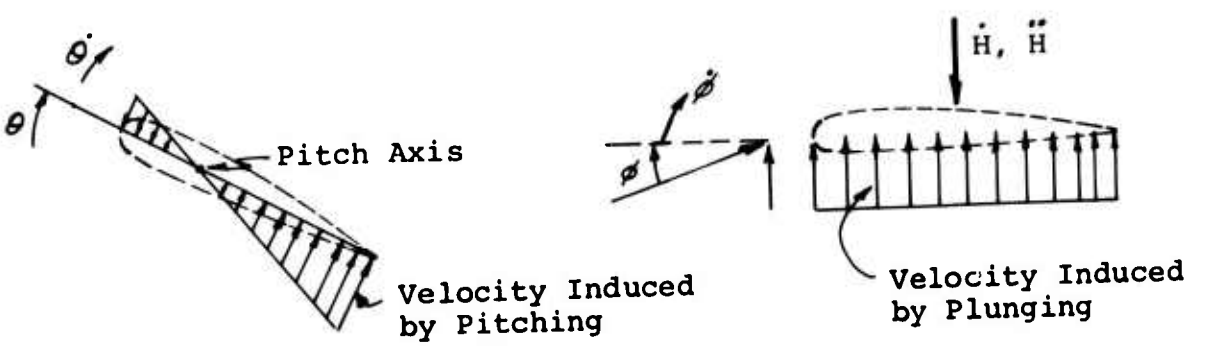

$\dot{\theta}$ and $\dot{\phi}$ Are Not Equivalent

(b) Induced Angle for a Vibratory Vertical Velocity is Not Equivalent to a Vibratory Angle of Attach

Figure 21. Comparison of Pitching and Plunging.

Reasonable theory/test correlation was obtained below stall, but the results near stall are very poor as shown in Figure 22. The near-stall comparison shows that the test results have not stalled while the theoretical prediction has. Therefore, a deficiency in the plunging representation may exist in the analysis that becomes apparent for model test conditions where large plunging induced cyclic angle-of-attack changes are present (neglecting elastic twist). It is probably this plunging deficiency that causes:

- The higher harmonic load in the predicted model waveform
- The premature stall inception prediction (see Figure 22)
- The poor flap angle prediction, which results in poor prediction of propulsive force

Other areas that may deteriorate the theoretical predictions include:

- The omission of oscillating tangential flow effects, which result from dV_T/dt due to μ effects around the azimuth
- An insufficient number of azimuth calculation points, (azimuth interval is 15 degrees) which may provide poor resolution of the higher harmonic airloads
- The omission of the dynamic C_M overshoot term discussed in Appendix IV
- The use of an approximate value for the lift stall delay parameter for a Mach number of 0.6

Even though the theory/test correlation can use improvement, the analysis correctly predicts the torsional load trend with C_T/σ and rotor blade torsional frequency for the model blade, and provides even better correlation for full-scale rotors (Reference 2).

ANALYTICAL INVESTIGATION OF STALL-INDUCED DYNAMIC LOADING

The Reference 1 study shows that changes of a blade's torsional natural frequency can change the stall-induced control loads. This study, however, considered only a single airspeed and a single blade loading. To further investigate the variation of stall-induced control loads, the previous study was expanded to:

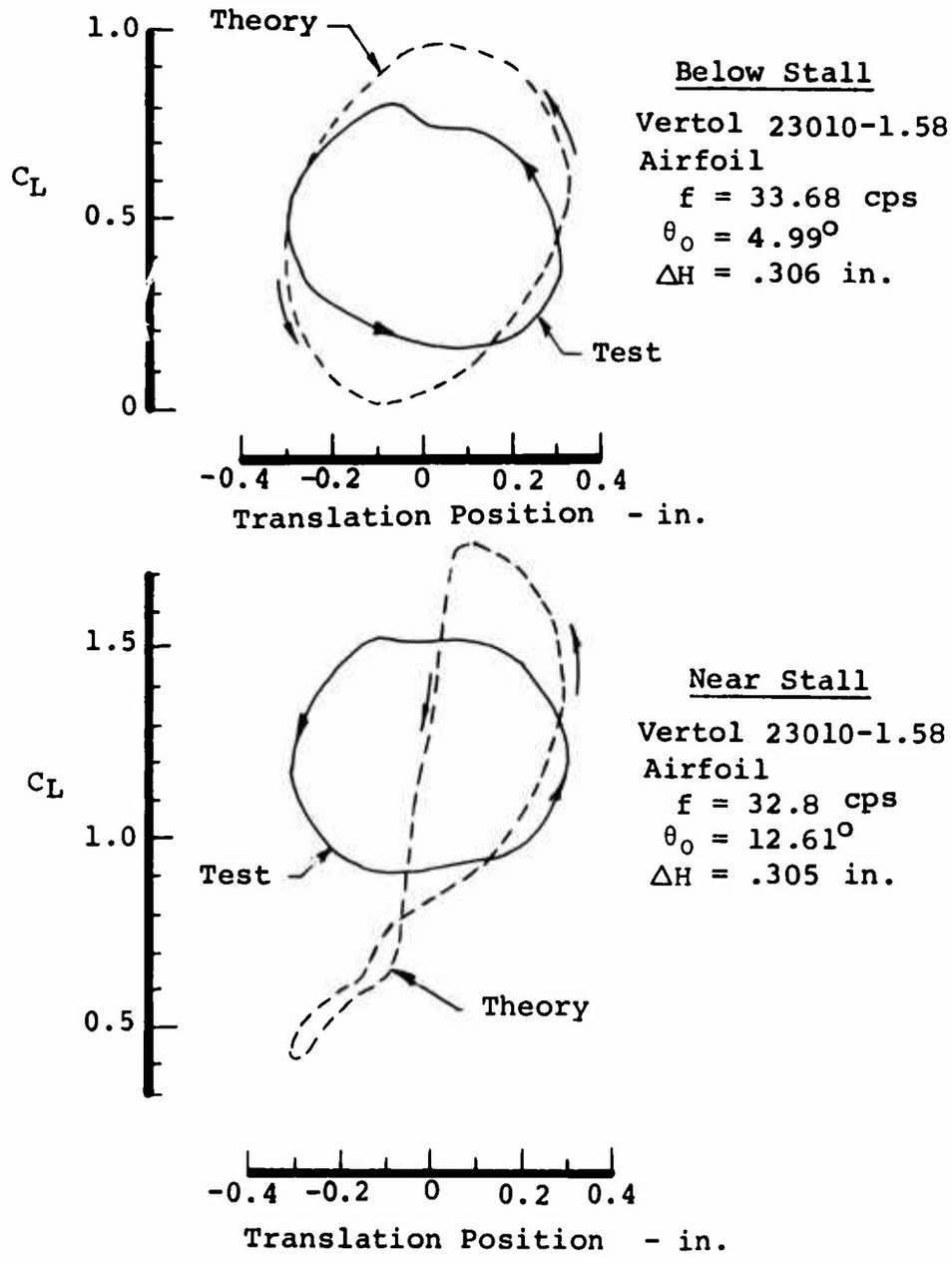

Figure 22. Comparison of Theory and Test C_L Variations for 2-D Plunging Data.

1) Determine the effect of various blade torsional natural frequencies (3/rev, 4/rev, 5.2/rev, 6.95/rev) on stall-induced torsional loads over a range of advance ratios (hover to 0.41) and blade loadings (0.05 to 0.18).

2) Determine the effect of blade pitch inertia, control system stiffness, blade twist, cyclic pitch, and torsional frequency (above 7/rev) on stall-induced control loads.

This study was performed using program C-60 (see Appendix I) to analyze a single-rotor aircraft. The previous section demonstrated the program's ability to predict torsional loads both in and out of stall, establishing its usefulness as a tool for performing the study.

The aircraft used for this study is a single-rotor helicopter with a CH-47C blade. A 20.1-square-foot frontal area was assumed for the fuselage, and a tail rotor sufficient for trim purposes was added. The main rotor consisted of three articulated 30-foot-radius blades with a constant chord of 25.25 inches. The blade cross section is a cambered NACA 23010 airfoil with negative 9.137 degrees of linear twist along the blade span. A full discussion of the blade's detailed physical properties is presented in Appendix III.

Varying Torsional Natural Frequency

The changes of the blade first torsional natural frequency for the vast majority of this study were accomplished by adjusting the blade torsional stiffness (GJ) of a standard CH-47C blade which has a torsional natural frequency of 5.165/rev. Natural frequencies of 3.0/rev, 4.04/rev, and 6.97/rev were obtained by multiplying the torsional stiffness distribution of the CH-47 by factors of 0.25, 0.5 and 3.3, respectively. This appears to be the most realistic parameter for change, since fiberglass and other composite materials make large torsional stiffness variations possible through various cross-ply lay-up techniques and selection of different modulus materials.

Changing the torsional natural frequency by varying the control system stiffness is not practical, since most of the torsional flexibility is obtained from the blade. Therefore, a large increase in control system stiffness would not significantly increase the blade torsional natural frequency due to the remaining flexibility of the blade. Large reductions in the control system stiffness would successfully lower the blade torsional frequency, but it would also reduce the allowable loads, since the strain would increase significantly. Electronically adjusting the control system stiffness through a feedback loop is possible, but the resulting induced damping (due to phase shifts) and impedance variations with blade harmonic

(due to system resonances) make this consideration complex and beyond the scope of this study. However, a very limited number of control stiffness variations were made to determine its effect.

Changes in torsional natural frequency can also be made by varying the blade pitch inertia. However, for a given blade geometry, it is very unlikely that significant changes in blade pitch inertia could be made in a cost and weight effective manner. Significant increases in inertia would result in larger blade weight and an inefficient rotor (from weight considerations). A significant reduction in inertia is probably not possible, but if it were, exotic and expensive blade material would be required to reduce the weight and inertia.

A much simpler method of changing torsional natural frequency with inertia is to simply vary the blade aspect ratio. A reduced chord blade would have a lower torsional inertia and a higher torsional frequency, and an increased chord blade would have higher inertia and a lower frequency. This, however, involves changes in the blade geometry, and analytically studying this blade is beyond the scope of this program.

In the aircraft industry, there are a number of helicopters with significantly different aspect ratios than the CH-47C. These include the low-aspect-ratio Bell rotors with a relatively large chord and the large-aspect-ratio Sikorsky rotors with a relatively small chord. Therefore, torsional frequency changes resulting from pitch inertia are a realistic occurrence in the aircraft industry. A limited study of large pitch inertia changes was undertaken to investigate this inertia effect, but it was limited to a blade with the CH-47C chord. Though these results may not be realistic for the chord size used, they are an indication of the effect of torsional inertia on blade control loads.

Extent of Study

Four rotor systems with different torsional natural frequencies blades were analyzed for 24 flight conditions, representing a total of 88 analytical data points. The extensive matrix of flight conditions was analyzed to investigate the interactive effects of blade frequency, airspeed, and blade loading. Using the results, control load trends with torsional natural frequency, blade loading, and airspeed were determined. Finally, a flight envelope was established for each blade frequency at a constant control load to allow a comparison over the whole range of flight conditions.

The study was expanded to investigate blade torsional frequencies, from 7/rev to 12/rev for a limited number of flight conditions, to establish the overall variation of torsional

load with frequency from 3/rev to 12/rev. Next, torsional frequency variations resulting from control system stiffness changes and torsional inertia changes were obtained for three flight conditions and compared with the results obtained by changing the blade torsional stiffness. Finally, variations of blade twist, cyclic pitch, and propulsive force were investigated to determine if other means for reducing the stall control loads could be found. This secondary study represented an additional 80 analytical data points.

Analytical Results of Flight Matrix

The first part of the control load study investigated the variation of control loads with changes in advance ratio and blade loading for blades with first torsional natural frequencies of 3.0/rev, 4.04/rev, 5.165/rev, and 6.97/rev. An extensive matrix of flight conditions was established to investigate interactive effects of blade frequency, airspeed, and blade loading by analyzing the four different torsional frequency blades at each flight condition. The full flight condition matrix is given below:

Airspeed	0 kt	125 kt	150 kt	175 kt
C_T/σ				
0.05				X
0.06			X	
0.07			X	X
0.08		X		X
0.09		X	X	X
0.10		X	X	X
0.105		X		
0.11		X	X	X
0.115	X	X	X	
0.12	X	X		
0.15	X			
0.165	X			
0.18	X			

The resulting torsional loads from the flight condition matrix were examined:

1) versus blade loading for constant airspeed and torsional frequency

2) versus torsional frequency for constant airspeed and blade loading

3) versus airspeed for constant torsional frequency and blade loading

These results showed that a significant reduction of the basic blade control loads can be realized over a considerable range of advance ratios and blade loading and that these reductions lead to a significant extension of the control load limiting aircraft flight envelope. This can be summarized by cross plotting and occasionally extrapolating the pitch-link load trends with blade loading and airspeed to obtain the flight condition (as a function of C_T/σ and μ) that first experiences a 2500-pound pitch-link load. The 2500-pound load represents approximately the original pitch-link endurance limit load for the CH-47C control system.

The above procedure yields a blade loading versus advance ratio envelope for the 2500-pound pitch-link load. Figure 23 compares the flight envelopes for each of the four different frequency blades investigated. The solid symbols represent flight conditions for a 2500-pound load obtained by interpolation. Open symbols were obtained by extrapolation. The lines represent the 2500-pound pitch-link load inception boundary as a function of blade loading and advance ratio for each of the blades studied. Flight conditions (C_T/σ and μ) that fall below the boundary have not yet reached the 2500-pound pitch-link load. Flight conditions above the boundary either have a pitch-link load above 2500 pounds or had to fly through such a load condition.

The basic blade (torsional natural frequency of 5.2/rev) is represented by the solid line. This load boundary (solid line) is approximately constant at a blade loading of 0.11 up to an advance ratio of 0.35. For higher advance ratios, the boundary shows a sharp decrease, reducing to a blade loading of 0.08 at an advance ratio of 0.42.

As Figure 23 shows, a blade with a torsional natural frequency of 4/rev (dashed line) has the best load boundary and represents a significant improvement over the basic blade configuration. The 4/rev load boundary has essentially the same shape as the basic blade, but it occurs at a higher blade loading. The basic blade boundary is at a blade loading 0.015 below the 4/rev blade at an advance ratio of 0.3. This means that at an advance ratio of 0.3 the basic blade would reach a pitch-link load of 2500 pounds at a blade loading of 0.11, while the 4/rev blade pitch-link load reaches this value at 0.125. At an advance ratio of 0.38, the basic and 4/rev blade are approximately equal; but, at an advance ratio of 0.4, the 4/rev blade boundary is expanded beyond the basic blade by a blade loading of 0.005.

The 3/rev blade (short dashes) shows a different boundary trend. At an advance ratio below 0.29, the 3/rev blade has the best load boundary, with the 2500-pound load reached beyond a blade loading of 0.125. This figure is not exact

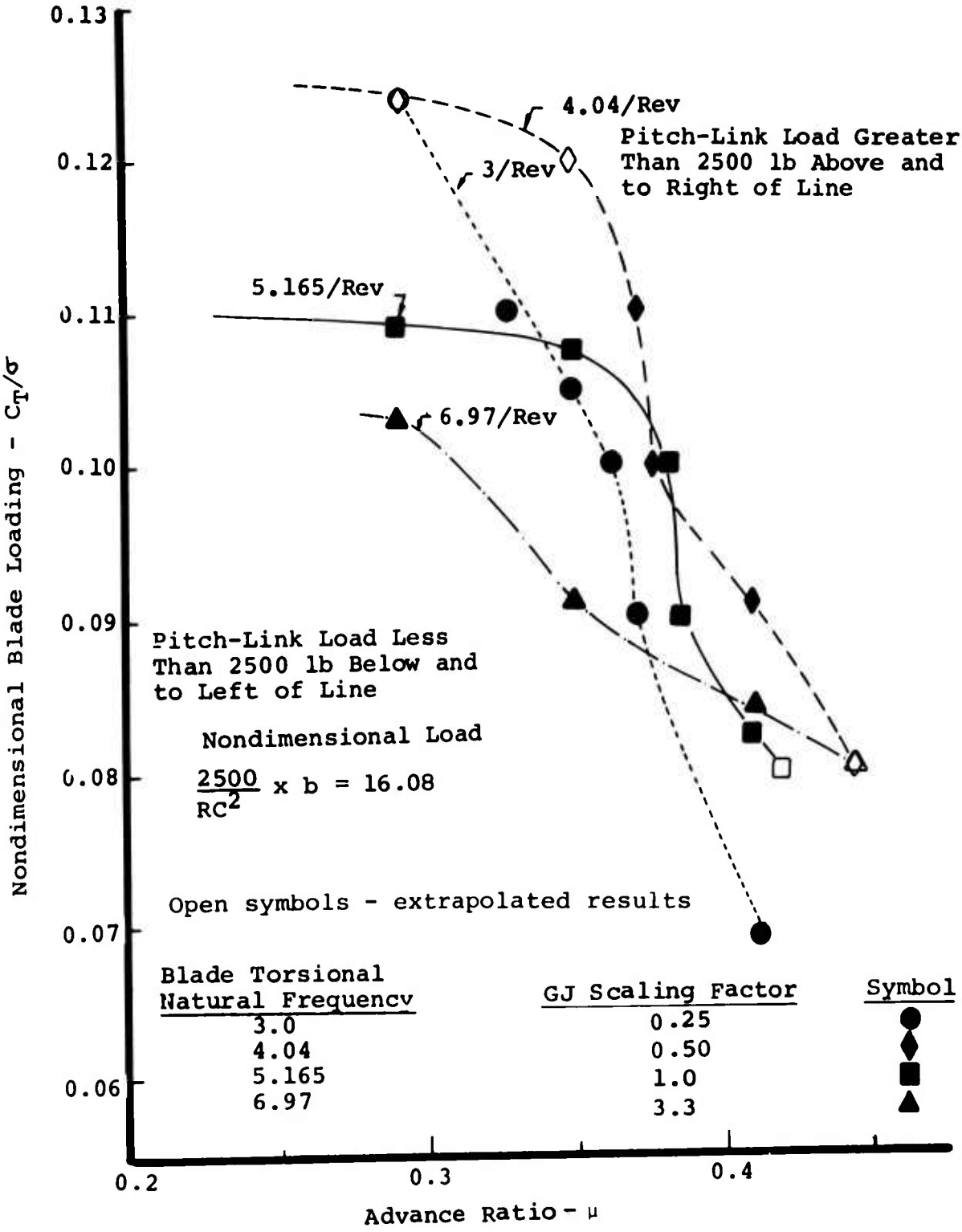

Figure 23. Control Load Boundaries for Blades With Torsional Natural Frequencies of 3, 4, 5.2 and 7/Rev.

since it was obtained by extrapolating lower blade loading data (the maximum load reached by the 3/rev blade at an advance ratio of 0.29 was 2,100 pounds at a blade loading of 0.12). The model test results, which were obtained at an advance ratio around 0.28, agree with these results, which showed that the 3/rev blade had lowest loads. However, the 3/rev boundary does not plateau like the 4/rev and 5.2/rev blades, but instead drops sharply with increasing advance ratio and eventually falls below the three other blades at a 0.375 advance ratio. Beyond an advance ratio of 0.34, the 3/rev blade is worse than the basic blade. The sharp boundary reduction of this blade at the higher advance ratios is due to a large load growth, which eventually becomes an instability. The instabilities are experienced at an advance ratio of 0.35 and beyond, and clearly mark the 3/rev blade as unacceptable, at least for the current pitch-link controlled configuration.

The 7/rev blade clearly has the poorest load boundary up to an advance ratio of about 0.37. At the higher advance ratios (above 0.35) the 7/rev blade has the smallest reduction of blade loading capability with increasing advance ratio, which can be seen below:

	REDUCTION OF C_T/σ PER 0.1 μ INCREASE ABOVE $\mu = 0.35$
3/rev	0.060
4/rev	0.054
5.2/rev	0.045
7/rev	0.012

The 7/rev boundary reduction is about one quarter that of the other blades. In this region the 7/rev blade surpasses the 3/rev blade at an advance ratio of 0.37, surpasses the basic blade at 0.40, and apparently will surpass the 4/rev blade around 0.44. The 7/rev blade may very well prove to have the best load boundary beyond an advance ratio of 0.44.

In summary, the study shows that the stall-induced control loads can be reduced by lowering the rotor blade torsional stiffness so that the first torsional natural frequency is reduced to about 4/rev. Larger reductions in torsional frequency (to 3/rev) reduce control loads for low advance ratios (below $\mu = 0.3$), but result in a large load increase and rotor instability at high advance ratios ($\mu > 0.35$). A higher frequency blade (7/rev) generated large stall loads at low and moderate airspeeds, but

may provide lower loads at high advance ratios ($\mu > 0.45$).

One further note--the endurance limit pitch-link load (2500 pounds) has been nondimensional so that this figure may be used for aircraft of different size. The pitch-link load has been divided by the radius times the chord squared and multiplied by the pitch arm (see figure below), all expressed in units of feet. The resulting number (16.08) can be converted to an equivalent load for any aircraft by multiplying by the aircraft's blade radius and chord squared and dividing by the pitch arm.

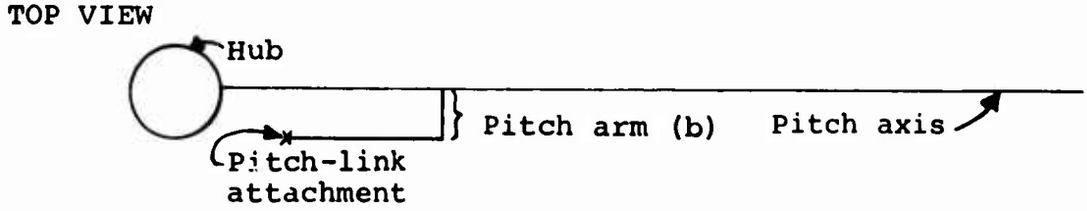

The following sections will:

1) examine the torsional load trends with blade loading and torsional natural frequency,

2) review the pitch-link load waveforms, and

3) determine the variation of propulsive force and rotor power.

Pitch-Link Load Variation With Blade Loading

The detailed results of this study can be presented in many ways. The choice of initially reviewing the variation of the pitch-link load with blade loading was made, since this format allows for a greater physical understanding than would an examination of the load trend with frequency. Figures 24 through 26 show the variation of pitch-link load with blade loading for each of the four different torsional frequency blades, at airspeeds of 125 knots, 150 knots, and 175 knots. For a given blade and airspeed, the figures show the variation of pitch-link load as the blade thrust is incrementally increased. Presenting all four blades at a given airspeed on the same plot allows direct comparison at the same flight conditions.

For all figures, the basic CH-47C blade (with a torsional natural frequency of 5.2/rev) is indicated by a solid line. At an airspeed of 125 knots (Figure 24), the basic blade pitch-link load increases slowly with blade loading up to a value of 0.10. In this region the pitch-link load waveform is predominantly

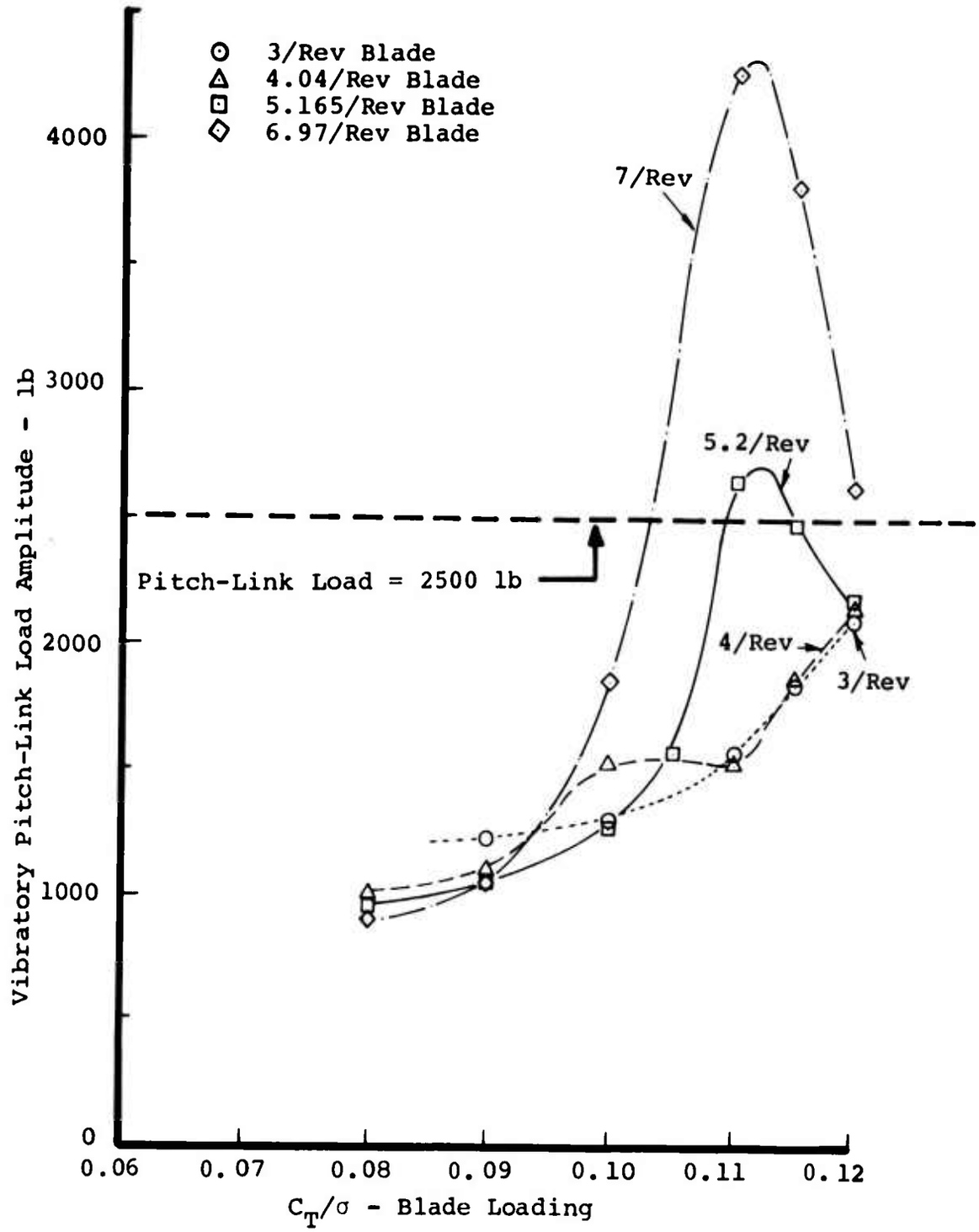

Figure 24. Variation of Pitch-Link Load Amplitude With Blade Loading at 125 Knots, $\mu = 0.288$.

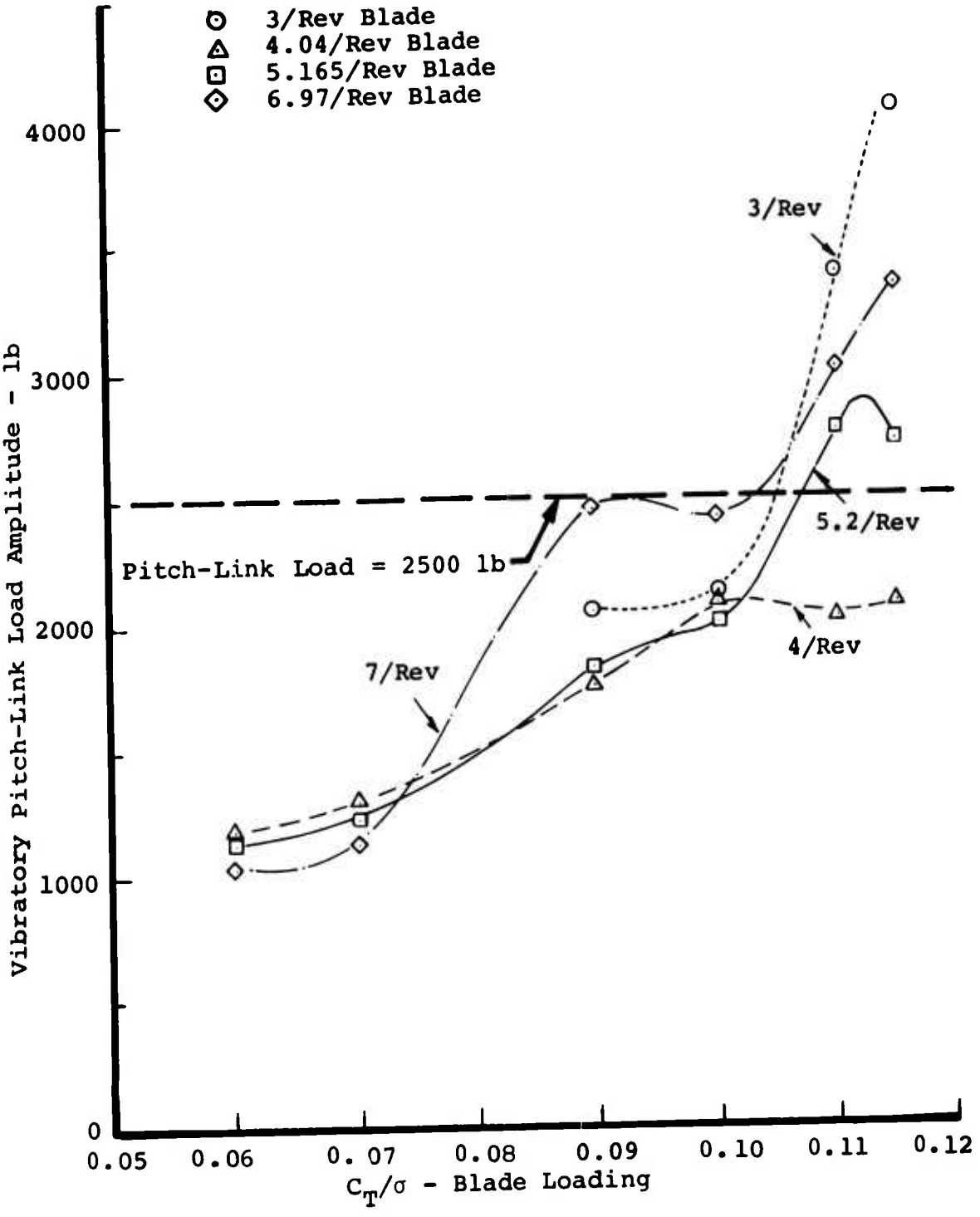

Figure 25. Variation of Pitch-Link Load Amplitude With Blade Loading at 150 Knots, $\mu = 0.344$.

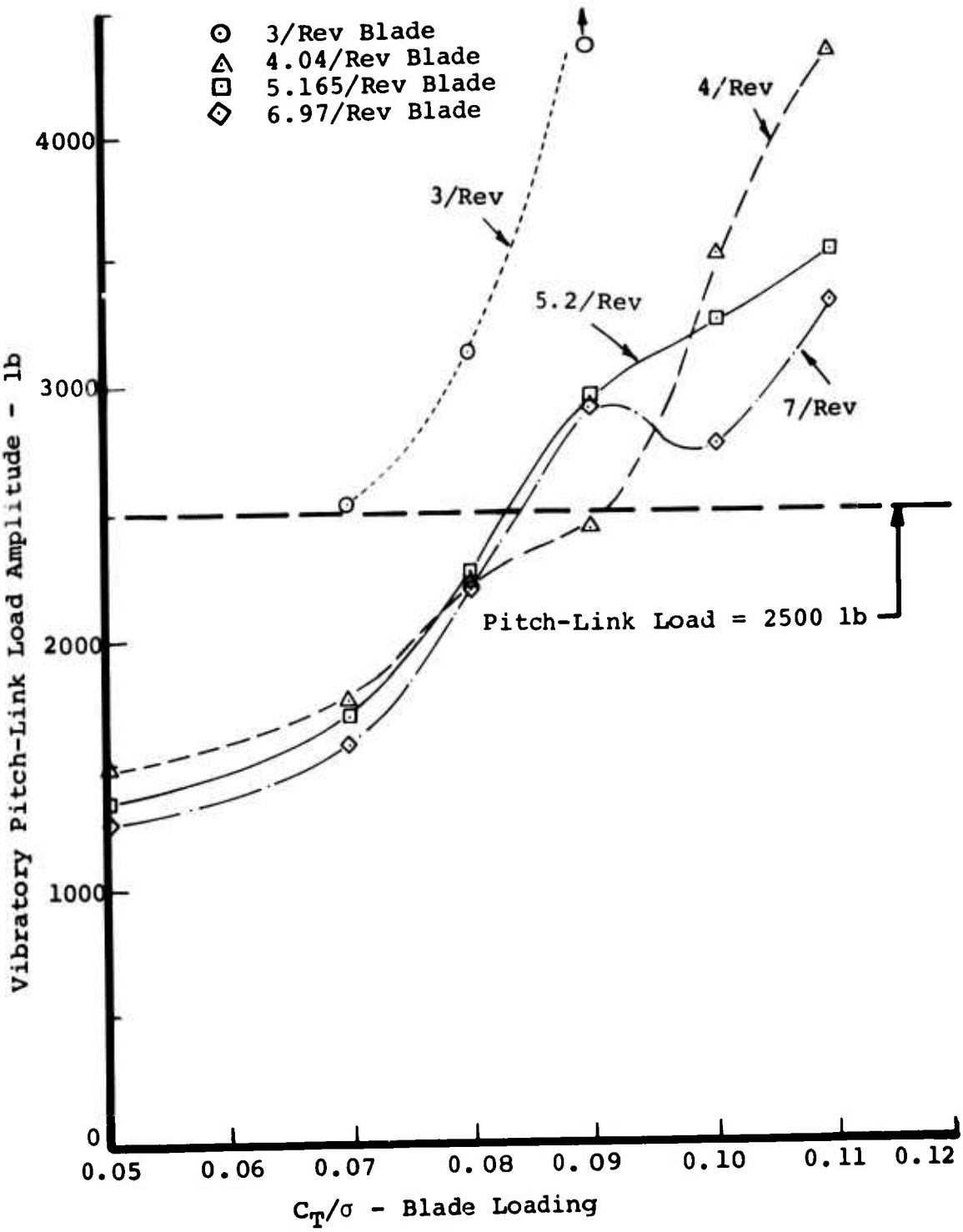

Figure 26. Variation of Pitch-Link Load Amplitude With Blade Loading at 175 Knots, $\mu = 0.397$.

1/rev and the loads are classified as unstalled (even though some stall is present). Stall inception occurs at a blade loading of about 0.103. The stall inception represents the flight condition at which the control loads begin to exhibit the rapid increase due to blade stall. In this region the pitch-link load waveform has a large high-frequency torsional load component which generally appears between 270 and 60 degrees azimuth, and usually determines the load amplitude.

The stalled pitch-link load continues to rise to 2650 pounds at a blade loading of 0.11. Increasing the blade loading beyond this point results in a load reduction. This reversal of the load trend may at first appear surprising, but it has been observed in model data (see Figure 6). There is also full-scale data that indicates the existence of the same phenomenon. CH-47C flight data shows that pitch-link loads do not continually increase with increasing rotor thrust as shown in Figure 27. The figure shows the stall-induced pitch-link load variation with increasing blade loading. The dotted line indicates the expected stalled pitch-link load growth, if no load reversal were present. Clearly, the bulk of the data falls below the expected no-reversal load line, indicating that load reductions do occur in deep stall. The figure used non-dimensional coordinates to reduce a variety of data to a single figure. Data included maneuver and level flight conditions with airspeeds up to 150 knots and load factors beyond 2.3 g's.

The 7/rev blade has generally the same pitch-link load trend with blade loading as the basic blade. There is an unstalled load region up to a blade loading of 0.09, a stalled load region typified by a large load increase with blade loading, and finally a load reversal at a blade loading of 0.11. As far as control loads are concerned, the 7/rev blade is significantly worse than the basic blade. In the unstalled region, the loads are about the same: in stall, the 7/rev blade loads are 65 percent larger; and stall inception occurs at a blade loading of about 0.095, which is 0.008 before the basic blade. Certainly, as far as stalled control loads at 125 knots are concerned, this blade is clearly the worst in the field.

The 4/rev pitch-link load trend with increasing blade loading is significantly different from the two blades discussed above. There is the typical unstalled region with little load growth up to a blade loading of 0.09. There is then a region of moderate load growth between 0.09 and 0.10, which is not typical of the stalled or unstalled load region. From a blade loading of 0.10 to 0.11, there is a load plateau, and stall inception occurs at 0.113. The unexpected load bump at 0.10 may be due to a local aeroelastic peak response, caused by a load reinforcing effect of the flight condition or trim combined with the larger live twist of the 4/rev blade. If this

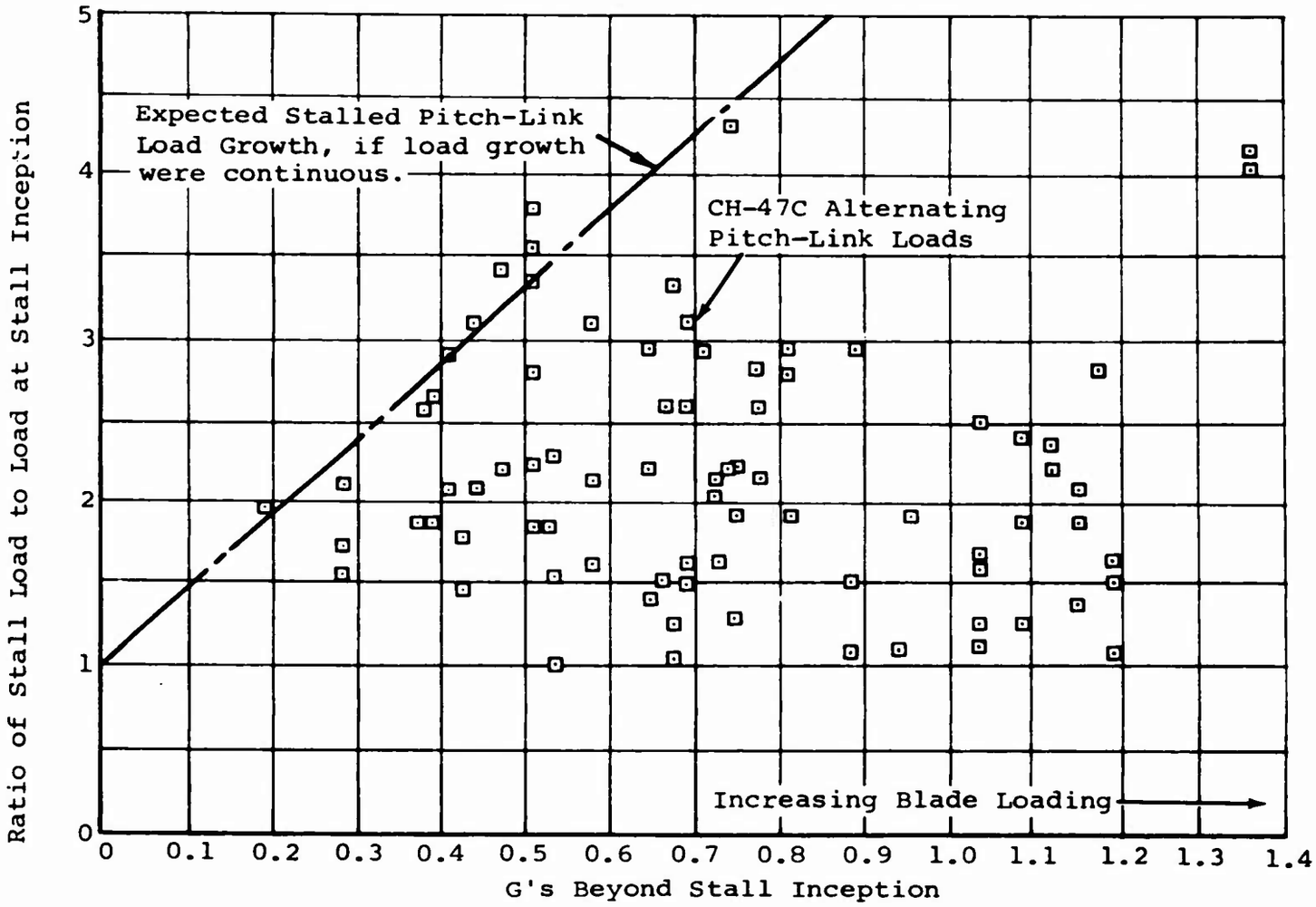

Figure 27. Pitch-Link Loads Do Not Continually Increase With Increasing Blade Loading.

load bump were not present, the low load growth rate associated with the substall condition would continue up to a blade loading of 0.11; and the basic control load trend with blade loading would be the same as the other blades.

As far as pitch-link loads are concerned, the 4/rev blade is significantly better than the basic blade. Below a blade loading of 0.105, the basic blade has slightly lower loads. Beyond 0.105, the 4/rev load is consistently lower than the basic blade; and, at 0.11 blade loading, it has only 58 percent of the basic blade load.

The 3/rev blade has the same load trend with blade loading as the other blades. The unstalled load region extends to a blade loading of 0.115. Stall inception does not occur until approximately 0.117. There is no doubt that the 3/rev blade has the lowest stall loads and is clearly the best blade for blade loadings beyond 0.10.

A review of the 125-knot results shows that:

1) The 3/rev blade provides the lowest stall-induced pitch-link loads.

2) The 4/rev blade stall-induced loads are approximately the same as the 3/rev blade load.

3) The 7/rev blade has the largest stall loads.

4) Stall inception occurs at a lower blade loading as blade frequency is increased (see table below).

Torsional Frequency	Stall Inception Blade Loading	Blade Loading Reduction Compared to 3/Rev Blade
3/rev	0.117	
4/rev	0.113	0.004
5.2/rev	0.103	0.014
7/rev	0.095	0.022

5) There is a good correlation between the blade loading reduction at stall inception (see right-hand column of table above) and the blade loading reduction at 2500 pounds (see right-hand column of table below). This indicates that earlier stall inception results in reduced blade loading capability.

Torsional Frequency	Pitch-Link Load	Blade Loading	Blade Loading Reduction
3/rev	2500	0.125	-
4/rev	2500	0.123	0.002
5.2/rev	2500	0.109	0.016
7/rev	2500	0.103	0.022

It is clear from these results that at 125 knots, the stall-induced pitch-link loads are lowest for blades with low torsional frequencies and largest for blades with high torsional frequencies.

CH-47C flight test data substantiates the conclusion that stall inception occurs at lower blade loadings as blade frequency is increased and that there is a load reversal at high blade loadings. Figure 28 shows the results of a CH-47C advanced-geometry blade flight test for aft rotor blades with a boron filament spar and a fiberglass spar, at an advance ratio of 0.2. The boron blade first torsional natural frequency is 6.53/rev and the fiberglass blade frequency is 5.45/rev. The boron blade stall inception occurred at a blade loading of 0.089, and the fiberglass blade inception occurs at 0.098. This represents a stall inception delay of 0.009 due to a reduction in torsional frequency from 6.53/rev to 5.45/rev. The single-rotor study results show a stall delay of 0.008 for reducing the torsional frequency from 7/rev to 5.2/rev, at an advance ratio of 0.3.

At 150 knots (see Figure 25) the basic blade experiences a load trend with blade loading similar to the 125-knot results but with some significant differences. There is an unstalled load region up to about 0.08, typified by a slow increase of pitch-link load with blade loading. Stall inception appears to occur around 0.103 with a rapid load increase. The load drops at a blade loading of 0.115, showing a load reversal as observed at 125 knots. In the region between 0.08 and 0.1, a different load trend is observed. The load increases gradually from 1500 pounds to 2000 pounds, but at a faster rate than the substall load growth. This load trend is similar to the 4/rev results at 125 knots, but an additional factor has been added. The pitch-link load waveform at 0.09, and especially at 0.10, shows all the signs of a stall-induced load waveform, but the loads do not grow rapidly with blade loading. It is probable that, at 150 knots with a different angle-of-attack distribution and reverse flow region, the stall-induced load trend is not the same as experienced at the lower speed flight conditions.

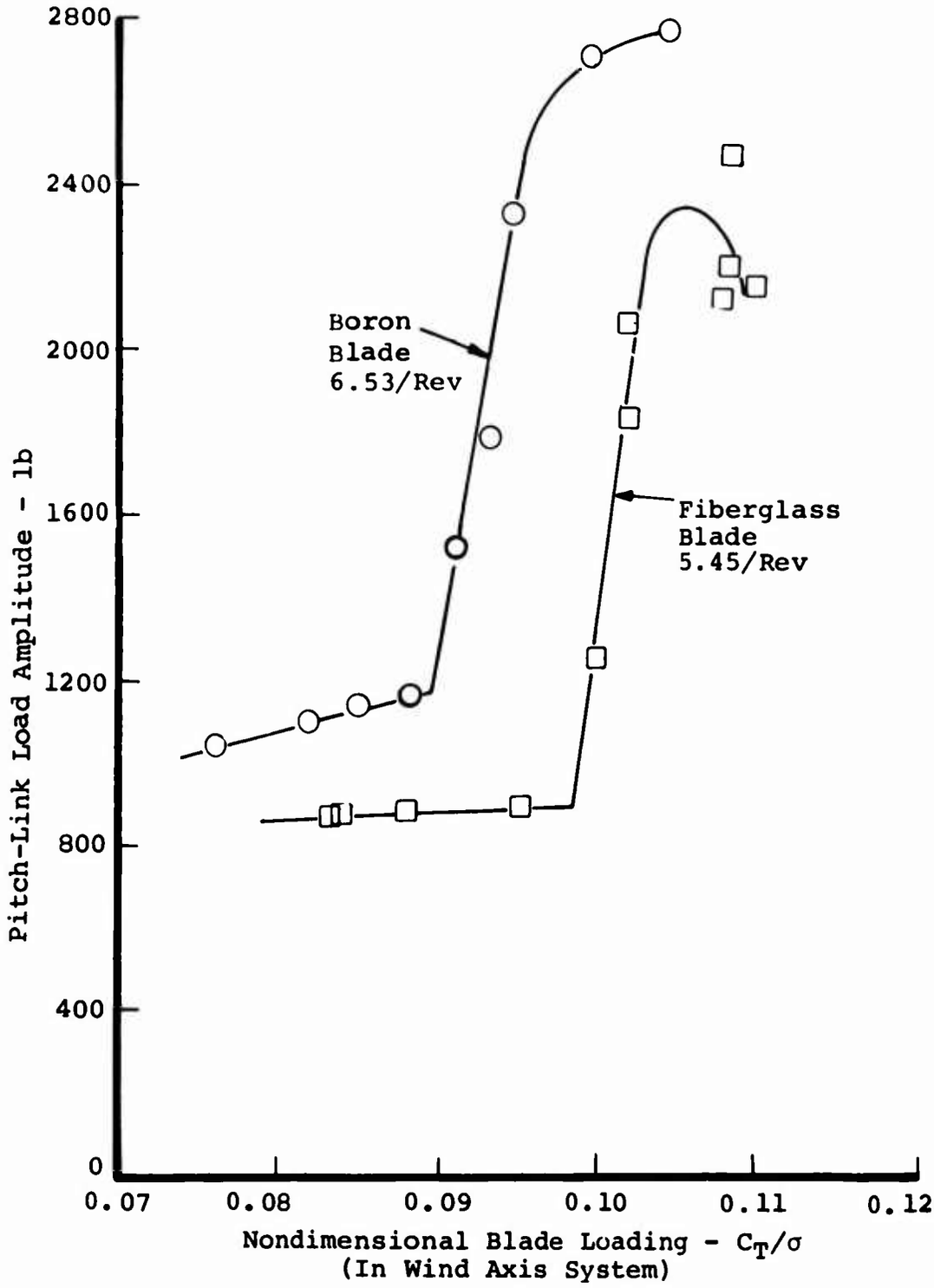

Figure 28. CH-47C Advanced-Geometry Blade Flight Test Data at an Advance Ratio of 0.2, V = 90 knots.

The 7/rev blade shows a similar load trend with blade loading as the basic blade, but with significantly larger stall loads. The unstalled loads occur up to 0.07. Stall inception occurs at approximately 0.075 with its typical rapid control load growth. The loads level out at 0.10, but then appear to reach a second stall inception near 0.105 and begin to grow at a very rapid rate. The strange load increase of the basic blade near 0.09 is very similar to the 7/rev first stall inception, in that both blades experienced load growth rates larger than for unstalled conditions and both experienced stall-induced pitch-link load waveforms.

The 4/rev blade appears to have no real stall inception. A typical unstalled load growth continues to about 0.09. A small load increase at 0.10, similar to the load bump at 125 knots for the same blade loading, is the only variation from a substall load growth rate. The load waveform shows the typical higher harmonics induced by stall, but they are relatively small and not typical of a fully stalled waveform (i.e., beyond stall inception). It is clear that this blade is behaving in a special way, since the load does not exceed 2100 pounds all the way up to a blade loading of 0.115.

The 3/rev blade shows a significantly different trend than it did at 125 knots. Up to a blade loading of 0.10, the loads appear reasonable, but beyond this the load grows at an extremely rapid rate. In fact, at a blade loading of 0.115, the blade is apparently unstable, since the loads have grown so large that the blade would probably fail. The 3/rev blade is experiencing an additional problem which is not apparent by simply observing the load trend. For all the load conditions calculated at 150 knots, the required power exceeds the available power. Apparently the blade is experiencing so much live twist that there is a significant increase in rotor drag. The other blades, by contrast, exceed the available power only at a blade loading of 0.115. (Note: none of the blades exceeded the available power at the 125-knot flight condition.) It is therefore obvious that the 3/rev blade is not an acceptable configuration for the 150-knot flight condition.

Summarizing the 150-knot results, it can be concluded that:

1) The 4/rev blade provides the lowest stall-induced loads.

2) The 3/rev blade is not a plausible configuration for the 150-knot flight environment.

3) The 7/rev blade has the largest loads of the three remaining blades.

4) The stall inception is no longer clearly defined, and the load trends are significantly different from the 125-knot results.

5) There is again excellent correlation between general stall load level and the blade loading at which a pitch-link load of 2500 pounds is reached, as shown below:

Torsional Frequency	Pitch-Link Load	Blade Loading	Sequence of Stall Inception
4/rev	2500	0.124	4
5.2/rev	2500	0.1075	3
3/rev	2500	0.105	2
7/rev	2500	0.091	1

However, this does not show the 3/rev blade power limitation.

At 175 knots (see Figure 26) the basic blade load trend with blade loading is different from the trends for the previous airspeeds. Unstalled loads continue to a blade loading of 0.07, and stall inception occurs at about 0.075. The stalled load increases with the typically large growth rate up to 0.09; beyond this point, the load does not reverse as for previous airspeeds, but continues to increase at about one-half the load growth rate. The blade loading at stall inception shows a significant reduction with airspeed, dropping from 0.103 at 125 knots to 0.075 at 175 knots. This reduction reflects the increased angle of attack (and hence earlier stall) required to fly at larger advance ratios.

The 7/rev blade load trend at 175 knots is almost identical with the basic blade trend up to 0.09. This blade shows the load reversal typical of the lower airspeed, but then resumes the load increase at the typical stalled load growth rate. There is little to choose from between the basic blade and the 7/rev blade. Though the 7/rev blade has a load reversal at 0.1, its load growth with blade loading resumes at about twice the rate of the basic blade. The 7/rev blade also shows a significant reduction in blade loading at stall inception for increasing airspeed. At 125 knots, stall inception occurred at 0.095; at 150 knots, the value is 0.075; and at 175 knots, the value is around 0.065.

The 4/rev blade has a typical substall load growth up to 0.07 and generally follows the load trend of the 7/rev blade and the basic blade up to 0.08. Beyond this point the load growth rate drops dramatically; and at a blade loading of 0.09, the pitch-link load is 1000 pounds below the other two blades. However, beyond this point the load growth rate increases sharply; and, at 0.01 and beyond, the load is the largest, except for the 3/rev blade.

The 3/rev blade is not a serious consideration at this airspeed. The loads are 1500 pounds beyond any of the other blades, and an instability is apparent at 0.09. The large live twist must be leading to these extreme load problems. This comment is not meant to condemn all torsionally soft rotors at high-speed flight. A system like Kamans, which controls the live twist from near the tip with aero tabs, may survive in this environment.

Summarizing the 175-knot results, it can be concluded that:

1) The 3/rev blade as configured here is not practicable for the 175-knot environment.

2) None of the three remaining blades has a clear advantage at this airspeed. A reduced load at one blade loading is cancelled by a large load growth in another region.

3) The stall inception blade loading decreases significantly with increasing airspeed.

4) The three blades (excluding the 3/rev blade) have a stall inception around a blade loading of 0.075.

5) There is reasonable correlation between the general stall load level and the blade loading at which a pitch-link load of 2500 pounds is reached as shown below:

Torsional Frequency	Pitch-Link Load	Blade Loading
4/rev	2500	0.091
7/rev	2500	0.083
5.2/rev	2500	0.082
3/rev	2500	0.069

This section shows that the 4/rev blade best meets the overall objective of reduced stall-induced pitch-link loads over the entire airspeed and blade loading range investigated.

-Pitch-Link Load Variation With First Torsional Natural Frequency

Plots of blade pitch-link load versus torsional natural frequency for a constant airspeed and blade loading are presented in Figures 29 through 31. Though the same analytical results are involved as in the previous section, these plots provide a much easier means for evaluating the effects of torsional frequency to confirm the previous conclusions.

Figure 29 shows the pitch-link load variation with torsional frequency for blade loadings from 0.08 to 0.12 for an airspeed of 125 knots. Below stall (blade loadings of 0.08 and 0.09), there is a slight load increase (less than 100 pounds) as the blade frequency is reduced from 7/rev to 4/rev. There is an additional 100-pound load increase as the frequency is further reduced to 3/rev. At a blade loading of 0.10, the 7/rev blade has the largest load, and the 4/rev blade has a 200-pound larger load than the other two blades. This 4/rev load corresponds to the load bump indicated in the previous section.

In stall at blade loadings of 0.11 and 0.115, there is a sharp load increase with increasing blade frequency. The 3/rev and 4/rev blades have the lowest loads (around 1700 pounds) with very little difference between them. The basic blade (with a torsional frequency of 5.2/rev) has a load of around 2500 pounds, and the 7/rev blade has a load of around 4200 pounds. In deep stall (a blade loading of 0.12), the loads are around 2200 pounds for all blades, with the 7/rev blade 450 pounds larger.

It is clear from this figure that the 3/rev and 4/rev blades have the lowest stall-induced pitch-link loads, and there is a very large stalled load increase (47 percent at 5.2/rev and 145 percent at 7/rev) with increasing torsional frequency.

The pitch-link load variation with torsional frequency for an airspeed of 150 knots is shown in Figure 30. Three distinct load trends with frequency appear at this airspeed. First, there is the typical unstalled load trend (at 0.06 and 0.07) with about a 150-pound load reduction obtained by increasing the torsional natural frequency from 4/rev to 7/rev. Next, there is a blade loading region of semi-stall (0.09 and 0.10), where the loads are about 700 pounds larger than the unstalled condition but, except for the 7/rev blade, do not have all the elements of full stall. In this region there is no significant trend with frequency, except for the 7/rev blade, which is about 500 pounds larger than the others. The third trend is for the full stall-induced loads, at blade loadings of 0.11

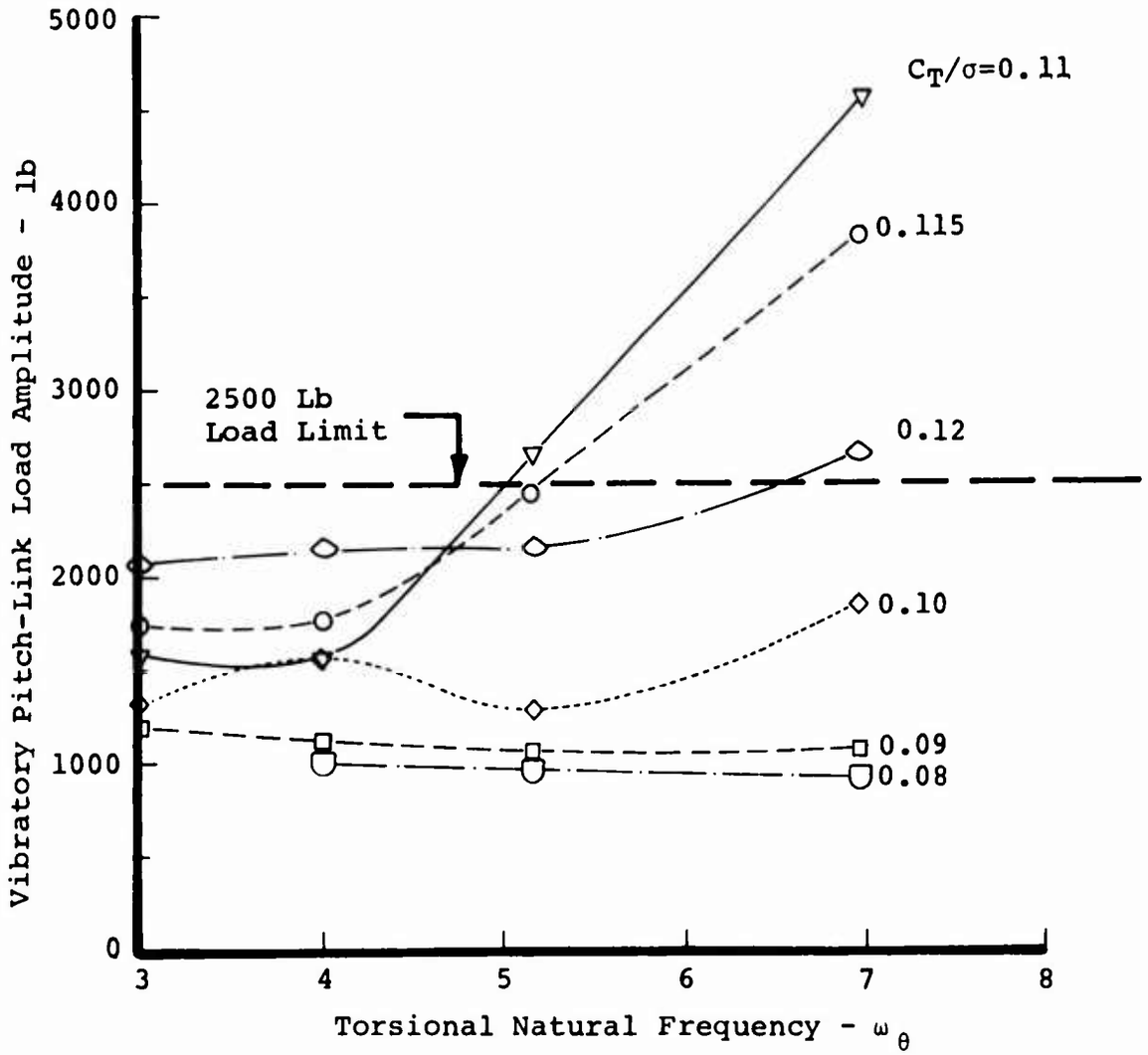

Figure 29. Variation of Pitch-Link Load Amplitude With Natural Frequency for 125 Knots, μ=0.289.

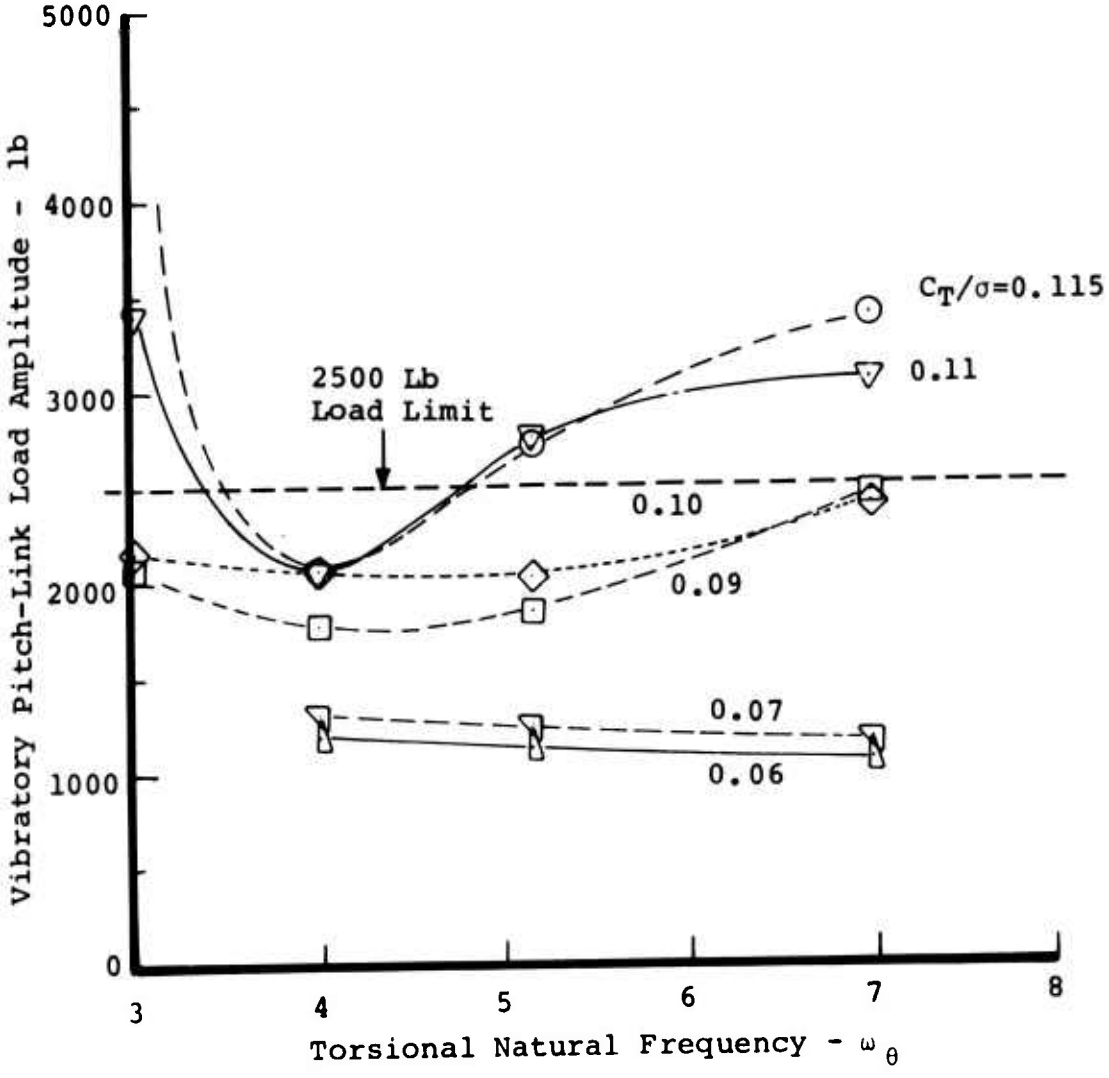

Figure 30. Variation of Pitch-Link Load Amplitude With Natural Frequency for 150 Knots, μ=0.344.

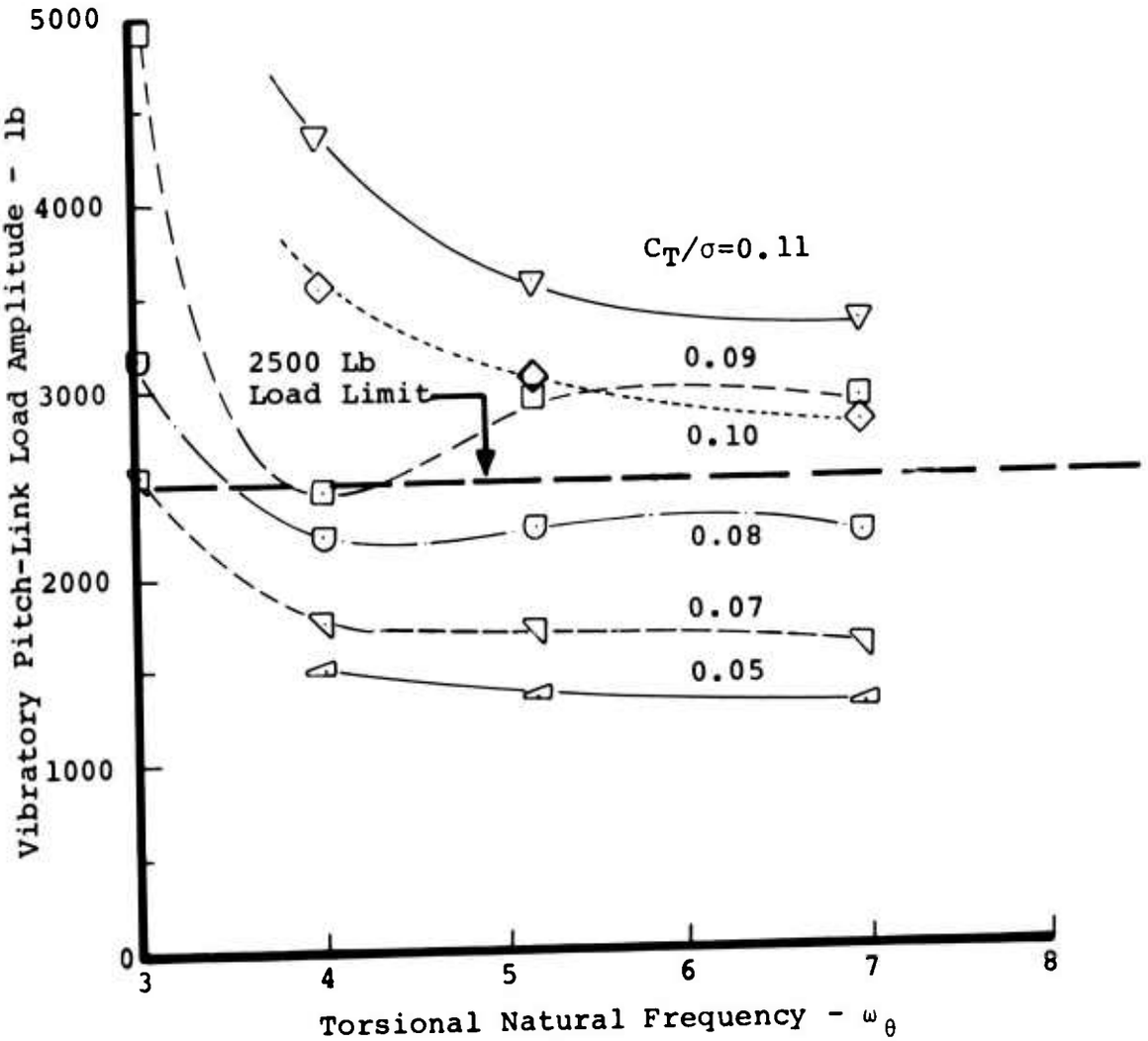

Figure 31. Variation of Pitch-Link Load Amplitude With Natural Frequency for 175 Knots, μ=0.397.

and 0.115. Here, the 3/rev blade's tendency toward instability is first observed. The instability is obvious at a blade loading of 0.115, where the calculated load exceeds 10 times the pitch-link endurance limit. The 4/rev blade has the lowest load at 2000 pounds. The 5.2/rev pitch-link load increases to 2750 pounds, while the 7/rev load is about 3200 pounds.

In summary, at 150 knots, the 4/rev blade has the lowest stall-induced pitch-link loads; the 3/rev blade is not practical at this airspeed; and again there is a stalled load growth with frequency (37 percent at 5.2/rev and 60 percent at 7/rev), but not as rapid as the 125-knot growth rate.

At an airspeed of 175 knots, there again are three distinct pitch-link load trends with torsional frequency, as shown in Figure 31. The first trend is the unstalled loads, which occur at blade loadings of 0.05 and 0.07 and show a load reduction of ?00 pounds by increasing the torsional frequency from 4/rev to 7/rev. A load increase of 800 pounds is obtained by reducing the torsional frequency from 4/rev to 3/rev at a 0.07 blade loading.

The second trend (obtained at 0.08 and 0.09) shows a large diverging load at 3/rev, a minimum load of about 2400 pounds at 4/rev, and an equal or increasing load at higher frequencies. At a blade loading of 0.08, the loads at 4/rev, 5.2/rev and 7/rev blades are within 100 pounds. However, at 0.09, the 5.2/rev and 7/rev blades are 500 pounds larger than the 4/rev blade.

In deep stall (0.10 and 0.11), the loads decrease with increasing frequency. The 3/rev blade is unstable; the 4/rev blade loads are about 4000 pounds; the 5.2/rev blade loads are about 3300 pounds (17 percent lower than the 4/rev); and the 7/rev blade loads are about 3200 pounds (20 percent lower). This is the only situation where increased stiffness results in a reduction of the stall-induced control load. However, these results must be viewed with caution, since the power limit is exceeded for all the blades in the deep stalled conditions. The reduced load trend for the higher frequency blade is still useful in the event that the available power is increased.

Overall, the 4/rev blade has the lowest stall-induced pitch-link loads. At 125 knots and 150 knots, the 4/rev blade clearly has the lowest stall loads. At 175 knots, for loads below the power limit, the 4/rev blade is equal to or better than the higher frequency blades.

-Pitch-Link Load Waveforms

Examination of the pitch-link load waveforms for the different frequency blades at various flight conditions will provide further understanding of the observed load trends. As a background for this discussion, three basic pitch-link load waveforms that have been obtained from CH-47C flight data will be

defined. The upper waveform in Figure 32 is a typical unstalled pitch-link load azimuthal variation. The waveform is predominantly 1/rev with some 2/rev. It exhibits a nosedown load around 90 degrees azimuth and a relatively level load from around 230 degrees to 0 degrees azimuth. The second waveform, in the middle of Figure 32, shows initial stall effects. There are stall-induced load spikes (i.e., high-frequency load variations) occurring on the retreating blade from approximately 250 degrees to 30 degrees azimuth. These spike loads do not determine the waveform peak-to-peak load and represent a transitional waveform between unstalled and the fully stall-induced high-frequency load. The bottom waveform illustrates the full stall-induced pitch-link load. For this waveform, the stall-induced spikes determine the blade peak-to-peak load.

At an airspeed of 125 knots, the four different frequency blades experience the first two waveform types (unstall and transitional stall), and all but the 3/rev blade experience the full stall waveform. The upper half of Figures 33 through 36 illustrate typical unstalled waveforms for the four blades. These unstalled waveforms correspond to the low pitch-link load regions at the low blade loadings. The lower half of these figures illustrate the full stall-induced waveform for the lowest blade loading with a full stall waveform.

The 3/rev blade, at a blade loading of 0.12, does not have a fully stalled waveform (see Figure 33). The 4/rev blade, at a blade loading of 0.12, just reaches a fully stalled waveform (see Figure 34) and, therefore, achieves a fully stalled waveform at a lower blade loading than the 3/rev blade. The basic blade (with a torsional natural frequency of 5.2/rev) has a fully developed stall waveform at 0.11 (see Figure 35), a full 0.01 earlier than the 4/rev blade. The 7/rev blade (see Figure 36) shows full stall at 0.10, which is 0.01 earlier than the basic blade. From these figures, it is clear that the stall-induced loads occur at lower blade loadings as the blade torsional frequency is increased.

Both the basic blade and the 7/rev blade experience a load reduction above a blade loading of 0.11. For both blades the pitch-link load waveform continues with the large stall-induced spikes, but the spike amplitude is reduced as the load reduction occurs.

Reviewing the stalled waveforms, it becomes apparent that the stall spike frequency is clearly increasing with increasing blade frequency. By measuring the azimuth region between adjacent stall spikes, a spike frequency may be determined. The table below shows the results of these measurements:

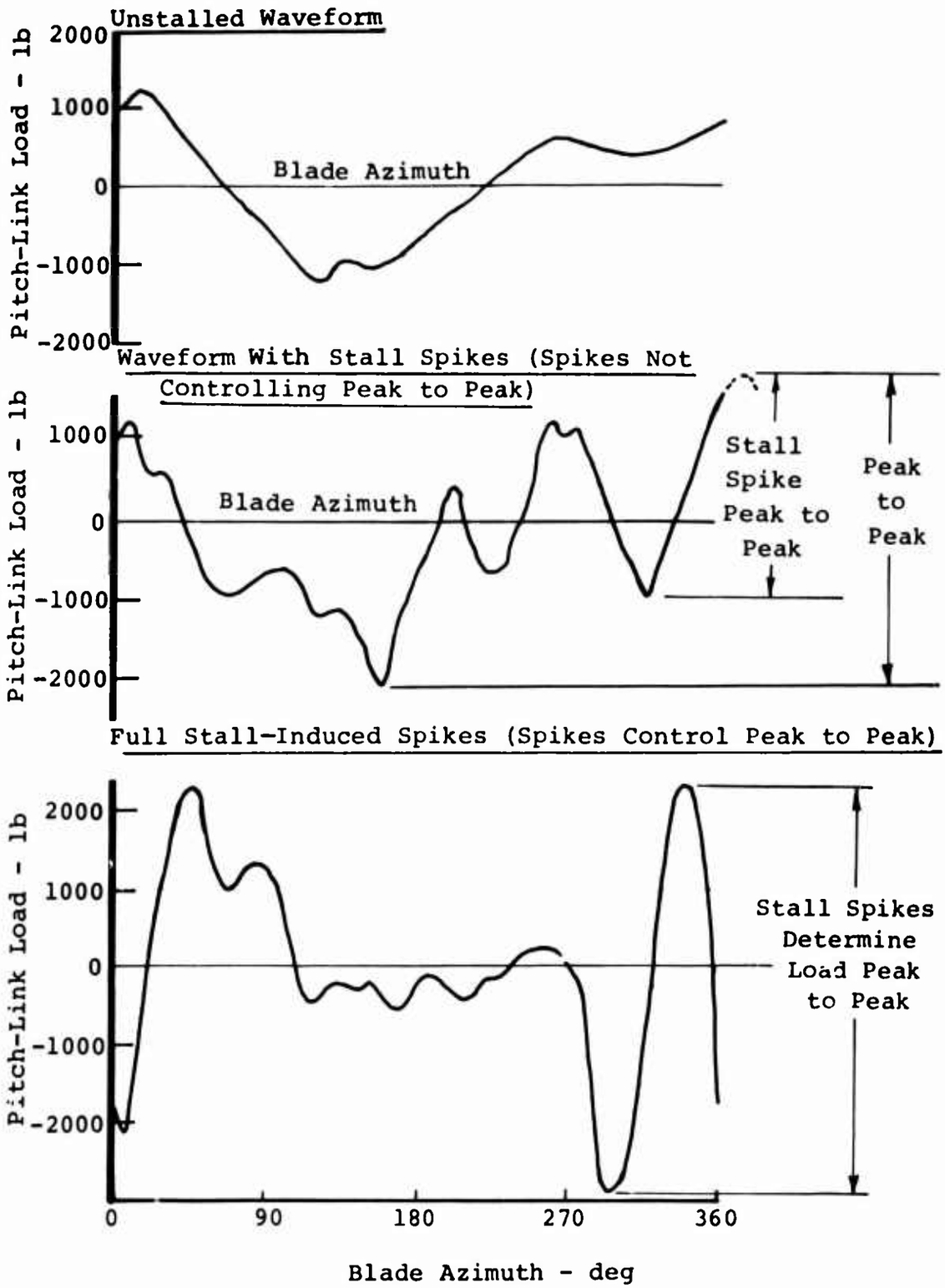

Figure 32. Typical CH-47C Waveforms.

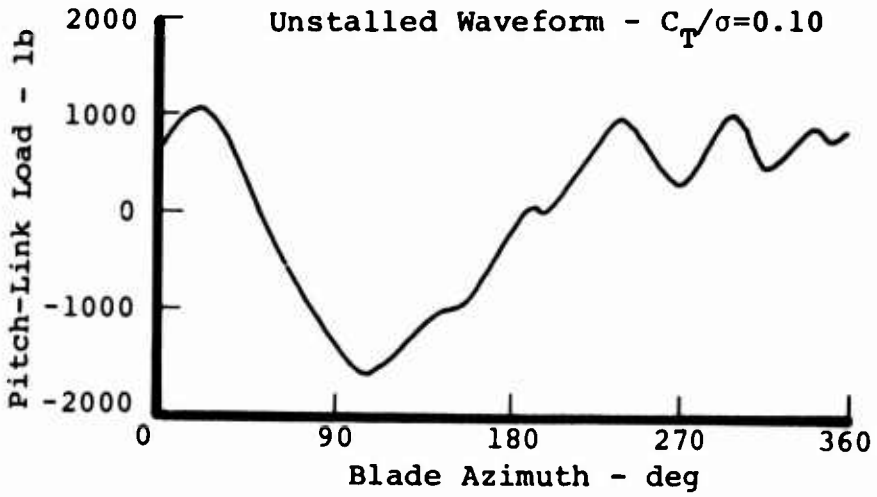

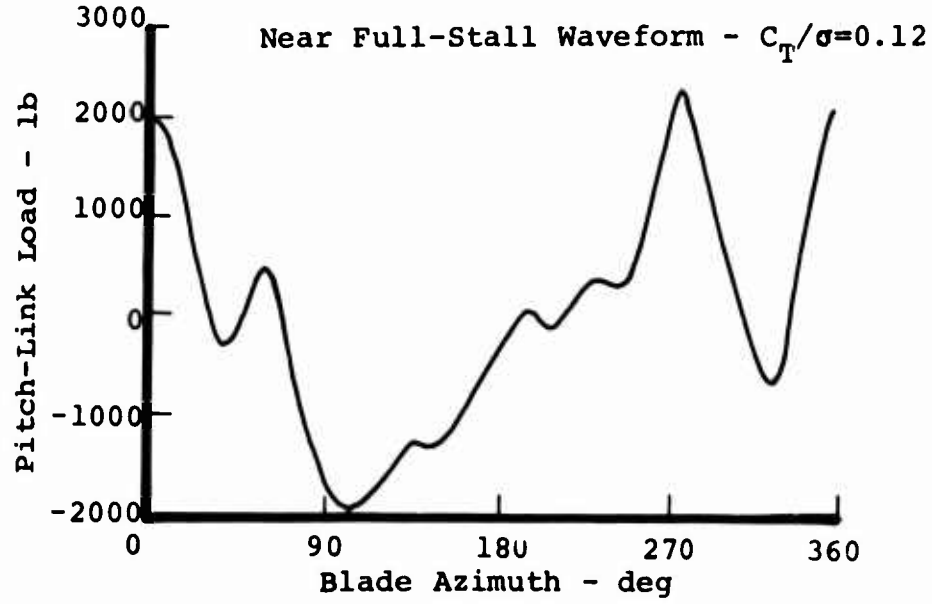

Figure 33. Typical Pitch-Link Load Waveforms for the 3/Rev Blade at 125 Knots, μ = 0.289.

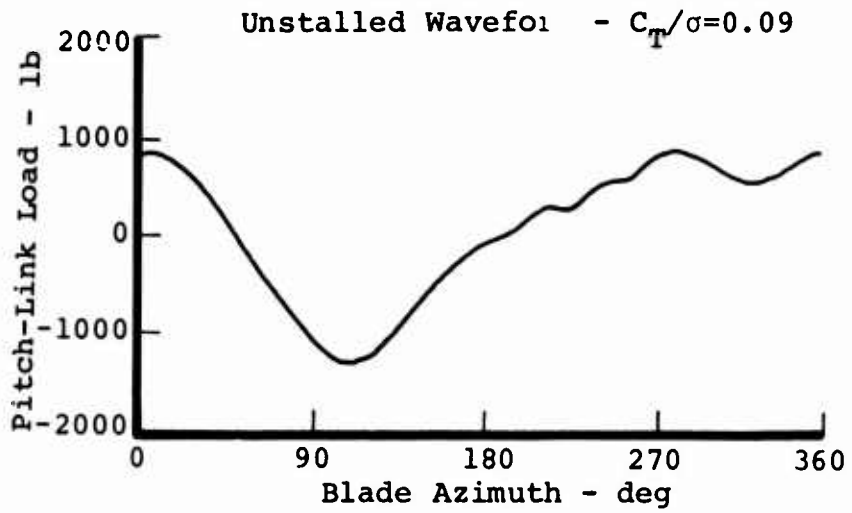

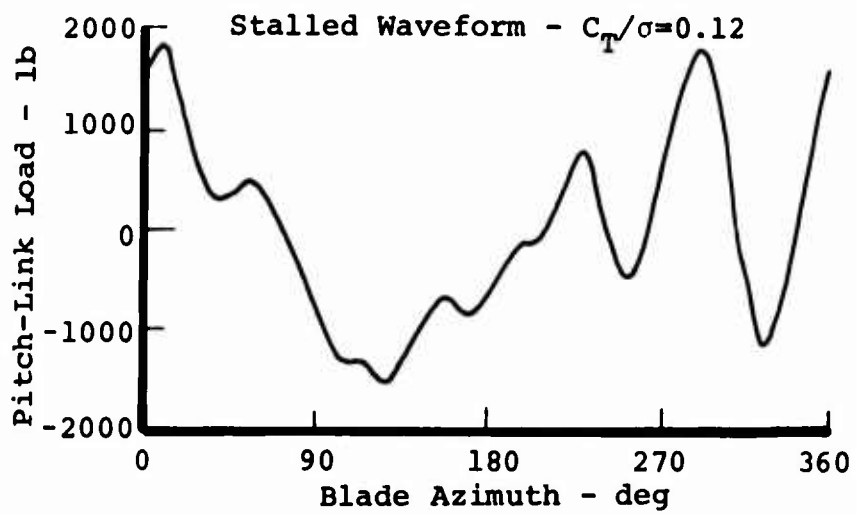

Figure 34. Typical Pitch-Link Load Waveforms for the 4/Rev Blade at 125 Knots, μ = 0.289.

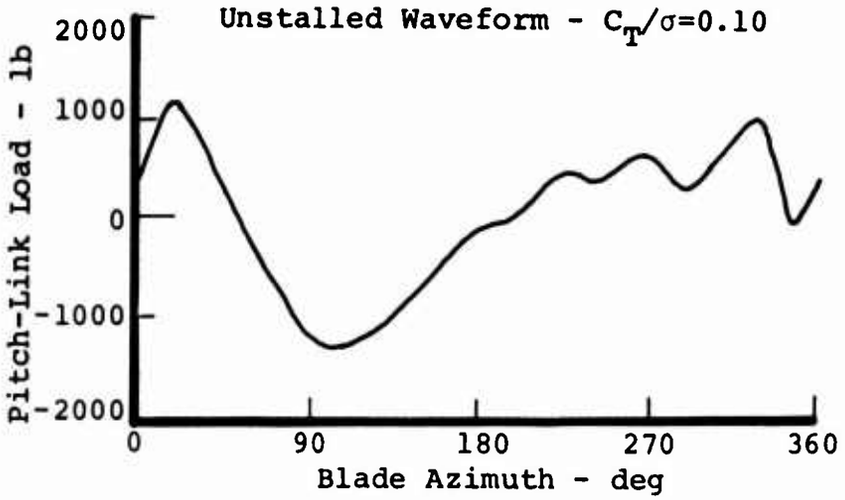

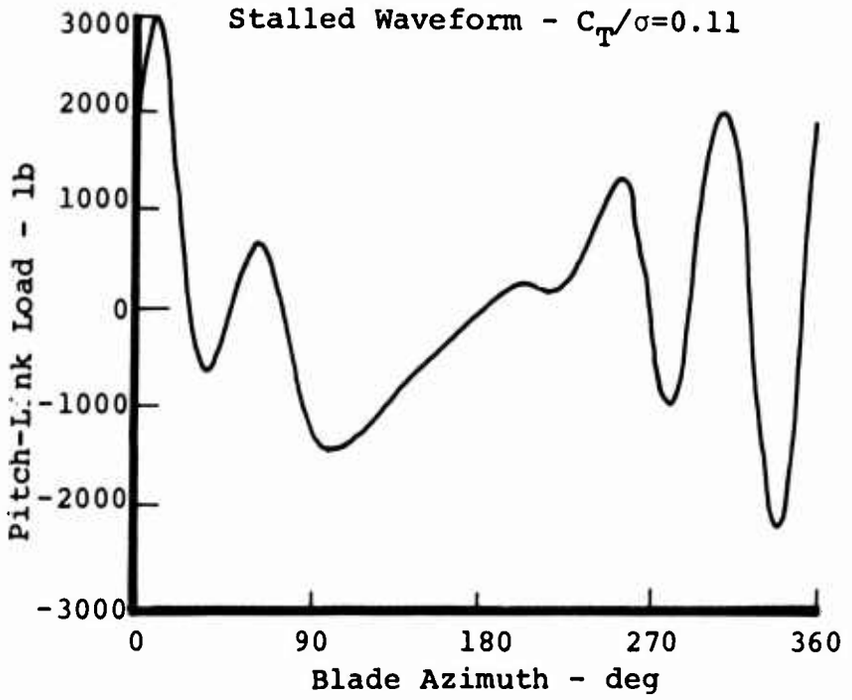

Figure 35. Typical Pitch-Link Load Waveforms for the 5.2/Rev Blade at 125 Knots, μ = 0.289.

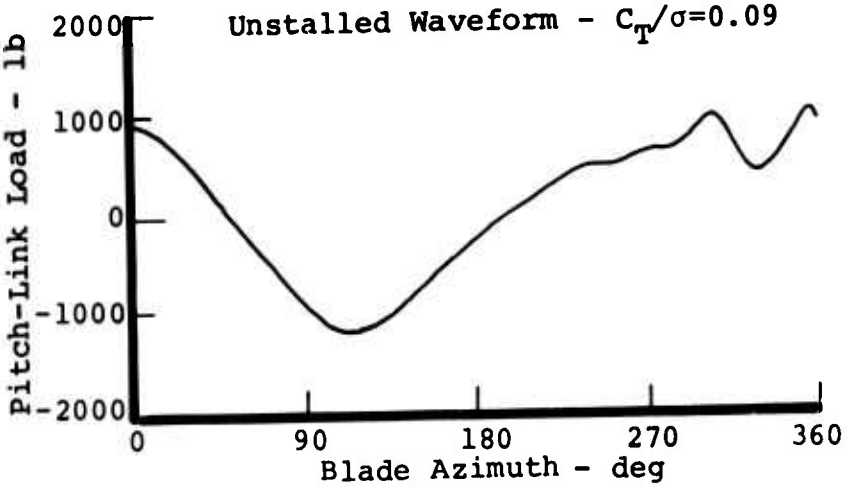

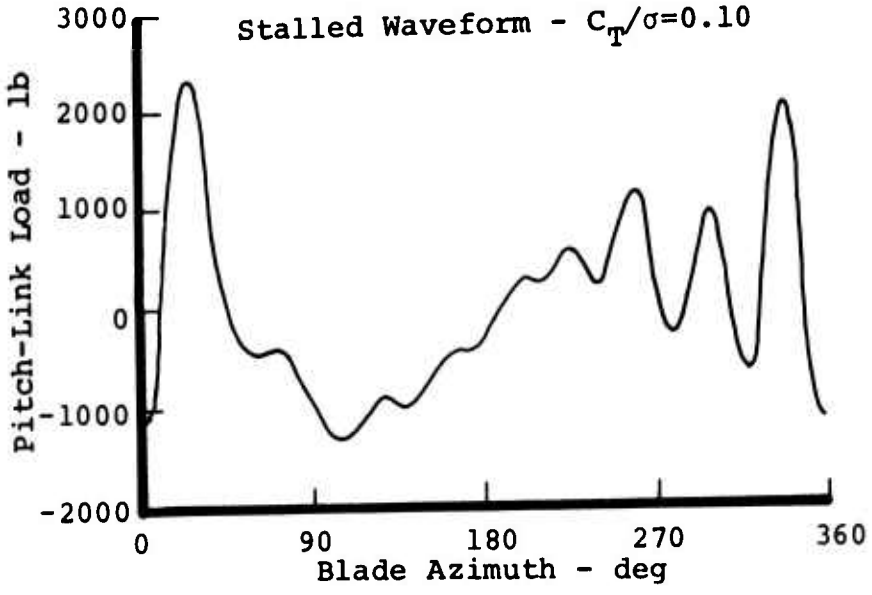

Figure 36. Typical Pitch-Link Load Waveforms for the 7/Rev Blade at 125 Knots, μ = 0.289.

Blade Frequency	Azimuth Between Spikes	Spike Frequency
3/rev	~83°	4.3/rev
4/rev	~72°	5.0/rev
5.2/rev	~58°	6.2/rev
7/rev	~45°	8.0/rev

This table shows that the stall spike frequency increases as the blade torsional frequency is increased. The spike frequency appears to be about 1/rev above the torsional natural frequency.

Figures 37 through 40 illustrate typical stalled waveforms for the four blades at airspeeds of 150 knots and 175 knots. A quick look through the figures shows a large variation in the stalled waveforms. The low-frequency blades show very little stall spikes for the retreating blade, but have a large compression load (airfoil nose down) for the advancing blade. The high-frequency blade pitch-link load continues to show the retreating blade stall spikes, but it also shows a large compression load for the advancing blade.

The 3/rev blade pitch-link load waveforms for 150 knots and 175 knots are given in Figure 37. These waveforms are at the largest blade loading for which a stable blade solution was obtained; increasing the blade loading by the next increment resulted in a divergent flight condition. This instability occurs at lower blade loadings as the airspeed is increased. The last stable data point at 150 knots is at a blade loading of 0.11, while the last point at 175 knots is at 0.08. As the figure shows, these pitch-link load waveforms do not have the large, stall-induced higher harmonic load spikes for the retreating blade. However, there is a large compression load for the advancing blade at 90 degrees blade azimuth. By examining the pitch-link load waveform for the unstable flight condition, it appears that the blade divergence involves a large advancing blade compression load that continually increases with each rotor revolution.

Figure 41 shows that the advancing blade compression load increases with airspeed. The upper figure shows the load waveforms for a blade loading of 0.11 at airspeeds of 125 knots and 150 knots. This 25-knot increase resulted in a 2000-pound compression load increase. The lower figure shows the effect of increasing airspeed by 50 knots at a low blade loading condition (0.09). As shown, the advancing blade compression load is increased by 2700 pounds at 175 knots even though the blade loading is reduced by 0.01. Therefore, the 3/rev blade is

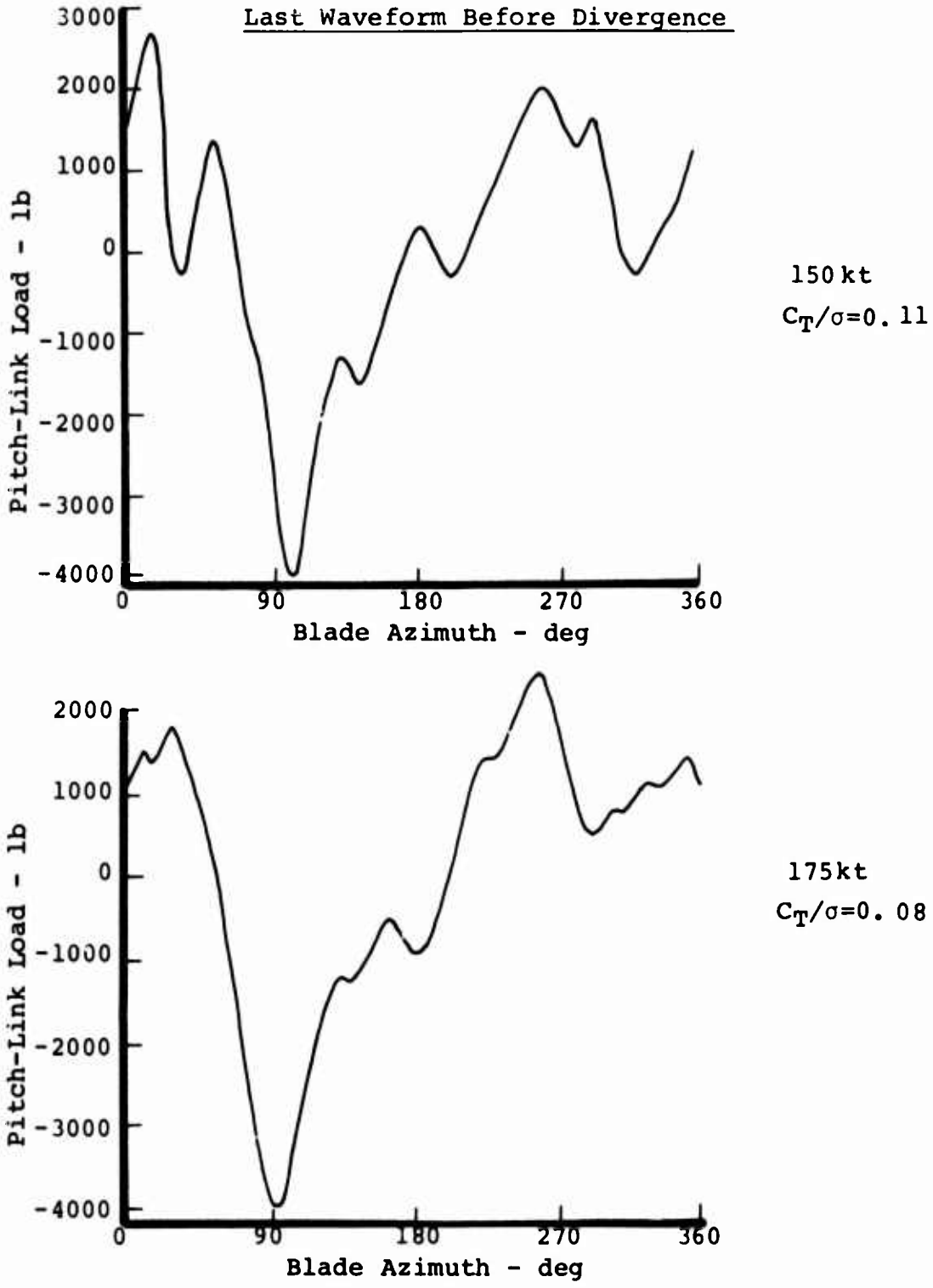

Figure 37. Typical Stalled Waveforms for the 3/Rev Blade at 150 and 175 Knots.

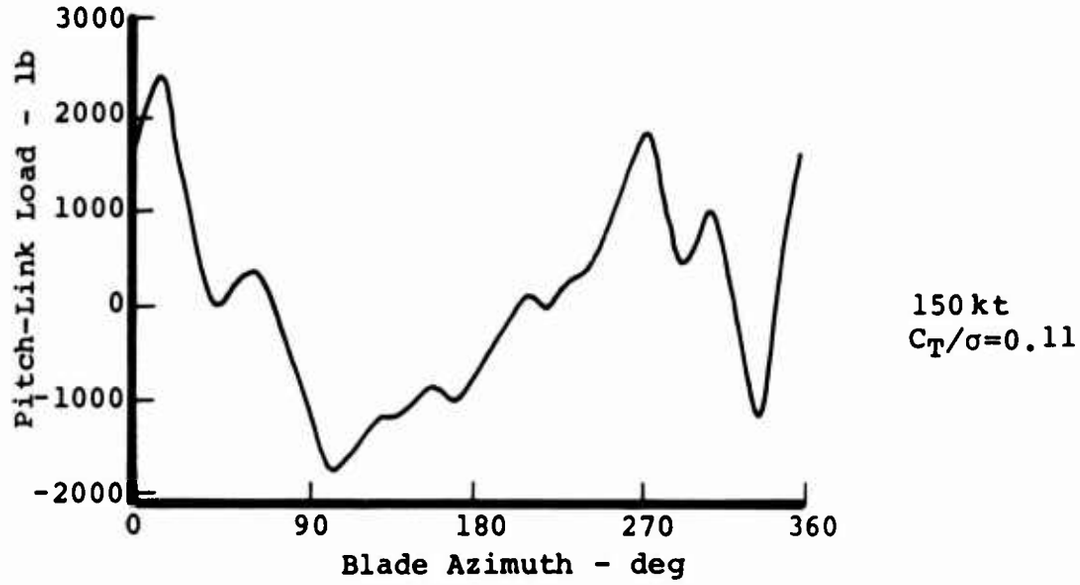

Figure 38. Typical Stalled Waveforms for the 4/Rev Blade at 150 and 175 Knots.

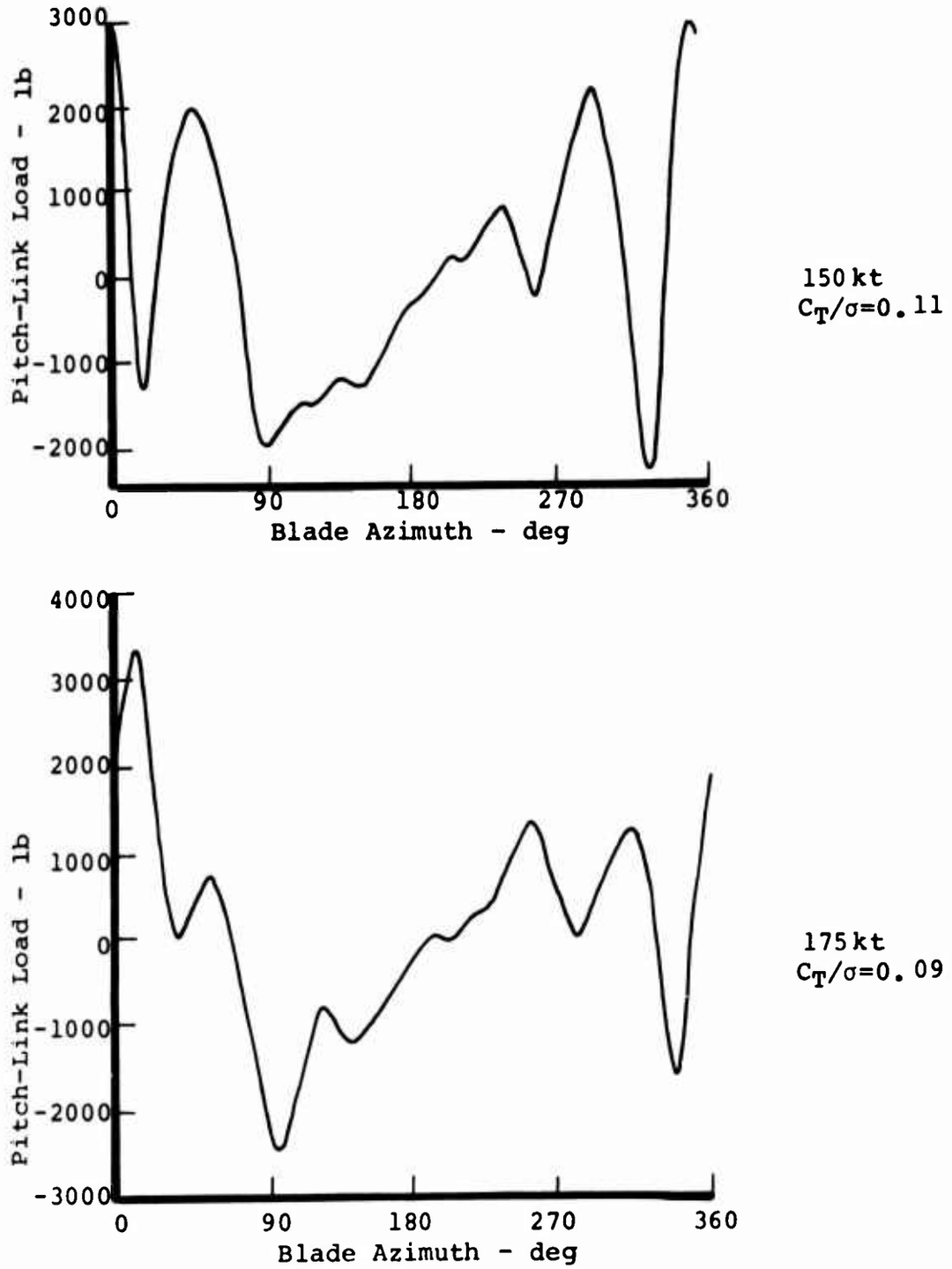

Figure 39. Typical Stalled Waveforms for the 5.2/Rev Blade at 150 and 175 Knots.

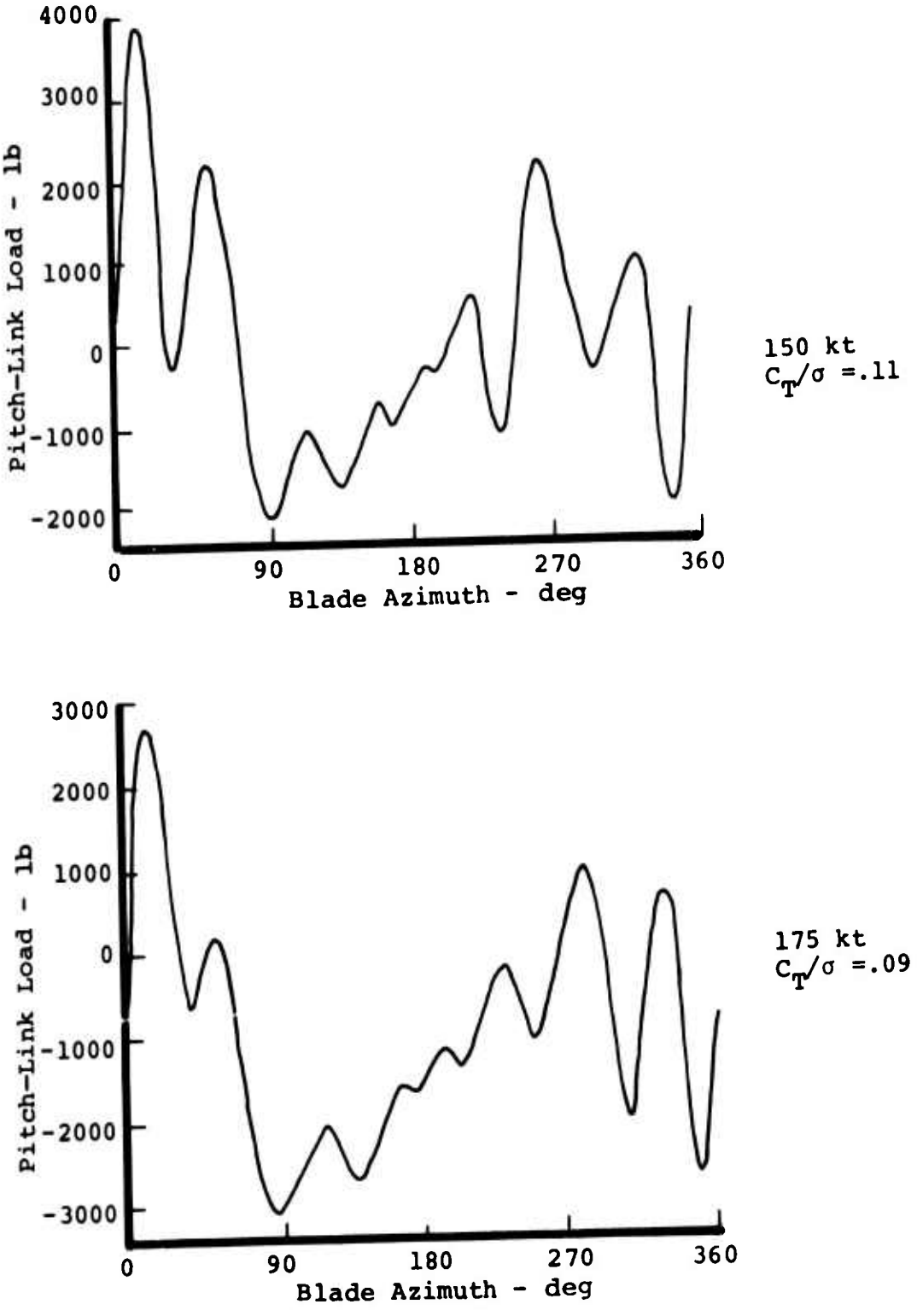

Figure 40. Typical Stalled Waveforms for the 7/Rev Blade at 150 and 175 Knots.

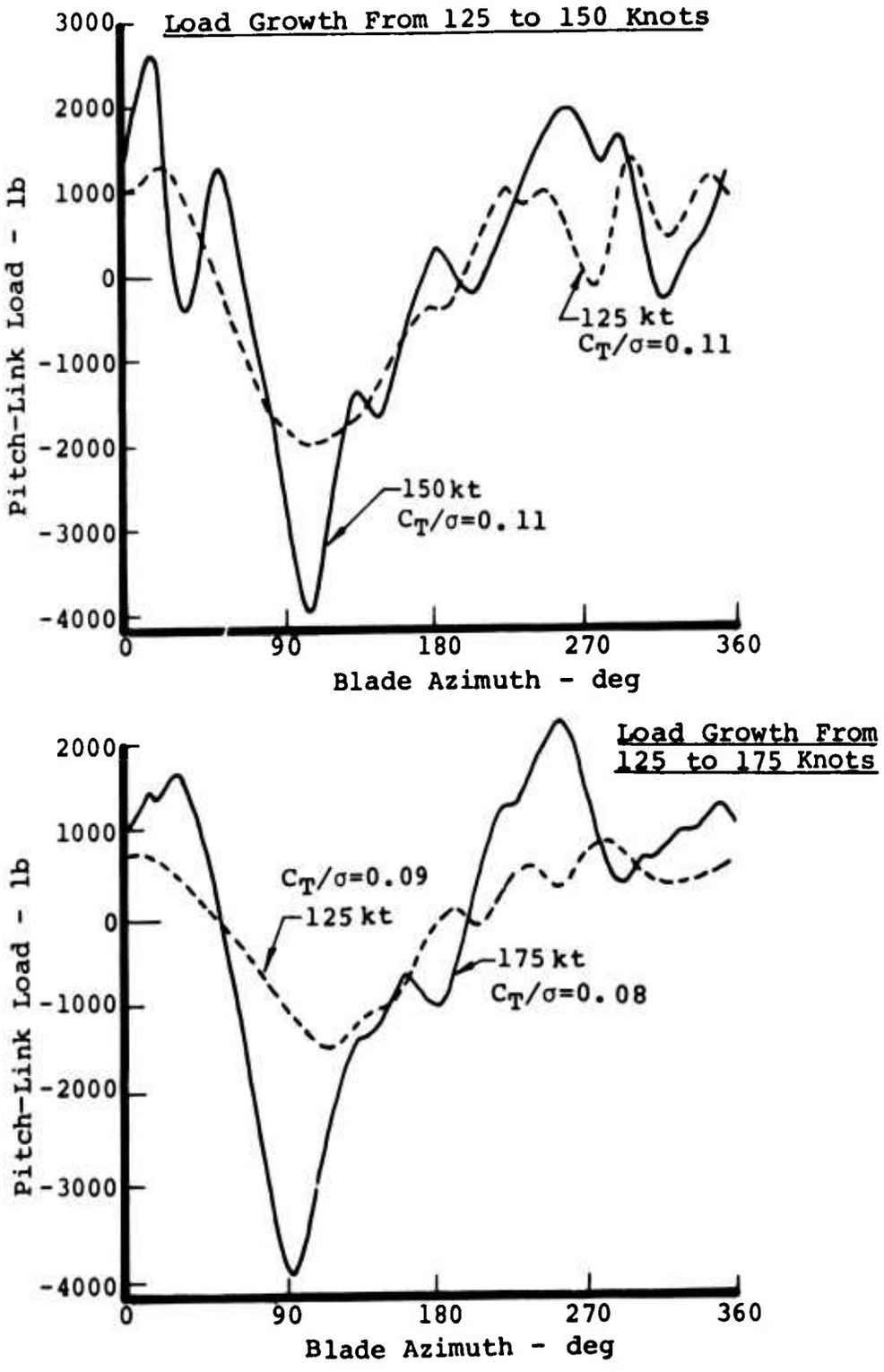

Figure 41. Advancing Blade Compression Load Increases With Airspeed for the 3/Rev Blade.

extremely limited by airspeed and is probably not a practical design for airspeeds much above 125 knots.

Figure 38 illustrates the typical stalled pitch-link load waveforms for the 4/rev blade at 150 knots and 175 knots. At 150 knots and a blade loading of 0.11, the load waveform is very similar to the 125-knot results with a large retreating blade stall spike that approximates the peak-to-peak load (compare with the waveform at the bottom of Figure 33). The upper half of Figure 42 compares the 125-knot and 150-knot waveforms at a lower blade loading (0.10), verifying that there is little change. At 175 knots, the pitch-link load waveform is very similar to the 3/rev blade; the retreating blade stall spikes are small, and the major feature of the waveform is an advancing blade compression load at 90 degrees of blade azimuth. The lower half of Figure 42 shows a 1000-pound compression load increase due to increasing the airspeed from 150 knots to 175 knots at a blade loading of 0.10. Figure 43 shows a 3500 pound compression load increase due to increasing the airspeed from 150 knots to 175 knots at a blade loading of 0.11. This indicates that the blade is experiencing an advancing blade load problem similar to the 3/rev blade, but at significantly higher airspeeds and blade loadings.

Typical stalled pitch-link load waveforms for the basic blade (torsional natural frequency of 5.2/rev) at airspeeds of 150 knots and 175 knots are given in Figure 39. At 150 knots the load waveform is very similar to a typical stall-induced waveform at 125 knots (see the upper half of Figure 44). There are large stall-induced spikes on the retreating blade that determine the peak-to-peak load. At 175 knots and a blade loading of 0.09 (see lower half of Figure 39), large retreating blade stall spikes are present but no longer control the peak-to-peak load, and a large advancing blade compression load is also observed. Comparing waveforms at 150 knots and 175 knots at a blade loading of 0.11 (lower half of Figure 44), a 2200-pound advancing blade compression load increase occurs at the 175-knot condition, along with a stall spike reduction. Therefore, the 5.2/rev blade also experiences an advancing blade load problem similar to the 3/rev blade, but the compression load for this blade is 1200 pounds smaller than the 4/rev blade at a blade loading of 0.11.

Figure 40 illustrates the typical stalled pitch-link load waveform for the 7/rev blade at 150 knots and 175 knots. Both the 150-knot and 175-knot waveform show the retreating blade stall spikes with some indication of an advancing blade compression load. Figure 45 compares waveforms between 125 knots and 150 knots (upper half of figure) and between 150 knots and 175 knots (lower half of figure) for a blade loading of 0.10. Both comparisons show large stall spikes and no essential change in the waveform's character. Figure 46 compares 150-knot

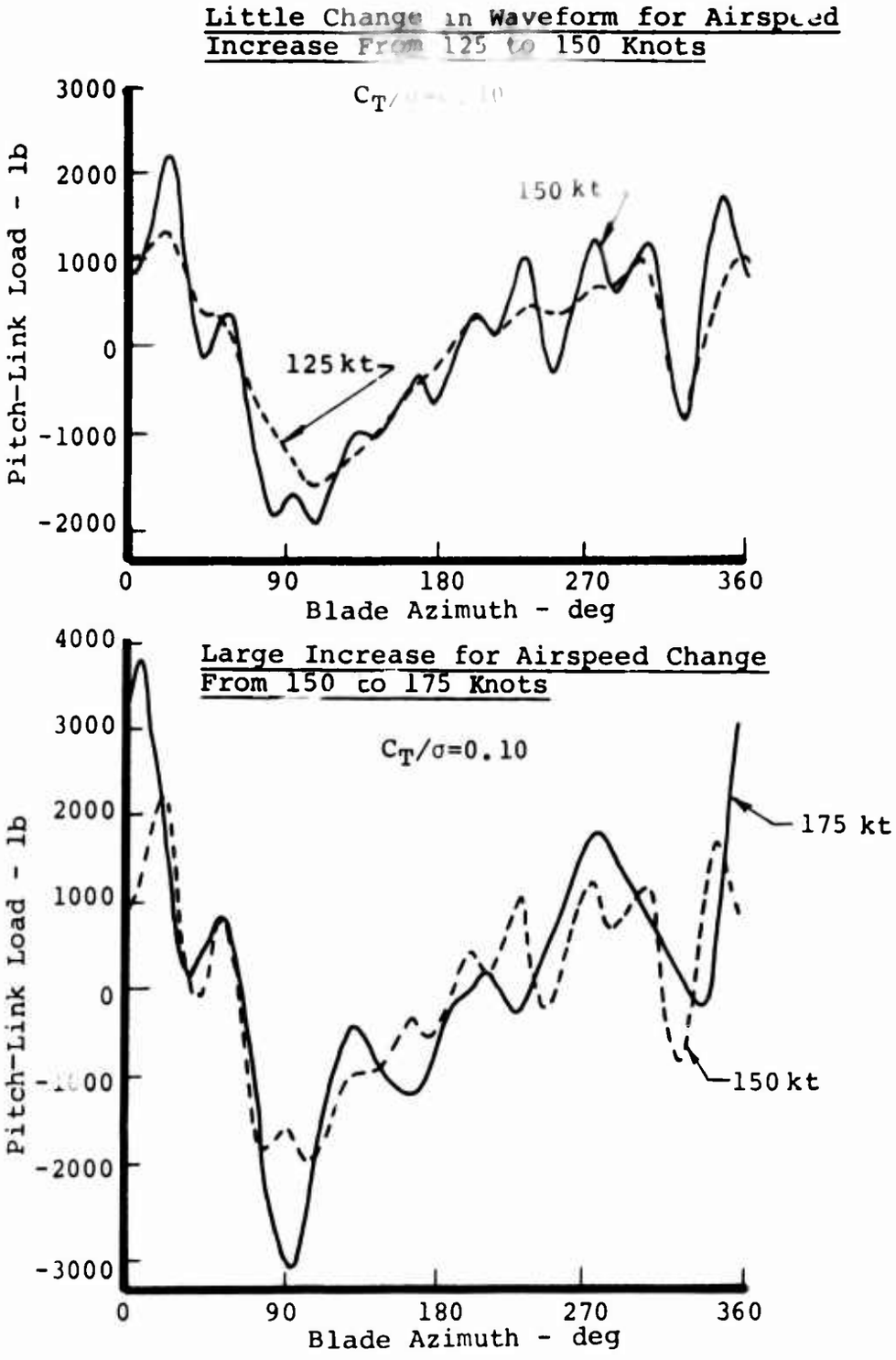

Figure 42. Waveform Changes With Airspeed for the 4/Rev Blade at a Blade Loading of 0.10.

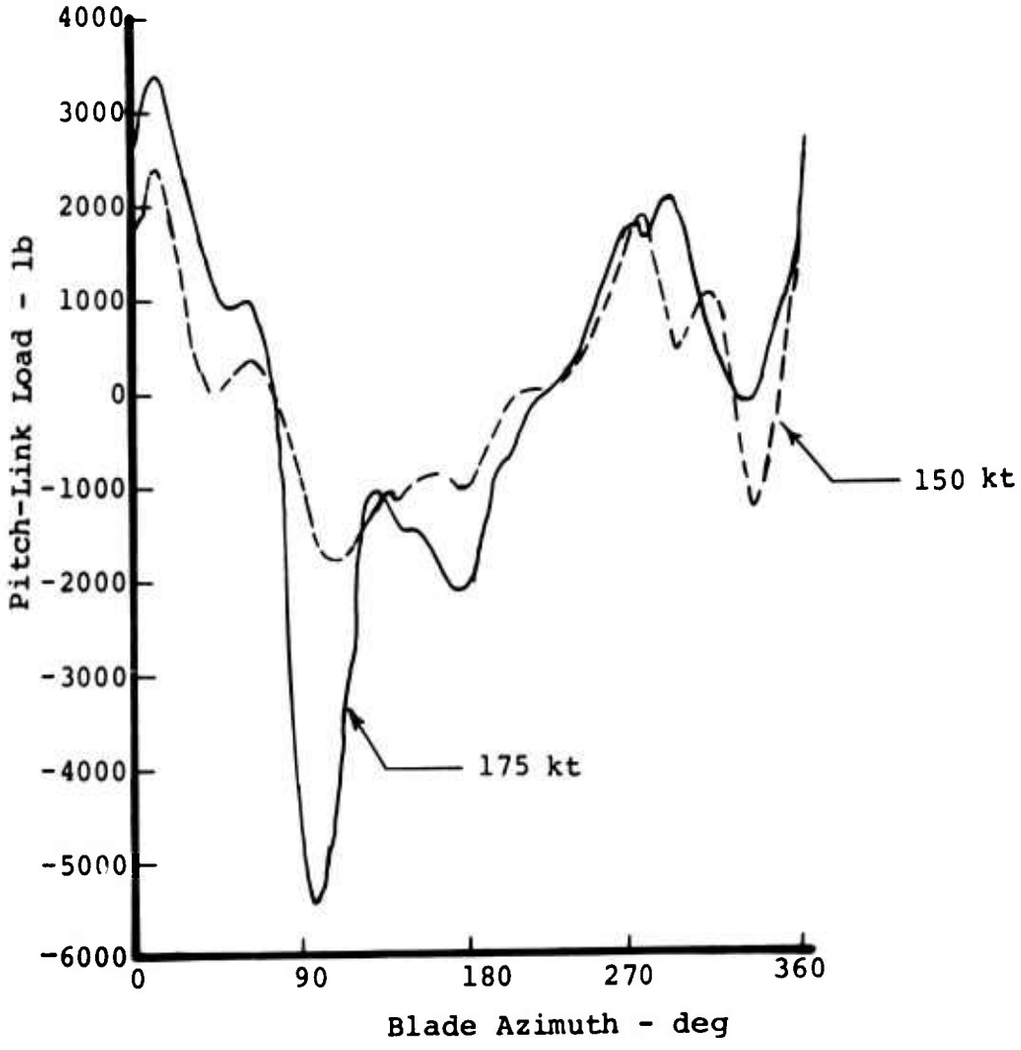

Figure 43. Waveform Change With Airspeed for the 4/Rev Blade at a Blade Loading of 0.11.

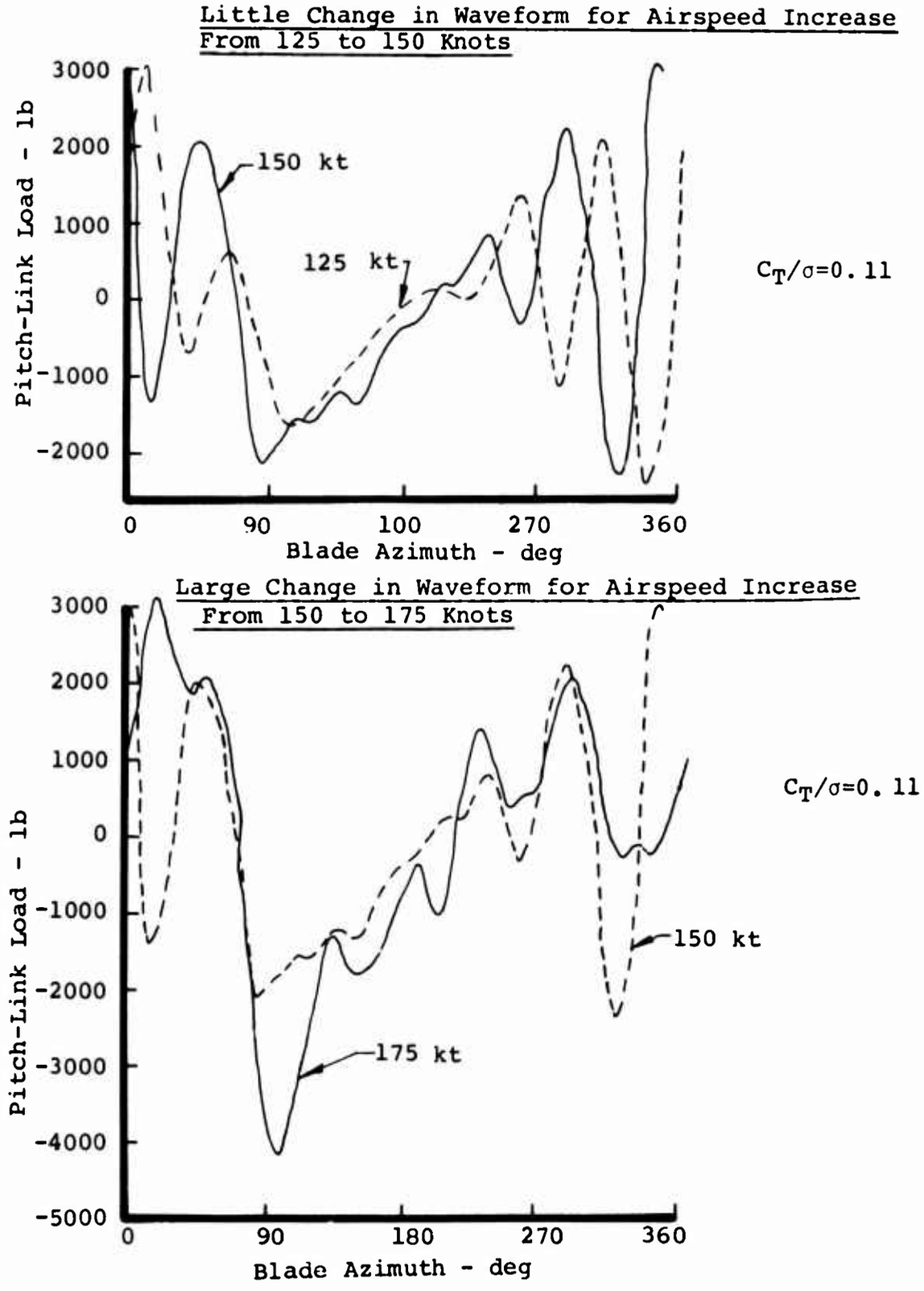

Figure 44. Waveform Change With Airspeed for the 5.2/Rev Blade.

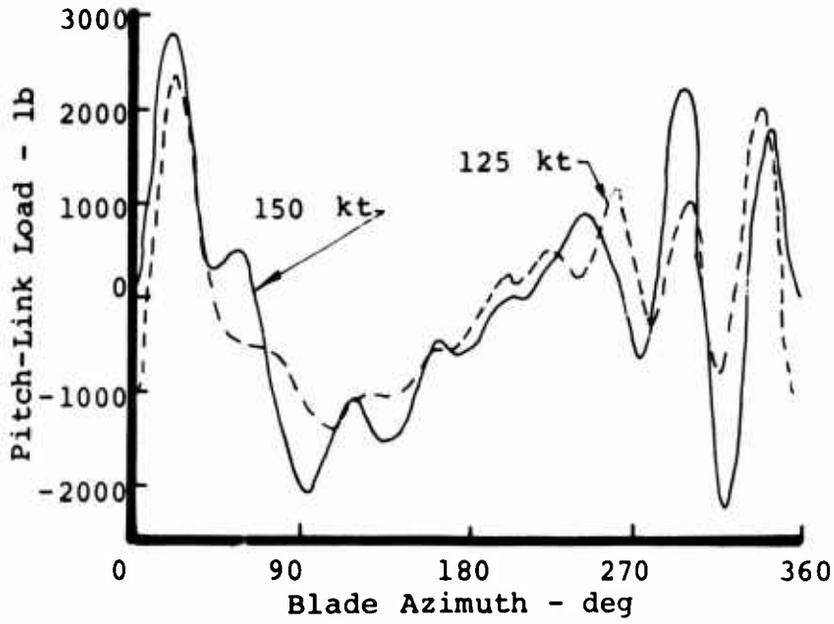

$C_T/\sigma=0.10$

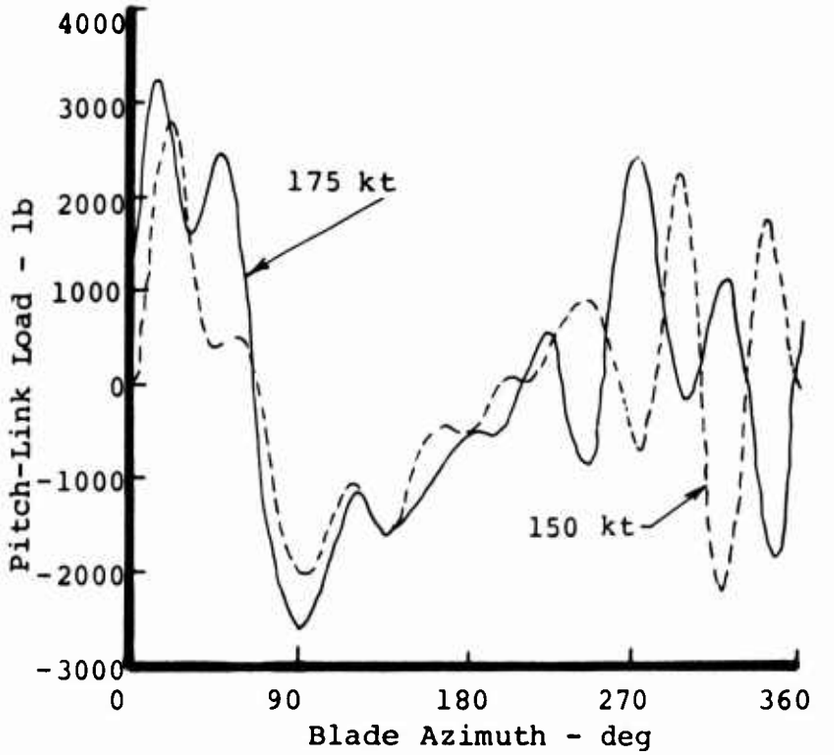

$C_T/\sigma=0.10$

Figure 45. Waveform Change With Airspeed for the 7/Rev Blade at a Blade Loading of 0.10.

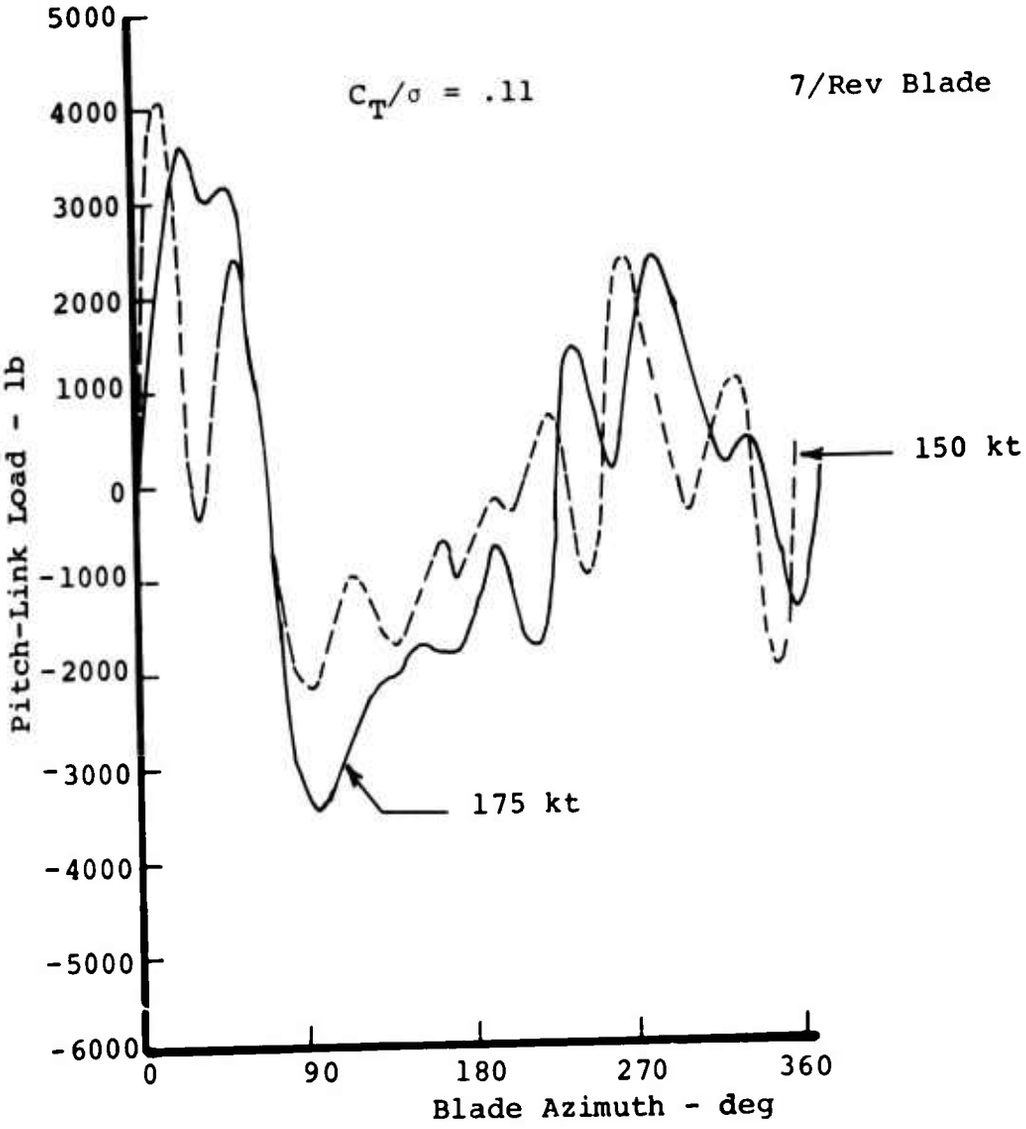

Figure 46. Waveform Change With Airspeed for the 7/Rev Blade at a Blade Loading of 0.11.

and 175-knot waveforms at a blade loading of 0.11, and shows a 1300-pound advancing blade compression load increase at 175 knots. This is 900 pounds less than the load increase experienced by the 5.2/rev blade at the same flight conditions.

In summary, the following conclusions can be made:

1) For airspeeds of 125 knots and 150 knots, large stall-induced retreating blade pitch-link load spikes cause a rapid load growth with increasing blade loading which can limit the aircraft flight envelope.

2) Stall inception occurs at lower blade loadings as the airspeed is increased (see Figure 47).

3) Stall inception occurs at lower blade loadings as the blade stiffness is increased at 125 knots and 150 knots (see Figure 48).

4) The 4/rev blade has the lowest stall loads for 125 knots and 150 knots, and a full-stall waveform with large retreating blade spikes does not develop until a blade loading of 0.11 or beyond.

5) The 3/rev blade does not develop a full-stall waveform with large retreating blade spikes within the flight envelope investigated, but it does become unstable at 150 knots and 175 knots.

6) The 3/rev blade instability results from a large advancing blade compression load. This load increases with airspeed and blade loading and becomes divergent at the following conditions:

Airspeed (knots)	Blade Loading (C_T/σ)
150	0.115
175	0.09

7) At 175 knots, all four blade pitch-link load waveforms show a significant increase of the advancing blade compression load.

8) The 7/rev blade has the lowest advancing blade load growth, as shown below:

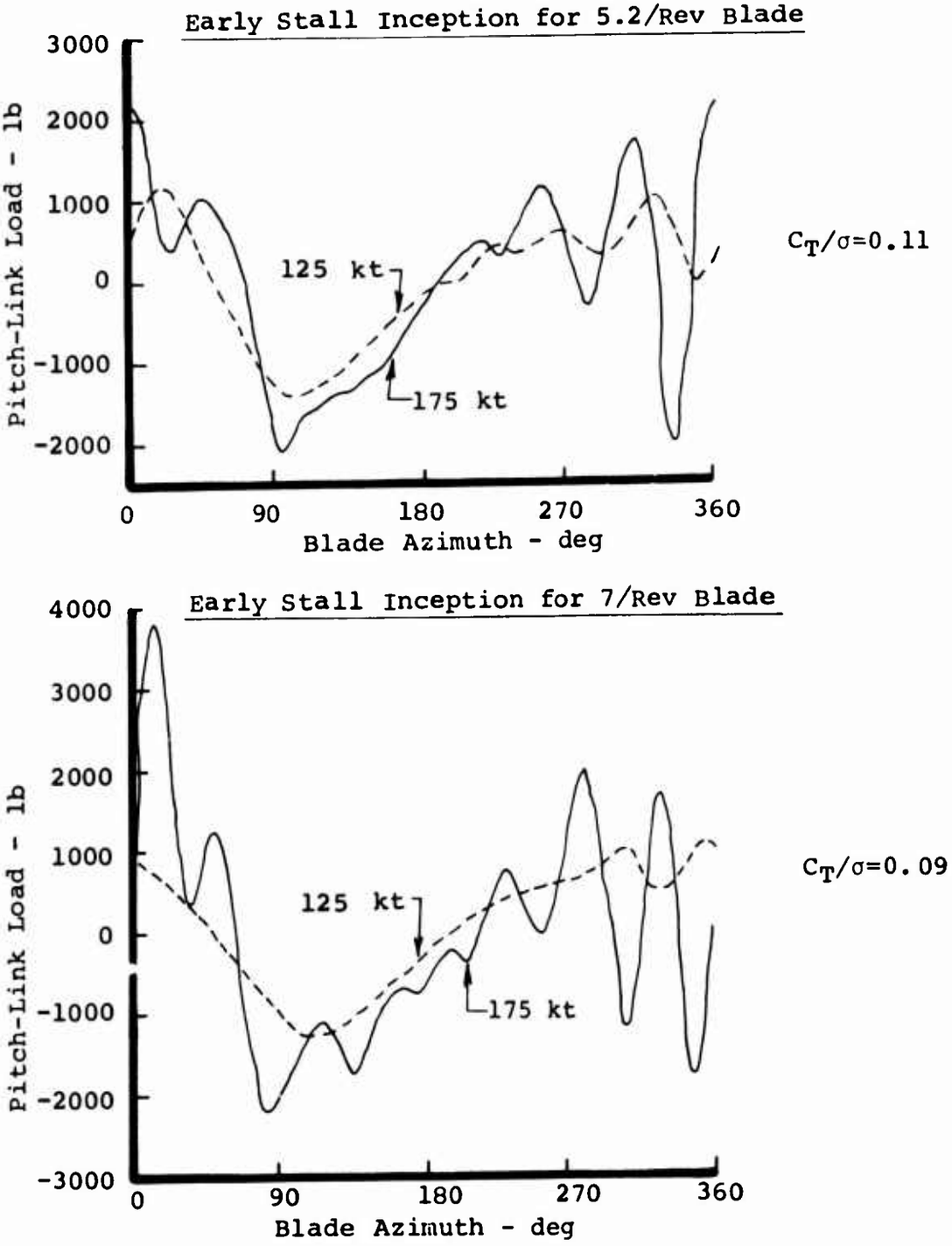

Figure 47. Stall Inception Occurs Earlier as Airspeed Increases.

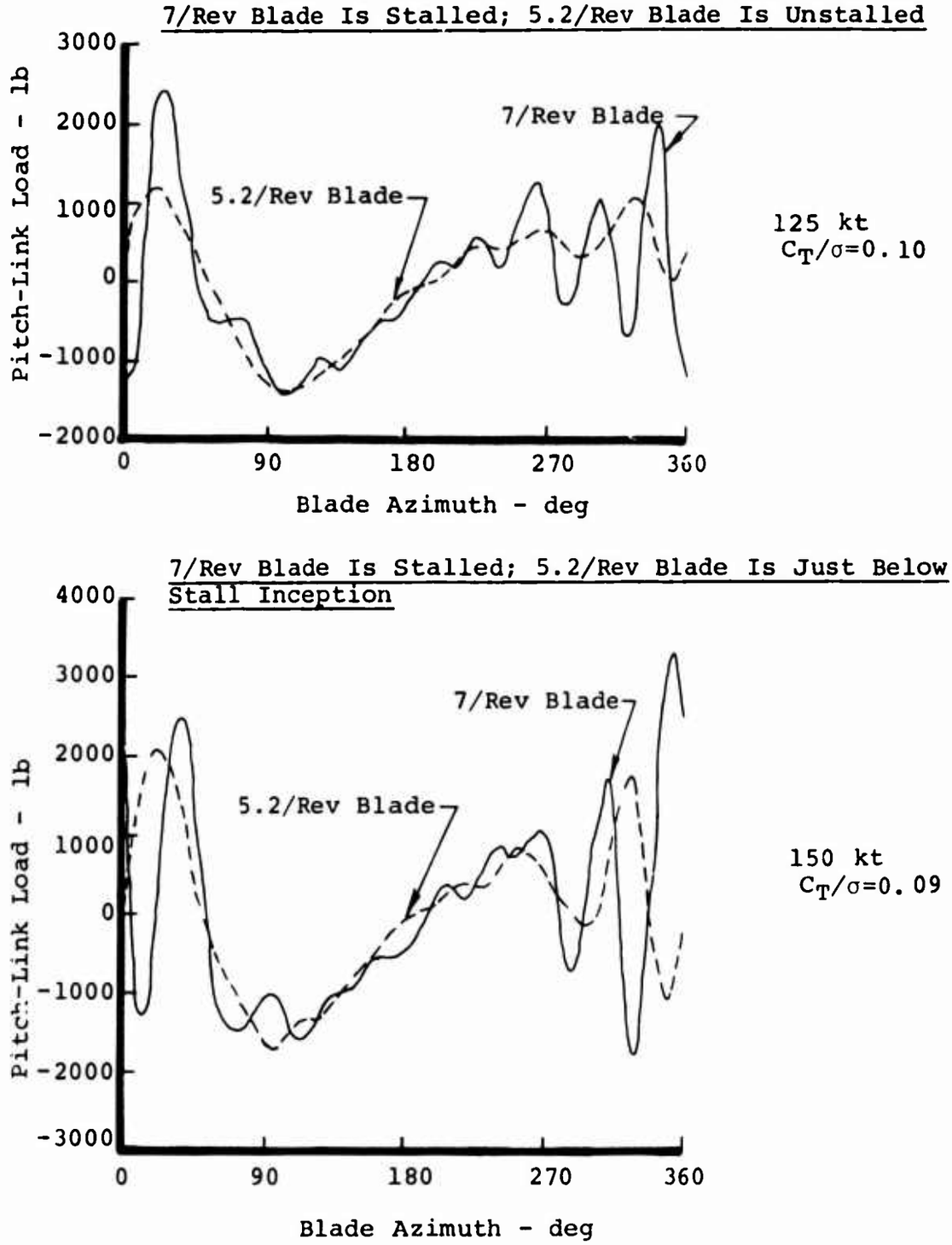

Figure 48. Stall Inception Occurs Earlier for the Stiffer Blades at 125 and 150 Knots.

Blade Frequency	Advancing Blade Load Increase From 150 to 175 Knots at $C_T/\sigma = 0.11$
7/rev	1300 pounds
5.2/rev	2200 pounds
4/rev	3500 pounds
3/rev	2700 pounds at $C_T/\sigma = 0.08$

The 4/rev blade is clearly superior for 125 knots and 150 knots, where large stall-induced spikes dominate the waveform. At 175 knots, a large advancing blade compression load begins to grow rapidly as blade loading increases. At this airspeed, the 7/rev blade has the lowest advancing blade load growth. However, for blade loadings of 0.09 and below, the 4/rev blade loads are about the same as the 5.2/rev and 7/rev blades. Therefore, considering the whole of the flight envelope investigated here, the 4/rev blade represents the best configuration, and the 7/rev blade appears to be the best above 175 knots.

--Effect of Blade Torsional Frequency on Rotor Performance

Throughout this report, the objective has been to determine the effect of blade torsional frequency on stall-induced pitch-link loads. However, for the pitch-link load results to have a practicable application, any secondary effects associated with torsional frequency change should be identified. The most significant secondary effect would be changes in rotor performance. This study hopes to lead to an expansion of the helicopter flight envelope by reducing the large stall pitch-link loads so that the aircraft will be power limited and not load limited. If, in the course of reducing the control loads, reductions in the performance envelope occur, it is possible that the gain from extending the load boundary could be cancelled by loss from shrinking the performance boundary.

Figures 49 through 51 show the variation of rotor power with blade loading at airspeeds of 125 knots, 150 knots, and 175 knots for the four blades studied. Generally, the rotor power increases with blade loading and airspeed for all blade frequencies. The 7/rev blade has the lowest rotor power, with the 5.2/rev blade slightly higher. The 4/rev blade power is even higher, with the difference between this blade and the 5.2/rev blade about twice as large as the difference between the 7/rev and 5.2/rev blades. In addition, the power difference between the 7/rev and 4/rev blade continually increases with airspeed, as shown below:

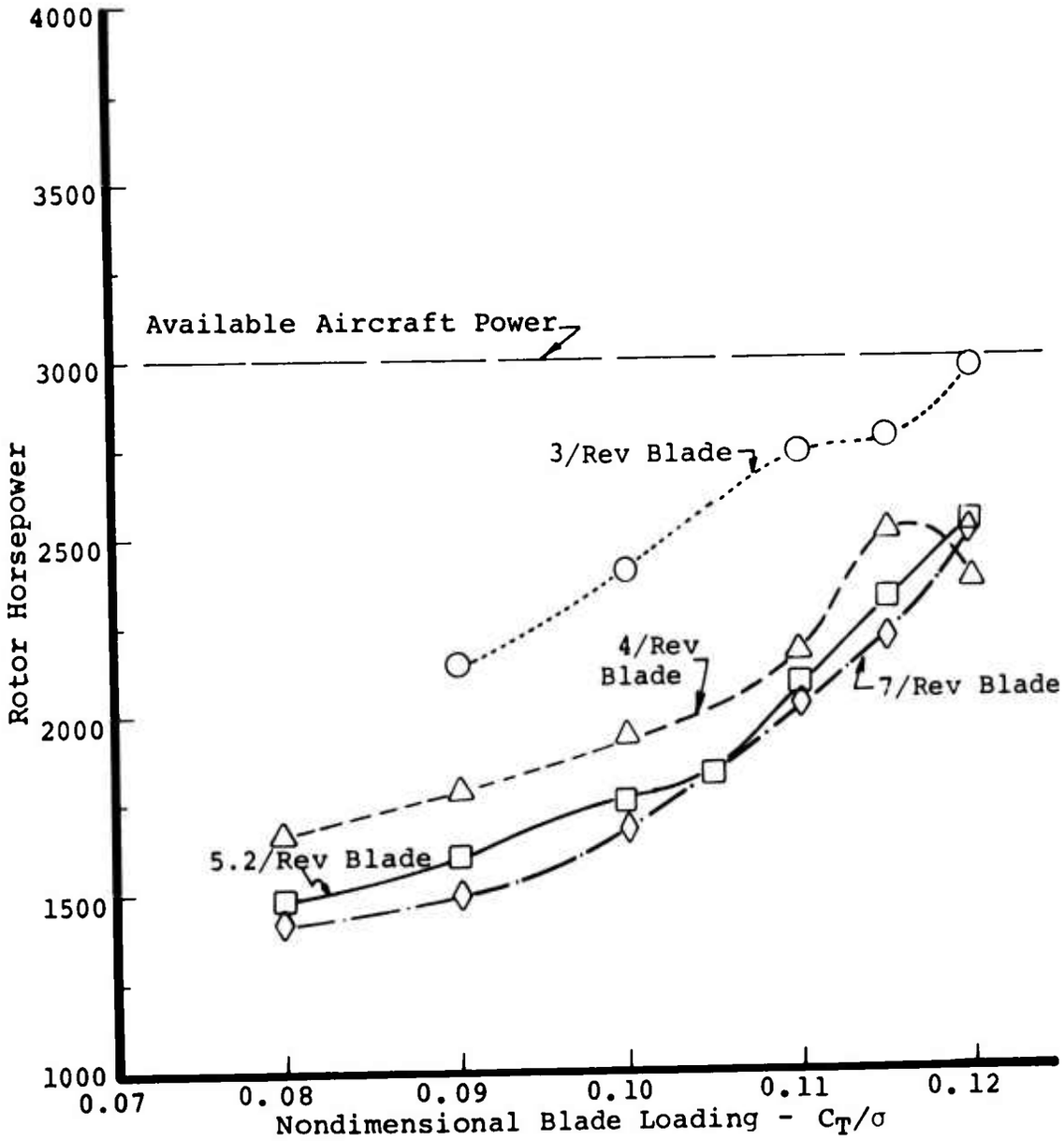

Figure 49. Variation of Rotor Power With Blade Loading for an Airspeed of 125 Knots.

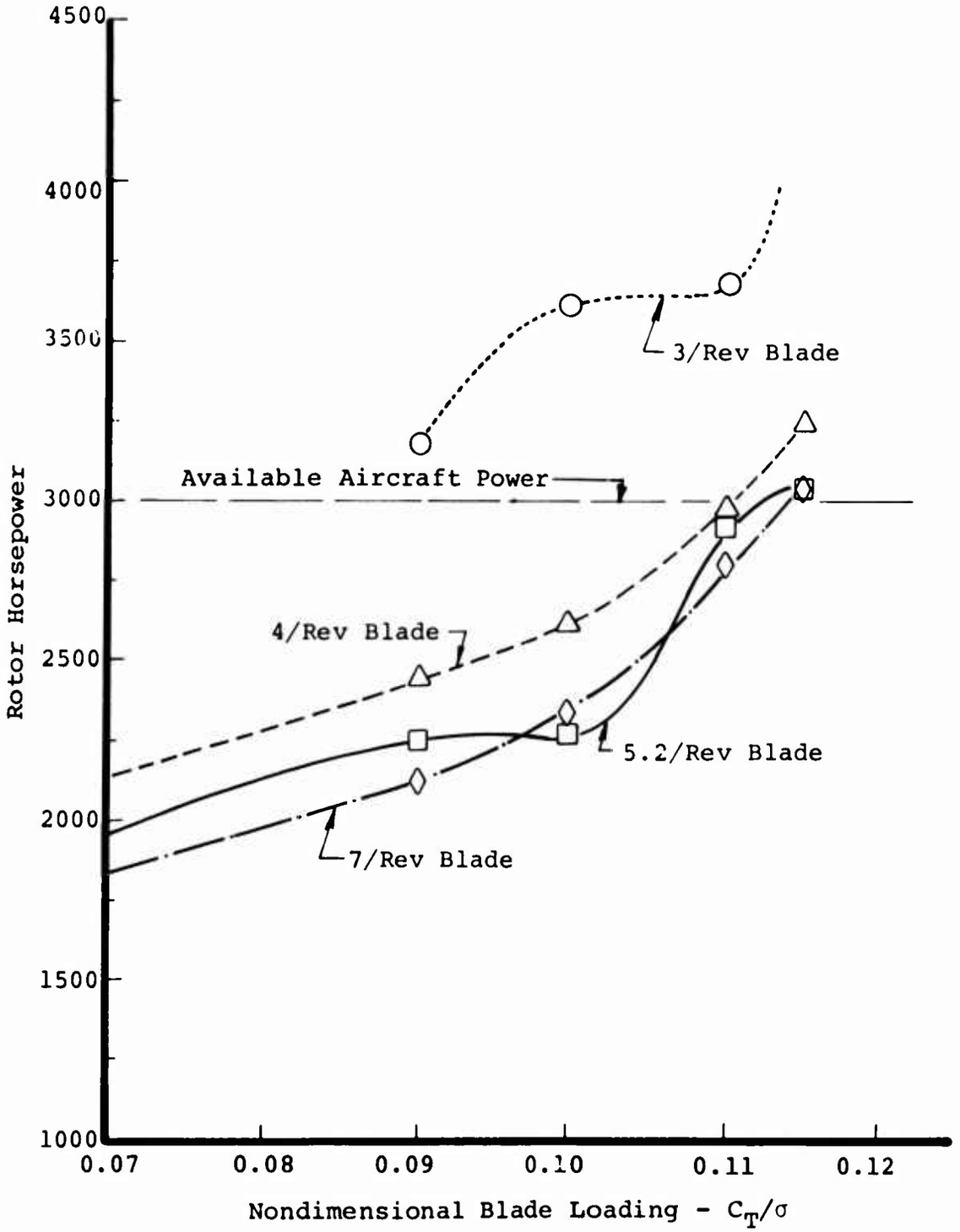

Figure 50. Variation of Rotor Power With Blade Loading for an Airspeed of 150 Knots.

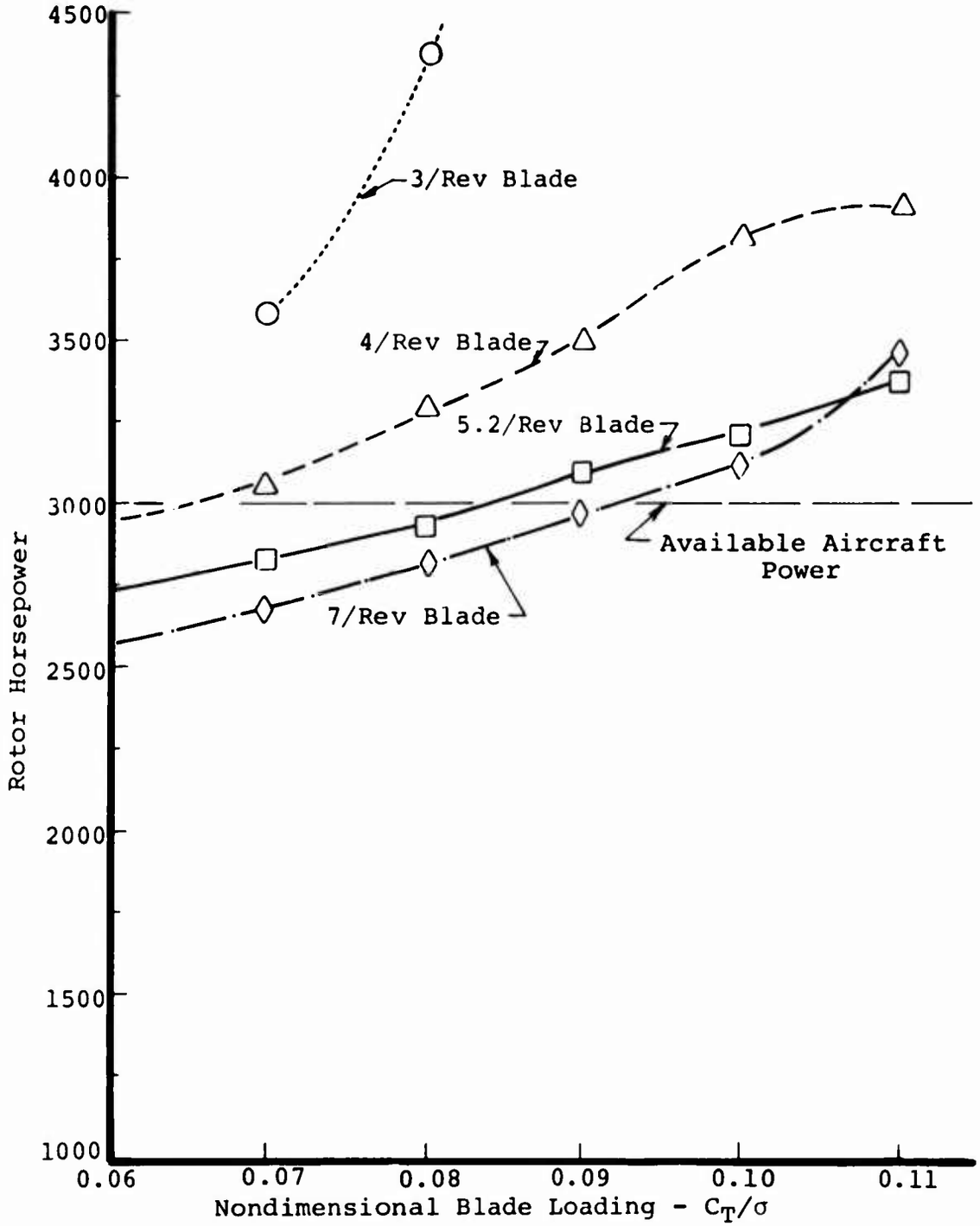

Figure 51. Variation of Rotor Power With Blade Loading for an Airspeed of 175 Knots.

4/REV BLADE POWER INCREASE RELATIVE
TO 7/REV BLADE AT $C_T/\sigma = 0.10$

Airspeed	Horsepower
125	250
150	300
175	700

The 3/rev blade clearly requires the most power, and only at 125 knots is the blade within 1000 horsepower of the 7/rev rotor.

The horizontal dashed line at 3000 horsepower across each of the figures represents an estimate of the available rotor power for a sea-level standard day. Increasing the altitude to 5000 feet reduces the power by 600 horsepower.

At an airspeed of 125 knots (Figure 49), all the blades are below the power limit, but the 3/rev blade is just below at a blade loading of 0.12. There is less than 300 horsepower difference between the 4/rev and 7/rev blade throughout this airspeed, while the 3/rev blade is as much as 700 horsepower higher than the 4/rev blade.

At 150 knots (Figure 50), the 3/rev blade is above the available power from a blade loading of 0.09 and above. All the blades exceed the power limit at 0.115 blade loading and are just below the limit (all within 200 horsepower) at 0.11. Again, there is little power variation (less than 350 horsepower) between the 4/rev, 5.2/rev and 7/rev blades.

At 175 knots (Figure 51), most of the flight conditions examined exceed the power limit. The 4/rev blade exceeds the power limit at a blade loading of 0.065, the 5.2/rev blade at 0.085, and the 7/rev blade at 0.0925. The 7/rev power boundary is a blade loading of 0.0275 better than the 4/rev blade and clearly represents a significant power savings. From these results it appears that the 7/rev blade is clearly superior to the others at this airspeed. However, all the performance data has not yet been presented.

This study uses single-rotor trim obtained from a trim analysis using an articulated rotor with rigid blades. The analysis gives rotor shaft attitude, cyclic pitch, rotor thrust, propulsive force, side force, and hub moments. The aeroelastic rotor analysis used for this study (program C-60) requires a trim input which consists of shaft attitude, rotor thrust,

and cyclic pitch as input. The other loads (i.e., propulsive force, side force, and hub moments) are calculated as part of the analysis and are not independent of the input. Since the trim can be obtained for only a rigid blade, the same trim will be used for the four different stiffness rotors. However, due to the live twist* of each blade, the propulsive force, side force, rotor power, and hub moments will be different for each blade torsional frequency.

Three of these hub load components (rotor thrust, propulsive force, and rotor power from blade torque) are essential in determining the rotor performance. For an aircraft to fly at a given gross weight and airspeed, the rotor must develop a specific rotor lift to balance the aircraft weight and a specific propulsive force to balance the total drag. These two forces, rotor lift and propulsive force, are a measure of the total force that the rotor must provide to remain at a given flight condition. Therefore, for a fair comparison of rotor power, the propulsive force and lift of the rotors to be compared should be approximately equal.**

As the rotor analysis is performed, the rotor thrust is equal for the four frequency blades at each flight condition. It remains to be seen how well the propulsive force agrees.

Figures 52 through 54 illustrate the variation of propulsive force with blade loading at 125 knots, 150 knots, and 175 knots for each blade. Generally, the propulsive force generated by the rotor increases as the airspeed increases and decreases as the blade stiffness increases. The trim analysis defines a constant propulsive force at each airspeed, having no variation with blade loading. However, due to elastic twist, there is a propulsive force reduction as the blade loading increases for each airspeed. The 3/rev blade frequently violates these general trends and will be excluded from the following discussion, since it is not a practical configuration.

---

*Live blade twist is the elastic pitch deformation of the blade caused by torsional loads. In general, the distribution of blade pitch angle along the span is the sum of the built-in twist, the live twist, collective pitch, and cyclic pitch.

**Strictly speaking, a direct power comparison should not be made until rotor lift, propulsive force, side force, rolling moment and pitching moment are identical for both rotors (i.e., hub load trim is maintained). To match these five loads requires iteration of collective pitch, cyclic pitch, shaft attitude, and sideslip angle. It would require a large number of cases to obtain a total hub load match, making this approach impractical.

The 4/rev blade generates the largest propulsive force at all flight conditions. The propulsive force is especially large at 150 knots for a blade loading of 0.09 and 0.10, and at 175 knots for 0.08 and 0.09. Therefore, the 4/rev blade requires

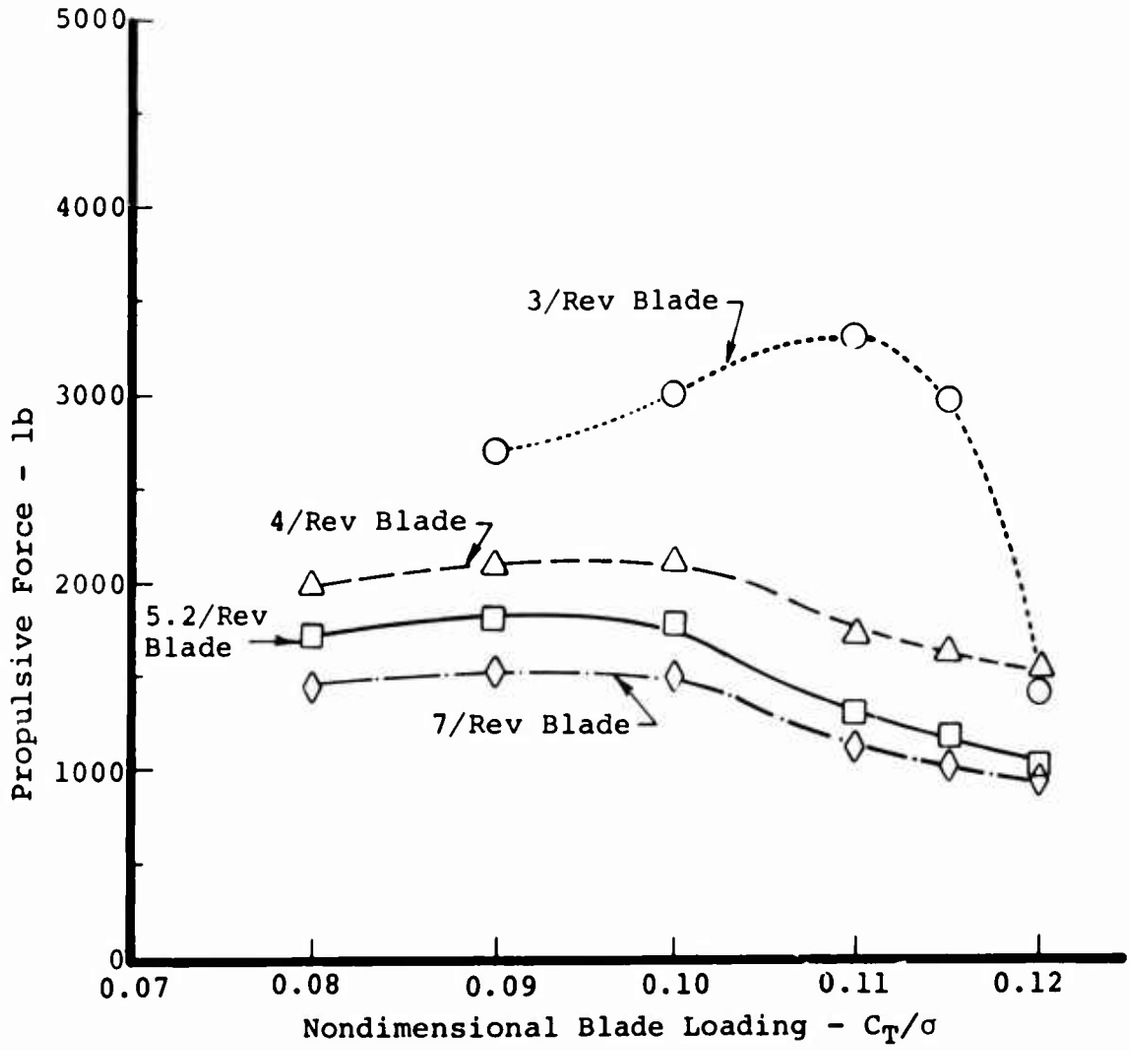

Figure 52. Variation of Propulsive Force With Blade Loading for an Airspeed of 125 Knots.

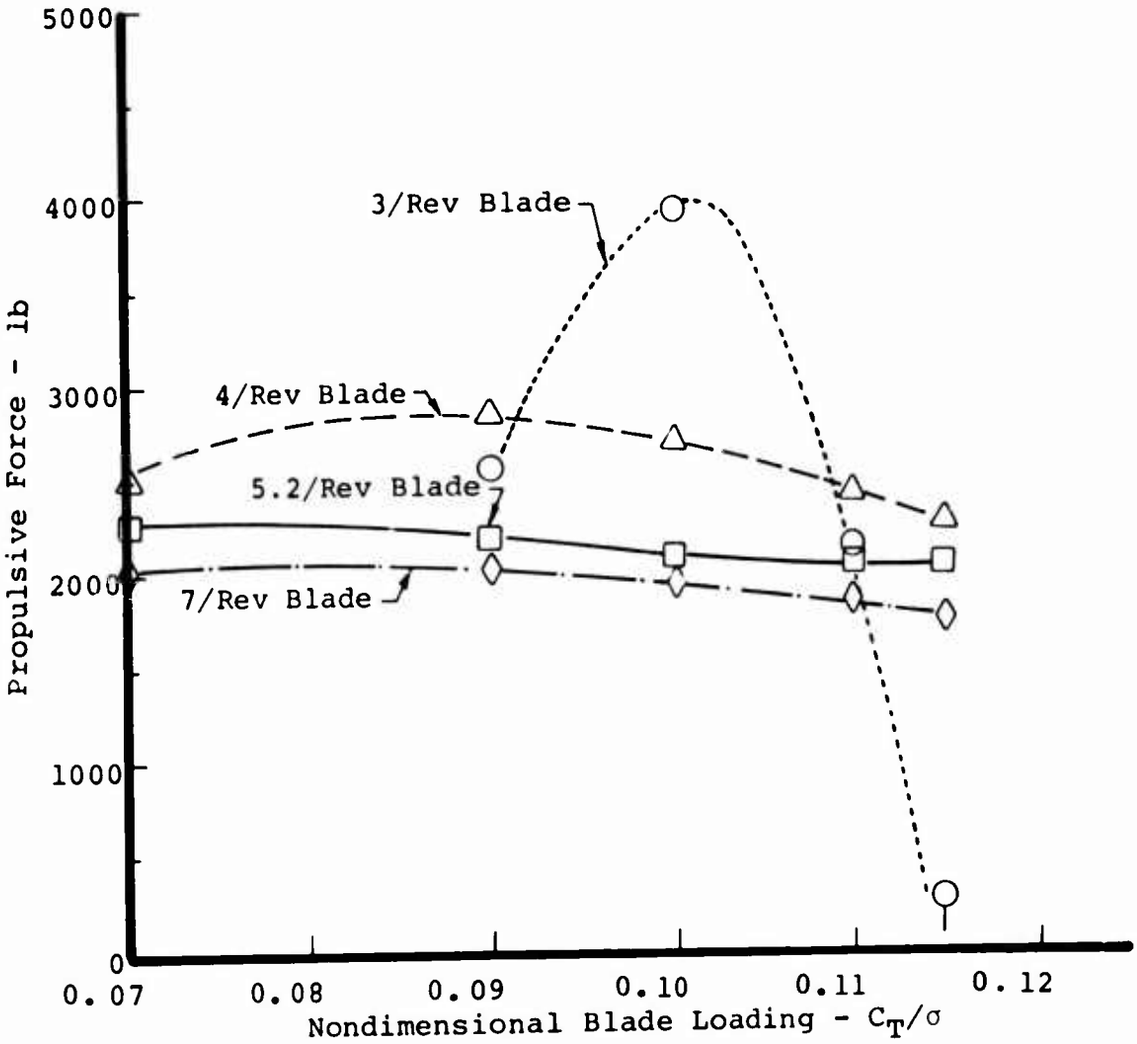

Figure 53. Variation of Propulsive Force With Blade Loading for an Airspeed of 150 Knots.

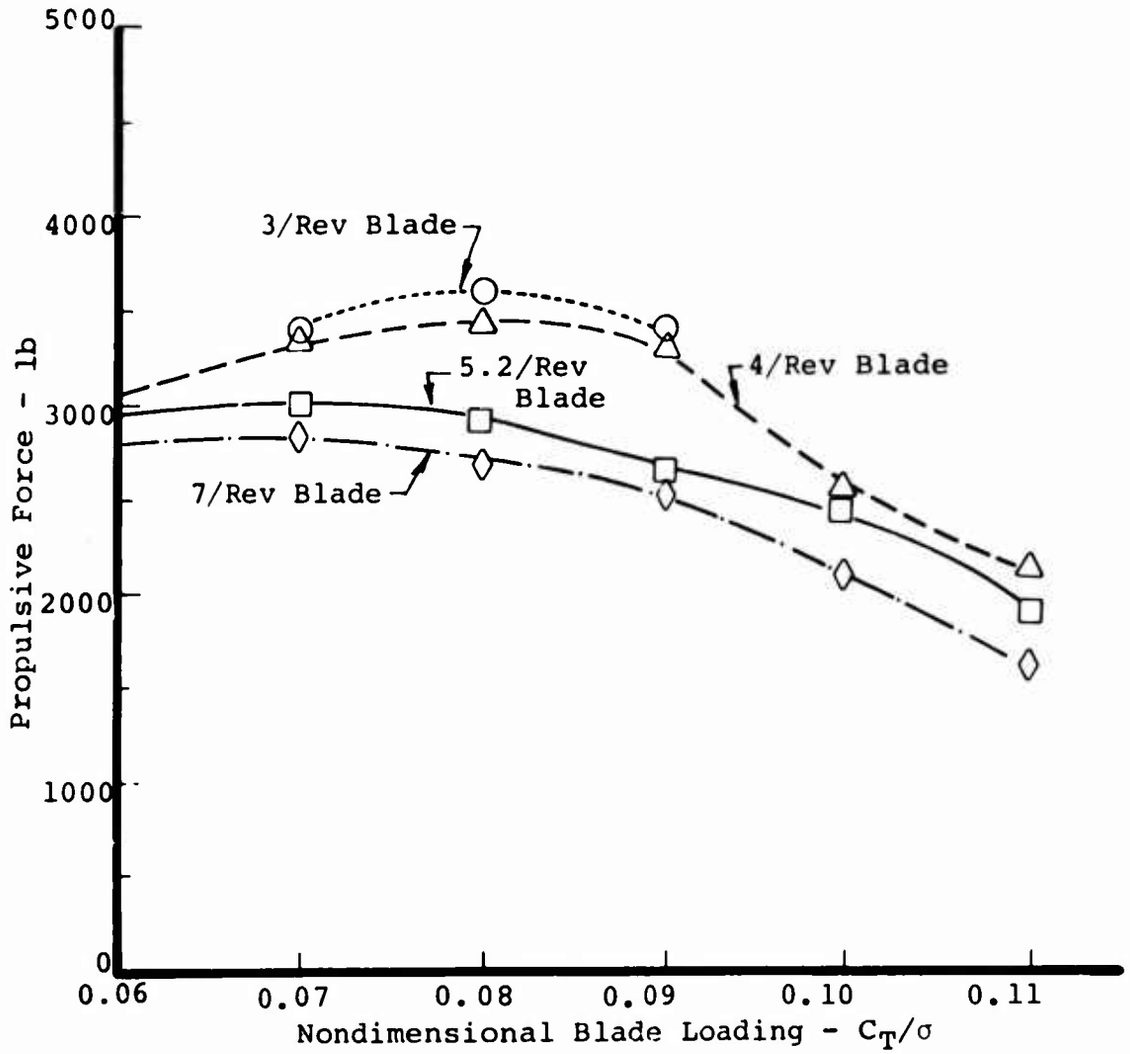

Figure 54. Variation of Propulsive Force With Blade Loading for an Airspeed of 175 Knots.

more power than the other two blades, but it also generates a larger propulsive force. To properly compare rotor power, the propulsive force should be adjusted so that only rotors with similar thrust and propulsive force are compared. Propulsive force matches at 125 knots and 175 knots were performed to evaluate the effect on required rotor power.

At 125 knots, the 3/rev, 4/rev and 7/rev cyclic pitch was adjusted to match the basic blade (5.2/rev) propulsive force. The results are shown in the table below for a blade loading of 0.115:

V = 125 knots $C_T/\sigma = 0.115$

Configuration	Propulsive Force (lb)	Rotor Power (hp)	Pitch-Link Load (lb)
Basic Blade (5.2/rev)	1159	2312	2478
4/rev - Basic Run	1605	2505	1766
4/rev - Adjusted Cyclic	1184	2354	1819
7/rev - Basic Run	1054	2216	3821
7/rev - Adjusted Cyclic	1150	2211	3163
3/rev - Basic Run	2981	2776	1737
3/rev - Adjusted Cyclic	Reasonable result not obtained		

The table shows that reducing the 4/rev propulsive force from 1605 pounds to 1184 pounds reduced the rotor power by 150 horsepower to within 42 horsepower of the basic blade power. Adjusting the 7/rev blade propulsive force resulted in essentially no power change. Attempts to adjust the 3/rev blade propulsive force led to a very large side force (i.e., two times the propulsive force). When the side force was adjusted, the propulsive force dropped further and the rotor power increased. Generally, changes in the 3/rev cyclic pitch frequently resulted in unexpected load changes, and it appears that this rotor would be very difficult to control.

At 175 knots, the 4/rev blade cyclic pitch was adjusted to match the 7/rev blade propulsive force at blade loadings of 0.08 and 0.09. For both cases the rotor power was reduced, as shown in the table below:

Configuration	Propulsive Force (lb)	Rotor Power (hp)	Pitch-Link Load (lb)
V = 175 Knots		$C_T/\sigma = 0.08$	
7/rev - Basic Run	2709	2812	2194
4/rev - Basic Run	3454	3292	2210
4/rev - Adjusted Cyclic	2645	2824	2163
V = 175 Knots		$C_T/\sigma = 0.09$	
7/rev - Basic Run	2522	2985	2939
4/rev - Basic Run	3358	3506	2451
4/rev - Adjusted Cyclic	2504	3054	2528

For the worst case (blade loading of 0.09), the propulsive force was within 18 pounds, out of 2522 pounds, and the power for the 4/rev blade was 69 horsepower larger than the 7/rev blade out of 2985 horsepower (i.e., 2.2 percent larger).

It should be pointed out here that the propulsive force/rotor power trade-off may not work out favorably for the 4/rev blade at blade loadings of 0.10 and 0.11 at 175 knots. At these flight conditions, the 4/rev and 7/rev propulsive forces are relatively close and the power difference is relatively large. However, these flight conditions may not be practical for either frequency blade, due to the strong presence of rotor stall and the large required power.

In addition to investigating the secondary effects on performance, changes in blade and hub loads should also be reviewed. However, these load effects are generally not as important as performance, since there are few instances where the flight envelope is actually limited by these loads. In addition, to determine the effect of torsional frequency on the rotor loads would require extensive investigation of all the spanwise blade load distributions plus all the rotor hub load components, which is beyond the scope of this contract.

In summary, the following conclusions can be made:

1) A match of rotor thrust and propulsive force is required before a power comparison can be made.

2) Reducing rotor propulsive force generally reduces the required rotor horsepower.

3) When the thrust and propulsive forces are matched, the 7/rev and 4/rev blades require approximately the same power. Generally, the two blades are nearly equivalent at 175 knots for both pitch-link loads and performance.

-Pitch-Link Load Variation in Hover

In addition to the investigation of stall-induced pitch-link loads over a range of airspeeds, a limited study was performed to determine the effect of blade torsional frequency on stall-induced pitch-link loads in hover. Stall loads are strong functions of both blade loading and airspeed, as shown in the previous results. This study allows stall-induced pitch-link loads to be obtained with one major contributor to the loads eliminated; namely, advance ratio.

For the hover conditions, the tangential velocity is constant around the azimuth. The only cyclic angle-of-attack variation results from a 1-degree cyclic pitch and an induced angle due to blade flapping. The cyclic pitch was needed to provide some means of introducing a cyclic load variation. If this were not done, the analysis would predict only steady loads. In actual hover flight or whirl tower conditions at high blade loadings, cyclic pitch is not needed to obtain vibratory stall loads. There are turbulences in the air that would introduce varying angles of attack and eventually trigger cyclic stall pitch-link loads.

Figure 55 shows the variation of hover pitch-link load amplitude with torsional frequency for blade loadings of 0.115 to 0.18. At blade loadings of 0.115 and 0.12, the pitch-link load has a 1/rev waveform with an amplitude of about 100 pounds. These loads are probably for an unstalled condition, since there is virtually no load variation with blade loading or torsional natural frequency. At a blade loading of 0.15, the loads increase to between 200 pounds and 300 pounds, with the 3/rev and 4/rev blades having the lowest load. At this condition, the rotor power is around 4000 horsepower, which is well beyond the available rotor power.

At a blade loading of 0.165, the pitch-link load for the 3/rev blade increases sharply to 1000 pounds. The major portion of this load is a 950-pound 8/rev component. Since the blade torsional natural frequency is 3/rev, it was surprising to observe that there was little 3/rev load and a very large 8/rev load. Further examination revealed that the blade second torsional natural frequency is nearly exactly 8/rev, thereby explaining the source of the large load. It is not known why the torsionally soft blade prefers to oscillate in its second mode, and further investigation is necessary.

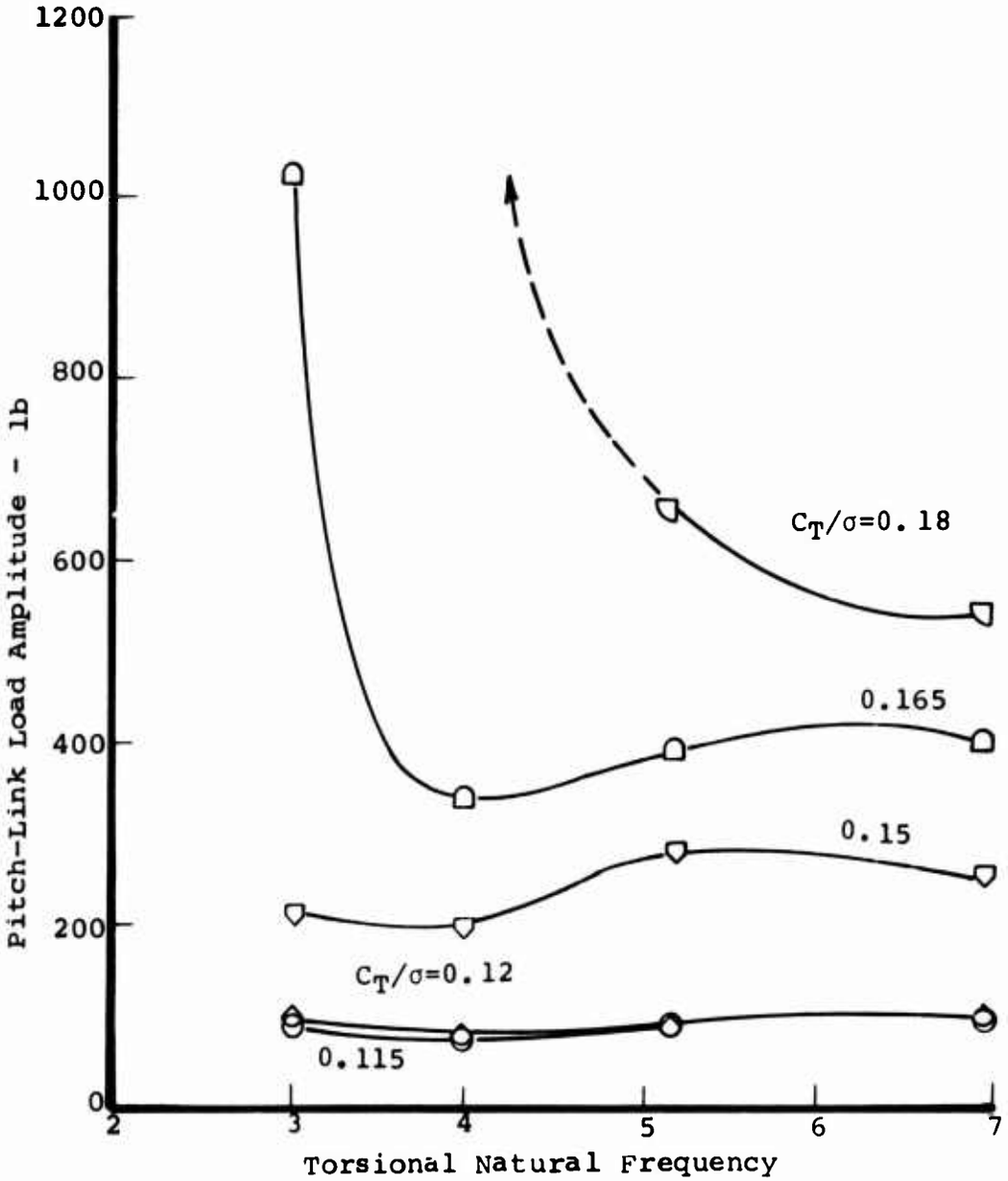

Figure 55. Variation of Pitch-Link Load Amplitude With Torsional Natural Frequency for Hover.

The 4/rev blade, at the same flight condition, has a pitch-link load of 340 pounds, which is the lowest of the four blades. The 5.2/rev and 7/rev blades had approximately the same load at about 400 pounds. The required rotor power for all blades is approximately 5000 horsepower, which is 66 percent larger than the available rotor power. Since the required power is so high, results at this blade loading (0.165), and above, probably have no practical application.

At a blade loading of 0.18, the 3/rev blade pitch-link load increases to 4500 pounds, with the 8/rev component again providing the largest load. The 4/rev blade also shows a large load increase, reaching a load of about 4000 pounds. However, the large load on this blade yields large torsional oscillations at the first torsional natural frequency (3600 pounds at 4/rev). The 5.2/rev blade has a load of 650 pounds and the 7/rev blade load is 540 pounds. At this condition the loads reduce with increasing torsional frequency. The required rotor power for this flight condition is over twice the available power, indicating that rotor stall is spreading over a larger portion of the blade.

Up to a blade loading of 0.165, the lower the blade torsional frequency, the lower the required rotor power. At a blade loading of 0.12, the 3/rev blade required about 100 horsepower less than the 7/rev blade; at 0.15, it requires 250 horsepower less. However, at a blade loading of 0.165, the 3/rev blade requires the highest power, 300 horsepower greater than the 4/rev blade. At 0.18, both the 3/rev and 4/rev blades required rotor power is 50 percent larger than the 7/rev blade required power.

To summarize, the following conclusions can be made:

1) The 4/rev blade has the lowest stall-induced pitch-link loads up through a blade loading of 0.165.

2) At a blade loading of 0.18, both the 3/rev and 4/rev blades become deeply stalled and have extremely large control loads. However, this flight condition probably has no practical application, since the required rotor power is more than three times the available power.

Analytical Results for Additional Effects

The previous two sections have:

1) established the ability of the aeroelastic rotor analysis to predict stall-induced pitch-link loads

2) determined the effect of blades with four different torsional natural frequencies on stall-induced pitch-link loads over a range of advance ratios and blade loadings

This section will further investigate the variation of stall-induced control loads by evaluating the effect of blade pitch inertia, control system stiffness, torsional frequency (above 7/rev), blade twist, and cyclic pitch. This additional study was performed to determine if other means for reducing the stall-induced pitch-link loads can be found.

-Control Load Trend With Blade Torsional Frequencies up to 12/Rev

In the previous section the relationship between pitch-link load amplitude and torsional natural frequency was examined for blades with frequencies between 3/rev and 7/rev for an extensive matrix of flight conditions. In order to more fully describe the overall relationship with frequency, five stalled flight conditions were studied for frequencies between 7/rev and 12/rev.

Due to the flexibility of the control system, obtaining frequencies above 7.25/rev by simply increasing the torsional stiffness was not possible. The maximum frequency obtained by increasing the torsional stiffness is 7.25/rev. Even if the blade flexibility were increased to infinity, the blade would vibrate as a rigid body under the action of the elasticity inherent in the control system. In order to obtain frequencies above 7.25/rev, the control system stiffness was made infinite. This enabled frequencies of 7/rev, 8/rev, 9/rev, 10/rev, 11/rev and 12/rev to be obtained by increasing the torsional stiffness by factors of 1.38, 1.82, 2.3, 2.8, 3.38 and 4.0, respectively. The 7/rev frequency was repeated using the infinitely stiff control system stiffness in order to provide a direct comparison with the previous finite control stiffness results.

Figure 56 shows the results obtained for the 125-knot flight condition at 0.11 blade loading. Pitch-link load amplitude increases rapidly with natural frequency from about 1500 pounds at 4/rev to a maximum 4900 pounds at 8/rev. Above 8/rev, the pitch-link amplitude decreases to 1400 pounds at 12/rev. At the 7/rev frequency, the infinite stiff control system (with a 1.38 factor applied to the torsional stiffness) lead to a reduction in pitch-link load from 4550 pounds to 4150 pounds compared to the flexible control system results (with a 3.7 factor applied to the torsional stiffness).

Figure 57 illustrates the relationship between pitch-link load amplitude and natural frequency for an aft rotor of a tandem helicopter at a flight condition of 123 knots and a blade

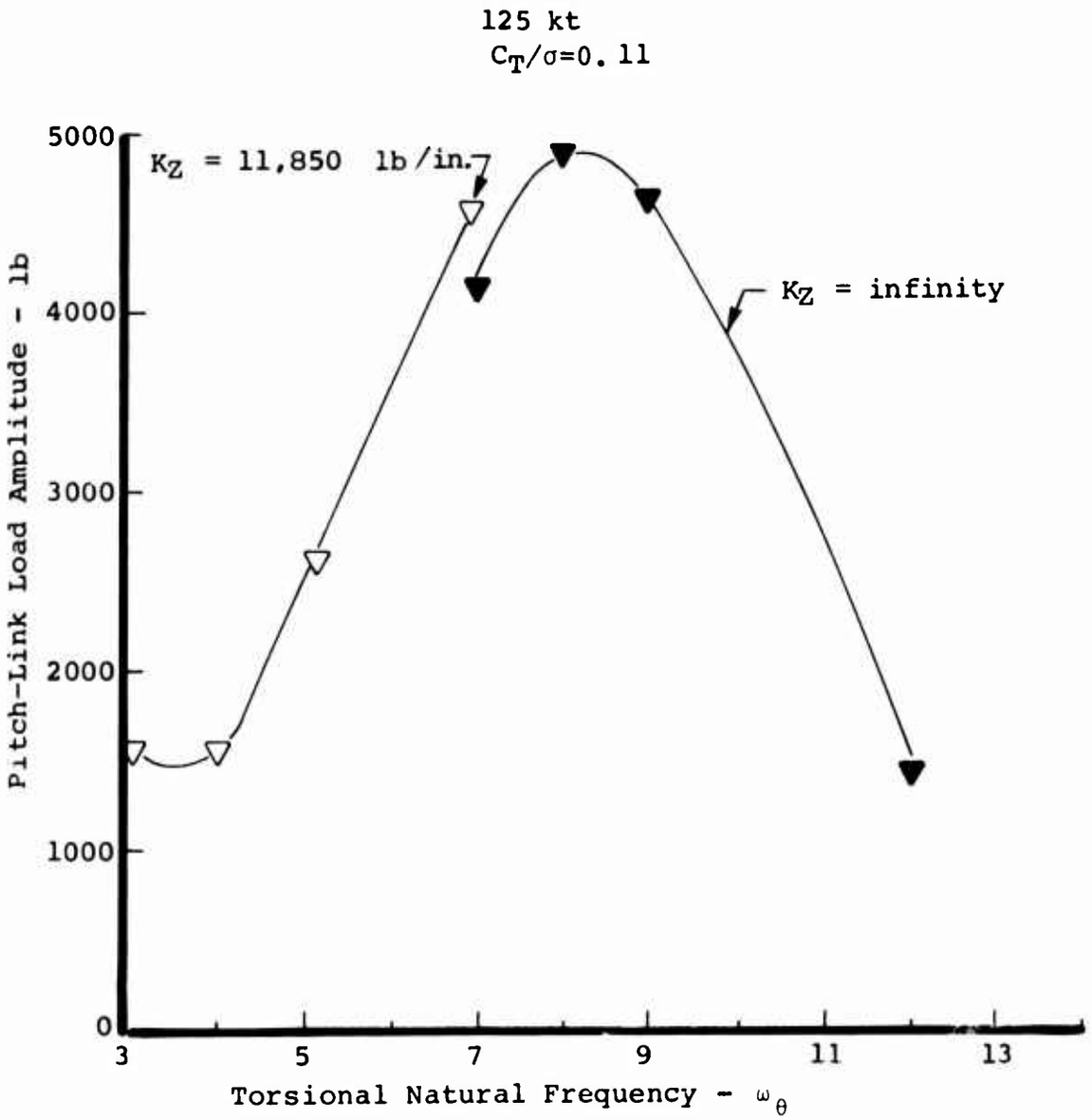

Figure 56. Variation of Pitch-Link Load Amplitude With Torsional Natural Frequency at 125 Knots, for Two Different Control Stiffnesses.

O = Control System Stiffness = 11,850 lbs/in.
Δ = Infinite Control System Stiffness

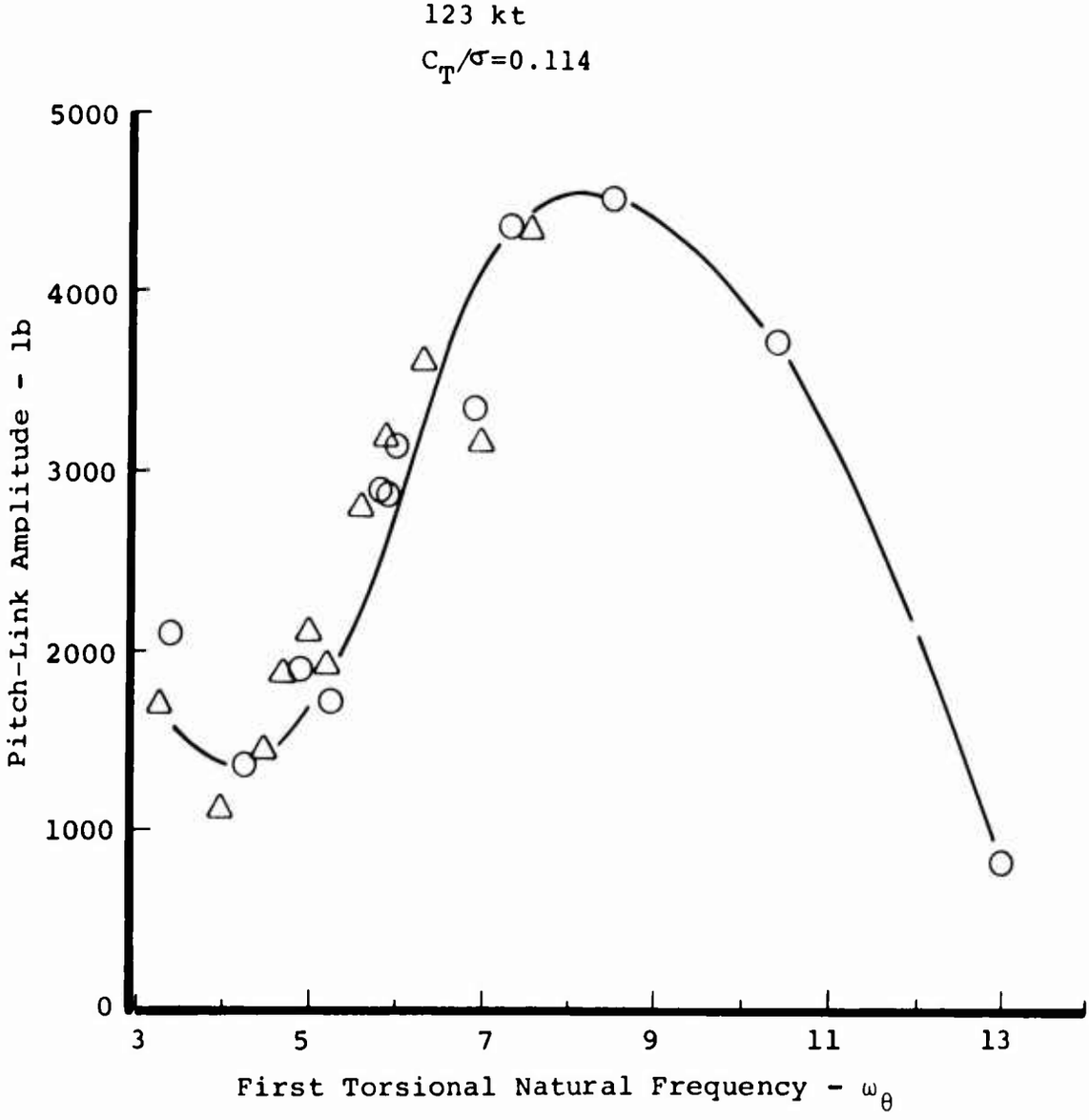

Figure 57. Variation of Pitch-Link Load Amplitude With Torsional Natural Frequency at 123 Knots.

loading of 0.114 (from Reference 1 results). The figure shows pitch-link loads for both nominal (11,850 pounds/inch) and an infinite control system stiffness.

These loads agree very well with the single-rotor results at 125 knots and a blade loading of 0.11 even though the airspeed, blade loading, and trim are different. The tandem rotor, at the nominal control system stiffness, exhibits a slightly deeper load bucket near 4/rev and a dip in the pitch-link load amplitude near 7/rev which is not evident in the single-rotor results. The infinite control system stiffness load trends agree very well for both the tandem and single rotor. It is clear from these results that there is a very significant and consistent trend of torsional load with frequency for the 125-knot flight condition.

At 150 knots, the extended frequency analysis was performed at blade loadings of 0.1, 0.11 and 0.115. The results are shown in Figure 58. Generally, there is little variation with torsional natural frequency at 150 knots. Ignoring the 3/rev blade instability, there is only 1600 pounds difference between the maximum and minimum load (there is a 3400 pound difference at 125 knots). At 4/rev there is a pronounced load bucket at blade loadings of 0.11 and 0.115. At 7/rev, reducing the blade torsional stiffness and assuming an infinitely stiff control system reduced the pitch-link load by 1300 pounds at 0.115 blade loading and 900 pounds at 0.11 blade loading, but there was no change at 0.10 blade loading.

Since increasing control system stiffness shows promise as a method of reducing control loads for the 7/rev blade, the same procedure was used for a 4/rev blade. The solid triangular symbol at 4/rev on Figure 58 indicates the pitch-link load amplitude obtained for an infinitely stiff control system. This reduces the pitch-link load amplitude by about 150 pounds. This result, along with similar results in the next section, establishes the feasibility of using increased control system stiffness with a corresponding reduced torsional stiffness (to keep frequency constant) as a method for reducing control loads.

Figure 59 illustrates the variation of pitch-link load amplitude with natural frequency for the 175-knot flight condition at a blade loading of 0.09. As expected, the 3/rev blade becomes totally unstable at this high speed. There is a load bucket at 4/rev and a load peak near 8/rev. The overall effect of natural frequency on pitch-link load amplitude is about the same as at 150 knots.

To summarize, the following conclusions may be drawn from the extended frequency trends:

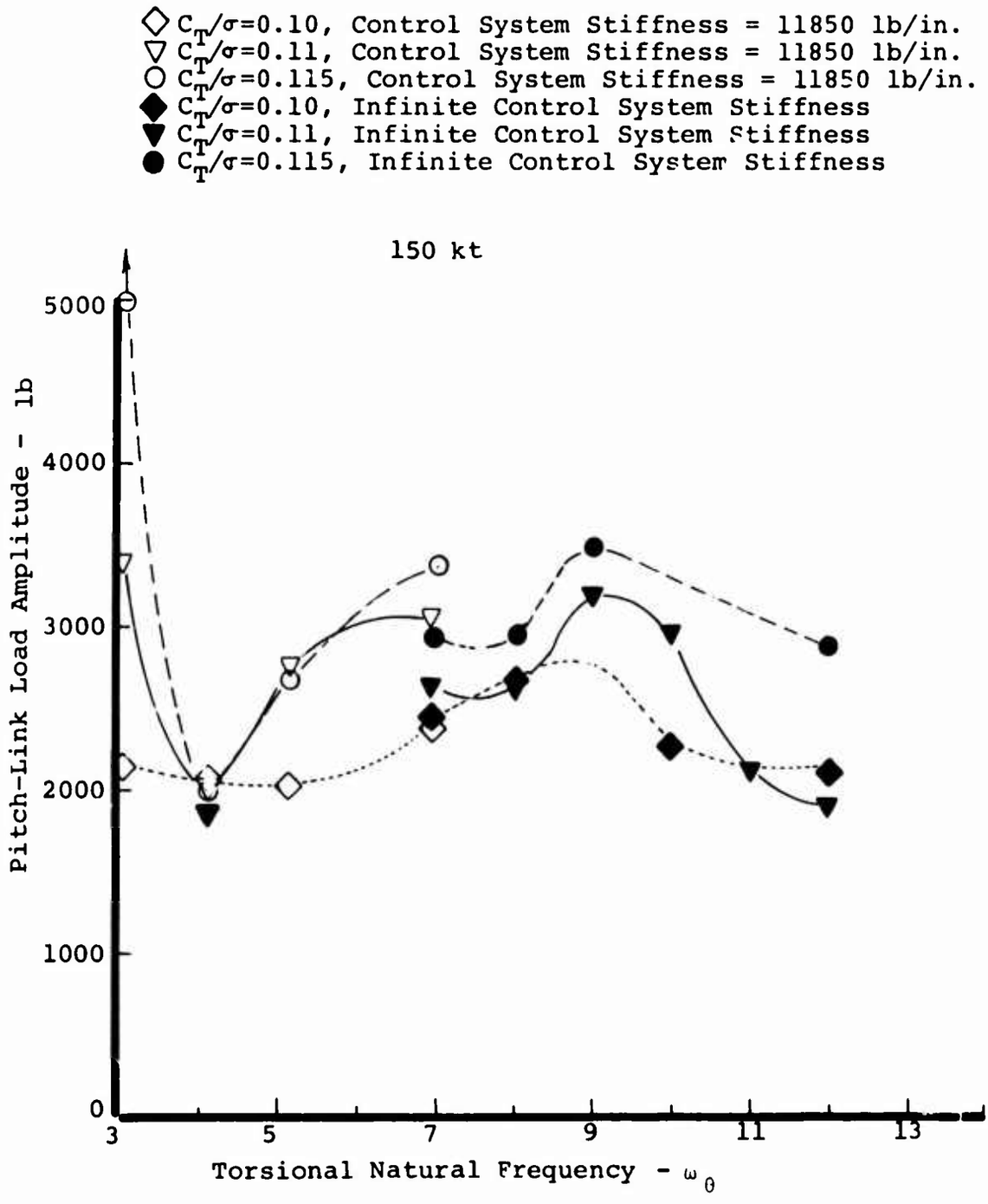

Figure 58. Variation of Pitch-Link Load Amplitude With Torsional Natural Frequency at 150 Knots for Various Blade Loadings.

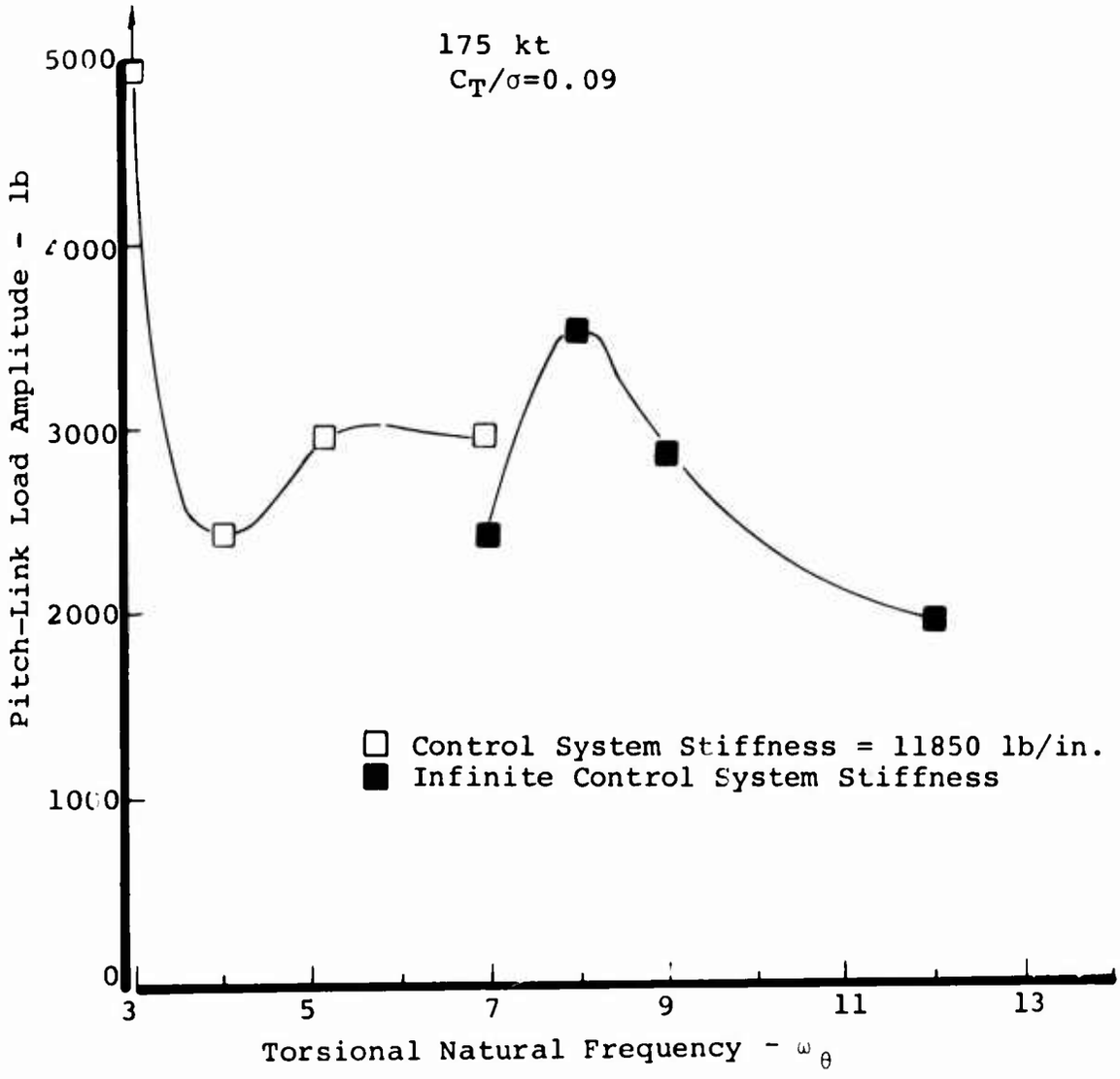

Figure 59. Variation of Pitch-Link Load Amplitude With Torsional Natural Frequency at 175 Knots.

1) At 125 knots there is a strong relationship between pitch-link load amplitude and torsional natural frequency. There is a load bucket near 4/rev and a load peak near 8/rev.

2) The effect of natural frequency on pitch-link load is much less pronounced at the 150-knot and 175-knot airspeeds. At both airspeeds the trend is characterized by a load bucket at 4/rev and a load peak near 8/rev or 9/rev.

3) A reduction in control load amplitude may be possible at a given frequency by increasing the control system stiffness and reducing the blade torsional stiffness.

-Other Methods of Varying Torsional Natural Frequency

In previous sections, torsional natural frequency was varied by changing the blade torsional stiffness distribution. This section investigates other methods of changing torsional frequency. The resulting pitch-link load variations with frequency were then compared with loads obtained by changing torsional stiffness.

To perform this study, frequency changes were made using two methods: changes in control system stiffness and changes in blade pitch inertia. Using the basic CH-47C blade as a baseline, torsional natural frequencies (5.2/rev) were varied from 3/rev to 6/rev at 125 knots by changing the control system stiffness. A control system stiffness of 1650 pounds/inch generated a frequency of 3/rev; 11,850 pounds/inch was used for the basic blade (torsional natural frequency = 5.2/rev); and an infinite stiffness produced a 6/rev frequency.

Frequency variation due to pitch inertia changes are divided into two regions above and below 7/rev: frequencies below 7/rev were obtained by scaling the blade pitch inertia distribution while holding all other blade properties at their nominal values (i.e., basic blade values); frequencies of 3, 4 and 7/rev were obtained by scaling the pitch inertia by factors of 3.08, 1.7 and 0.55, respectively. Frequencies above 7/rev were obtained by assuming an infinitely stiff control system and scaling the pitch inertia. The control system was made infinite because unrealistically small inertias would have been necessary if the nominal control system stiffness was used. Frequencies of 7/rev, 8/rev, 9/rev, 10/rev, 11/rev and 12/rev were obtained by using factors of 0.75, 0.56, 0.44, 0.36, 0.3 and 0.26 with an infinitely stiff control system. The 7/rev frequency was repeated using the infinite control system stiffness in order to provide a direct comparison with the finite control system stiffness results.

Figure 60 shows the relationship between pitch-link load amplitude and torsional frequency (3/rev to 7/rev) at an airspeed of 125 knots and a blade loading of 0.115 for the three methods of varying frequency. The solid line indicates changes in the torsional stiffness; the dashed line indicates changes in control system stiffness; and the dot-dash line shows the effect of pitch inertia changes. Each method of varying frequency produces approximately the same trend of pitch-link load amplitude with frequency. The maximum variation between methods occurs at 4/rev and is approximately 1000 pounds. The pitch inertia and control system stiffness variations led to higher loads than the torsional stiffness variation below 5.2/rev and lower loads above 5 2/rev.

When a frequency of 4/rev was generated by reducing the control system stiffness, the pitch-link load amplitude was 2150 pounds (triangular symbol). When the frequency was obtained by reducing the torsional stiffness, the load is reduced to 1750 pounds (circular symbol). This result is significant, since it supports the conclusion made in the previous section; i.e., that the control load can be reduced at a given torsional frequency by increasing the control system stiffness and compensating for this change by reducing blade torsional stiffness.

Figure 61 illustrates the relationship between pitch-link load amplitude and natural frequency for an aft rotor of a tandem helicopter at a flight condition of 123 knots at a blade loading of 0.114 (from Reference 1 results). For these analytical results, torsional frequency was varied by changing torsional stiffness, pitch inertia, and control system stiffness. Comparing these tandem-rotor results with the single-rotor results of Figure 60 shows that both sets of loads show the same general trend with frequency, even though there are differences in the flight condition and the methods of varying frequency. Disregarding the large load variation at 3/rev for the tandem rotor, both sets of results show about a 1000-pound maximum variation at a given frequency.

Figures 62 and 63 illustrate the variation of pitch-link load amplitude with natural frequency at the 150-knot airspeed and blade loadings of 0.115 and 0.11, respectively. The results of each method of varying frequency generally confirm that pitch-link load amplitude is less sensitive to natural frequency at 150 knots than at 125 knots. The results of the torsional stiffness variations at the two flight conditions are very similar (neglecting the 3/rev blade). Both exhibit a load bucket at 4/rev and a load peak near 9/rev. The results of the pitch inertia variations at both flight conditions yield similar trends with frequency. It should be noted that when the torsional stiffness variation peaks at 9/rev,

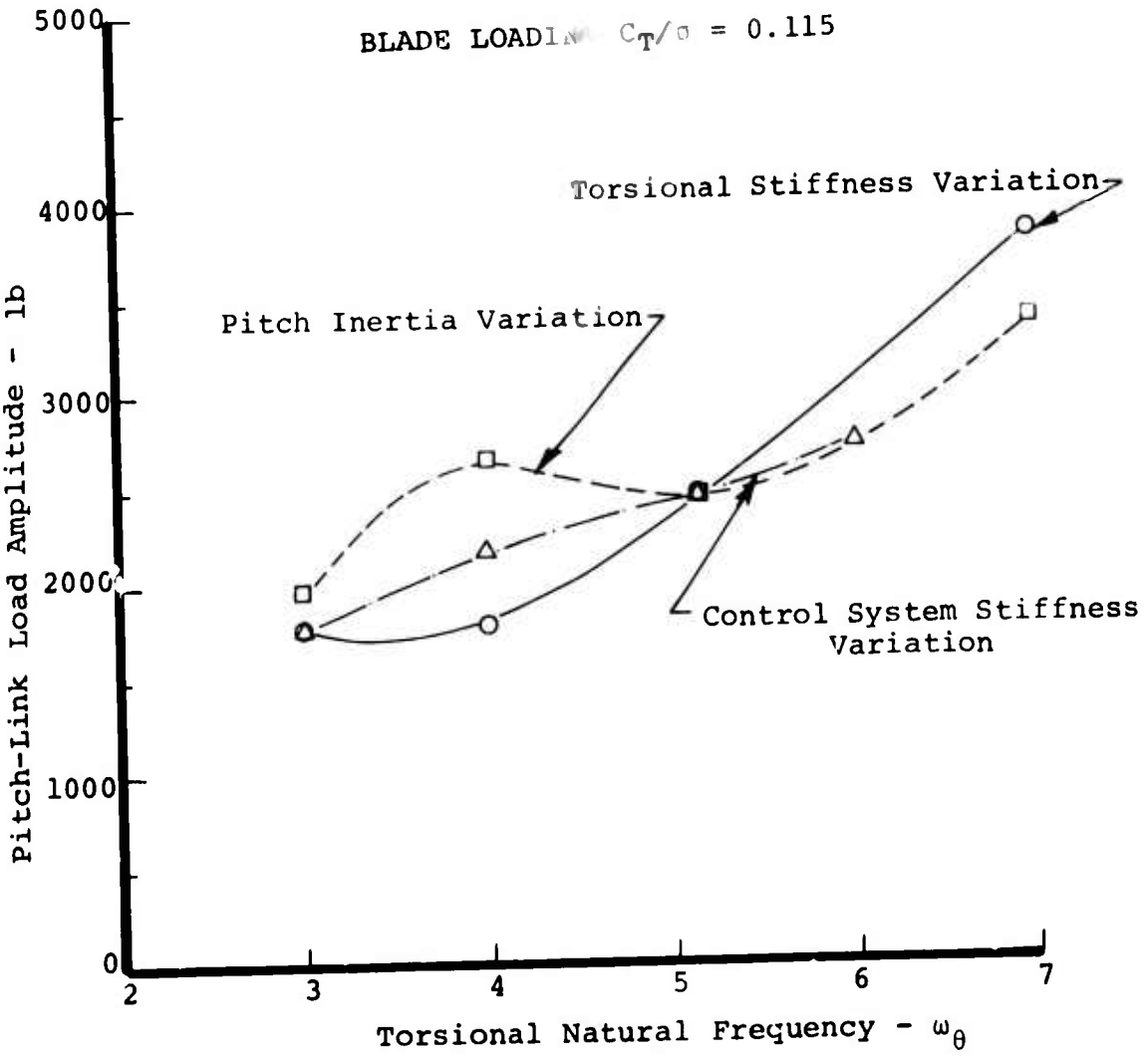

Figure 60. Variation of Pitch-Link Load Amplitude With Natural Frequency at 125 Knots.

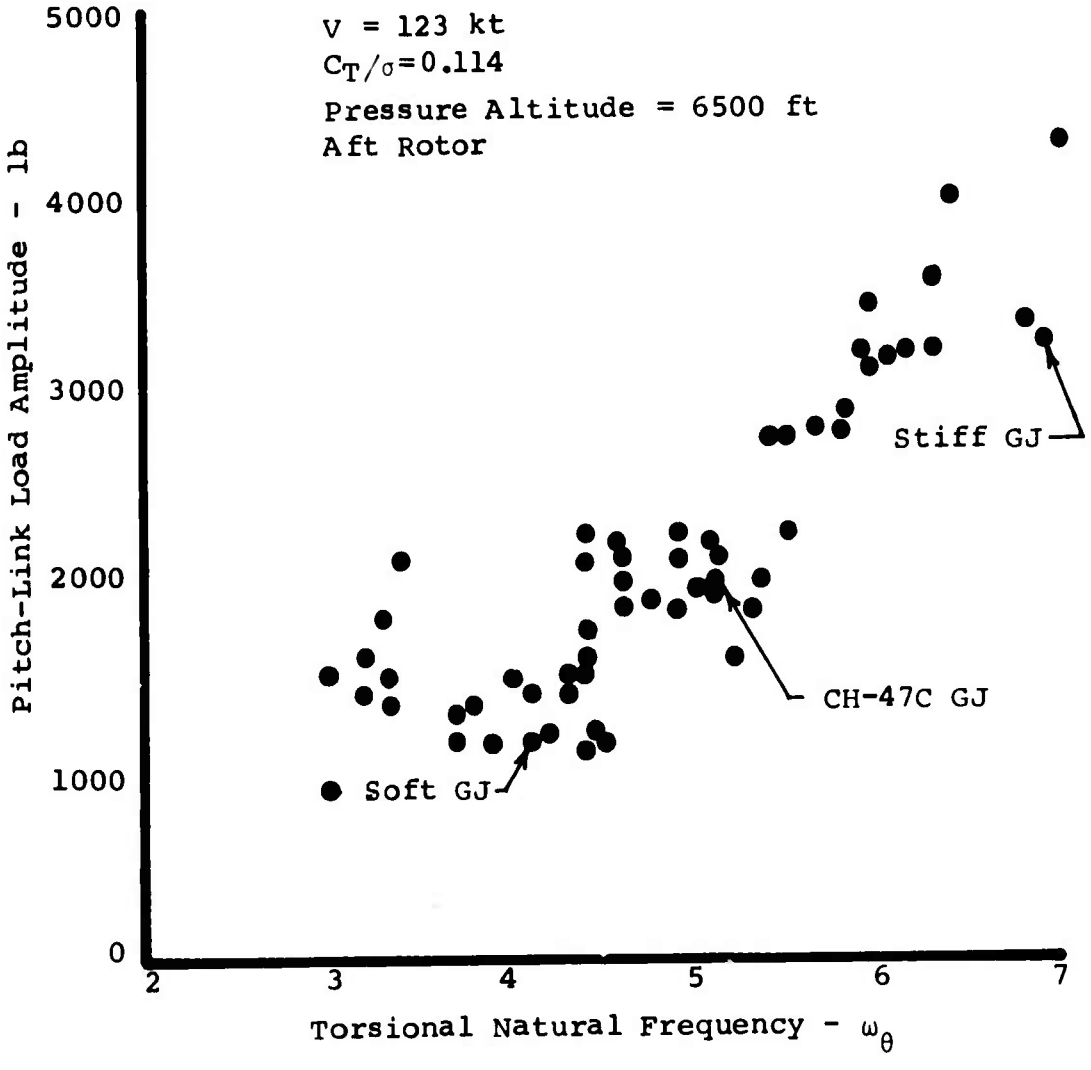

Figure 61. Effect of Torsional Frequency on Tandem-Rotor Pitch-Link Loads.

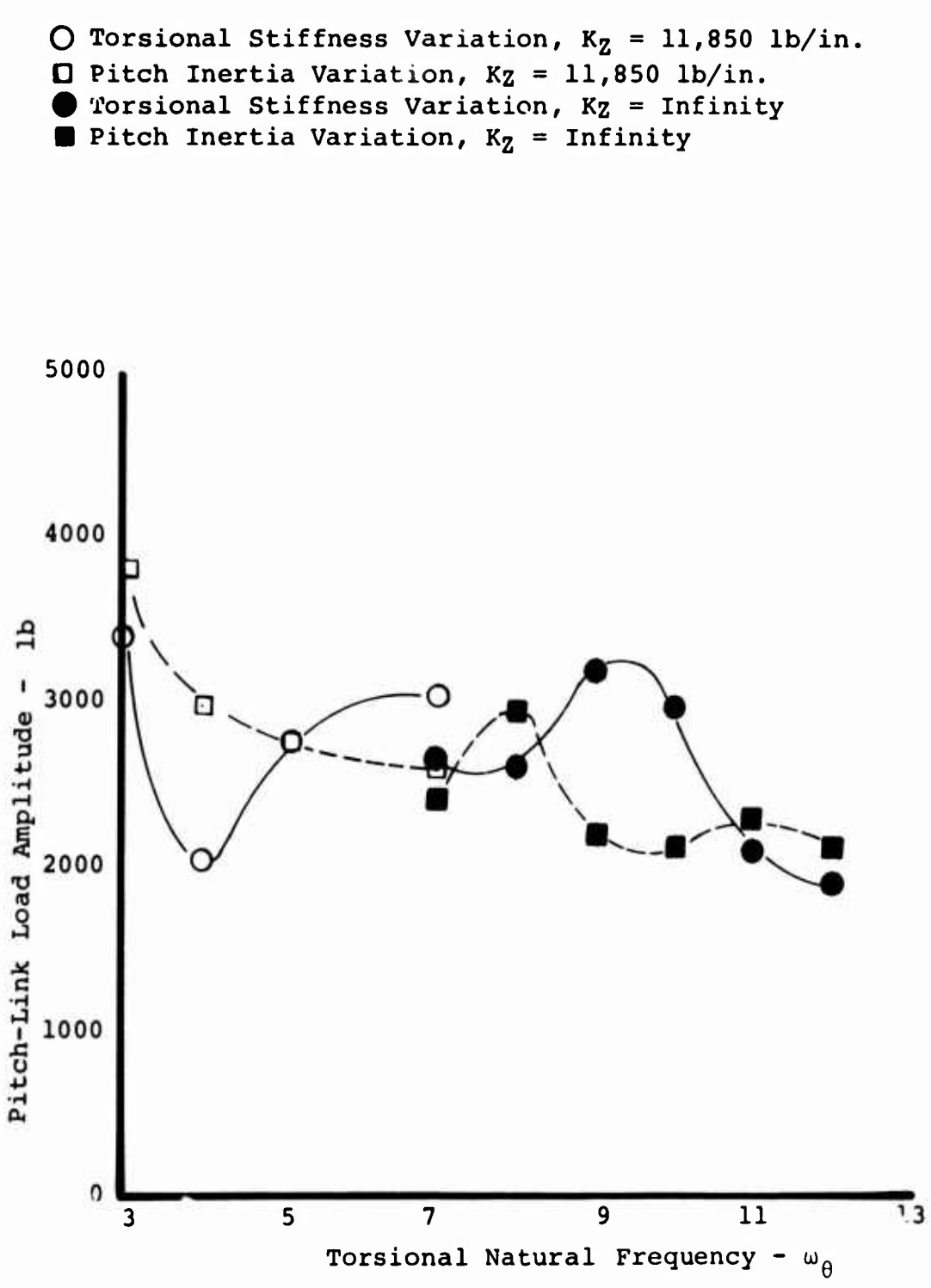

Figure 62. Variation of Pitch-Link Load Amplitude With Natural Frequency at 150 Knots and .115 Blade Loading.

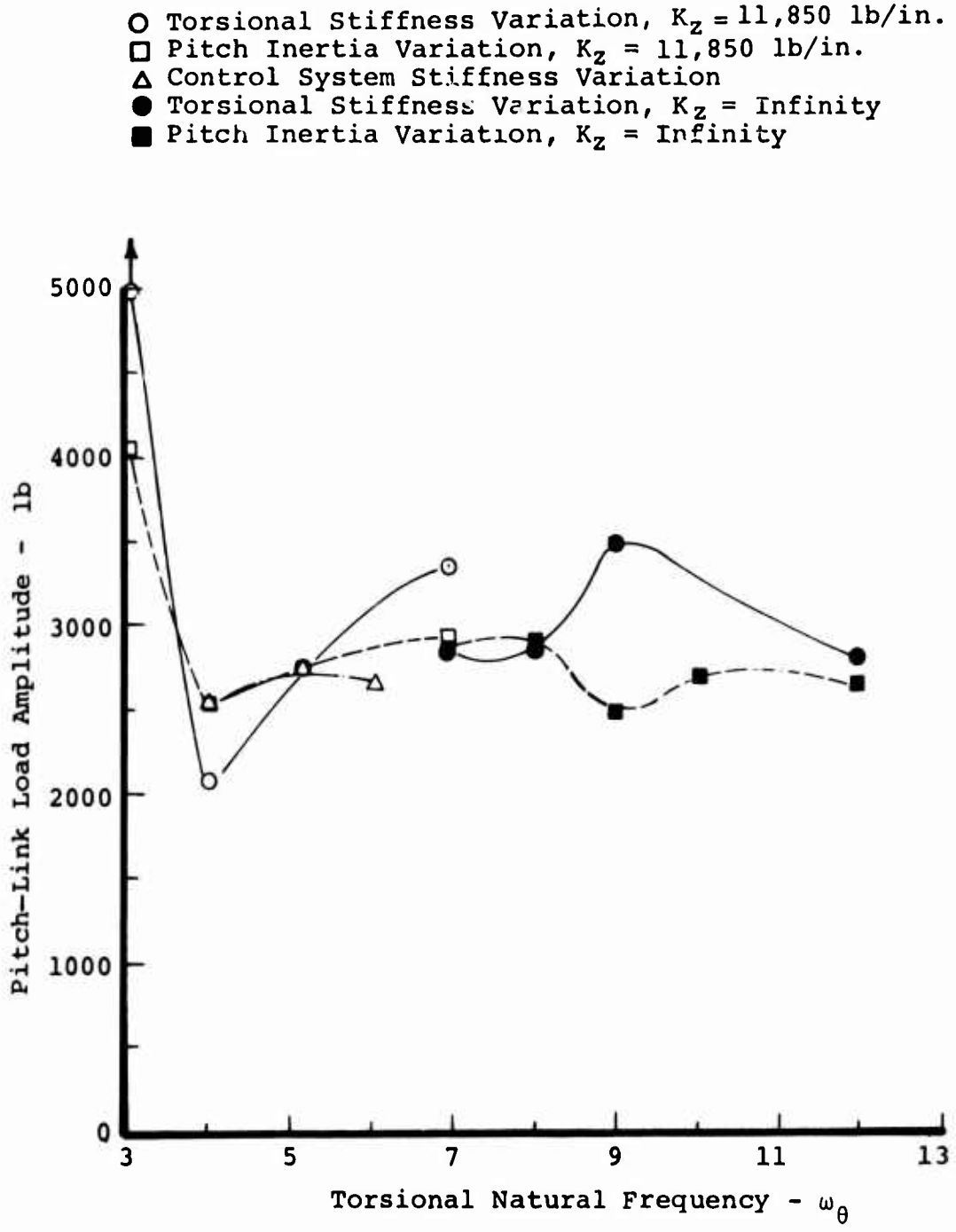

Figure 63. Variation of Pitch-Link Load Amplitude With Natural Frequency at 150 Knots and 0.115 Blade Loading.

the pitch inertia variation shows a slight dip in pitch-link load.

For both flight conditions, the variation in pitch-link load amplitude from one method of changing frequency to another is about 1000 pounds, which is in good agreement with the results obtained at 125 knots. This 1000-pound variation at a given frequency is comparable to the total variation over the range of frequencies. Therefore, at 150 knots, the method of generating a frequency is as important as the frequency obtained.

The figures show that variations in torsional stiffness lead to larger changes in pitch-link loads than do changes in control system stiffness or pitch inertia. This result was also observed at the 125-knot flight condition. This is particularly true for frequencies between 4/rev and 7/rev, where pitch inertia and control system stiffness variations also produce very small changes in pitch-link load amplitudes.

To summarize:

1) Changes in torsional stiffness are more effective in producing changes in pitch-link load amplitudes than changes in pitch inertia and control system stiffness.

2) At 125 knots, changes in torsional stiffness, control system stiffness, and pitch inertia lead to large changes in the pitch-link load with torsional natural frequency. At 150 knots, all the pitch-link load changes with torsional natural frequency are small (neglecting the 3/rev blade results).

3) The effect of torsional natural frequency at 125 knots is larger than the variation obtained between the different methods used to generate the frequencies. At 150 knots, the variation in pitch-link load amplitudes at a given frequency is as large as the variation with frequency.

4) Neglecting the 3/rev results, the maximum control loads occur near 9/rev and minimum control loads occur at 4/rev.

5) Reductions in control load magnitude at a given frequency are possible by simultaneously increasing the control system stiffness and reducing the torsional stiffness (i.e., by obtaining more elastic pitch deflection as blade live twist and less as blade pitch due to control system deflection).

-Effects of Blade Twist On Stall-Induced Control Loads

The effects of blade twist on stall-induced control loads were studied by changing the nominal 9-degree linear blade twist. This was done for blades having torsional natural frequencies of 3/rev, 4/rev, 5.2/rev and 7/rev at an airspeed of 125 knots for a blade loading of 0.115.

Figure 64 compares the trend of pitch-link load amplitude with natural frequency for each blade twist. Generally, each blade twist produces a trend of increasing pitch-link load amplitude with increasing natural frequency. The blades with 9 degrees and 12 degrees of twist have nearly the same load growth rate with increasing frequency up to a frequency of about 5.2/rev; above 5.2/rev, the blade with 12 degrees of twist has almost no load growth. The blade with 6 degrees of twist is insensitive to natural frequency changes for frequencies up to 5.2/rev. Above 5.2/rev, the load growth rate increases and is nearly the same as that of the standard 9-degree twist blade.

The figure also shows that at 3/rev, blade twist has almost no effect on the pitch-link load amplitude, while at 7/rev there is almost a 1000-pound load change. This may be due to the 3/rev blade's large live twist which allows the blade to elastically deform to nearly the same shape regardless of the built-in twist. On the other hand, the 7/rev blade is over 13 times stiffer in torsion than the 3/rev blade (torsional stiffness scaling factors of 0.25 and 3.3, respectively) and elastically deflects to a much lesser extent. Since the live twist is small, the built-in twist has a direct influence on the pitch angle distribution. Therefore, changes in built-in blade twist alter the pitch angle distribution resulting in pitch-link load changes.

For the blade frequencies examined, no one blade twist produces control loads which are either consistently higher or lower than any other. For example, the 12-degree blade twist produces the smallest pitch-link load at 3/rev and 7/rev; the highest load at 5.2/rev; and the median load at 4/rev. Therefore, pitch-link load amplitude appears to be a function of both blade twist and torsional frequency.

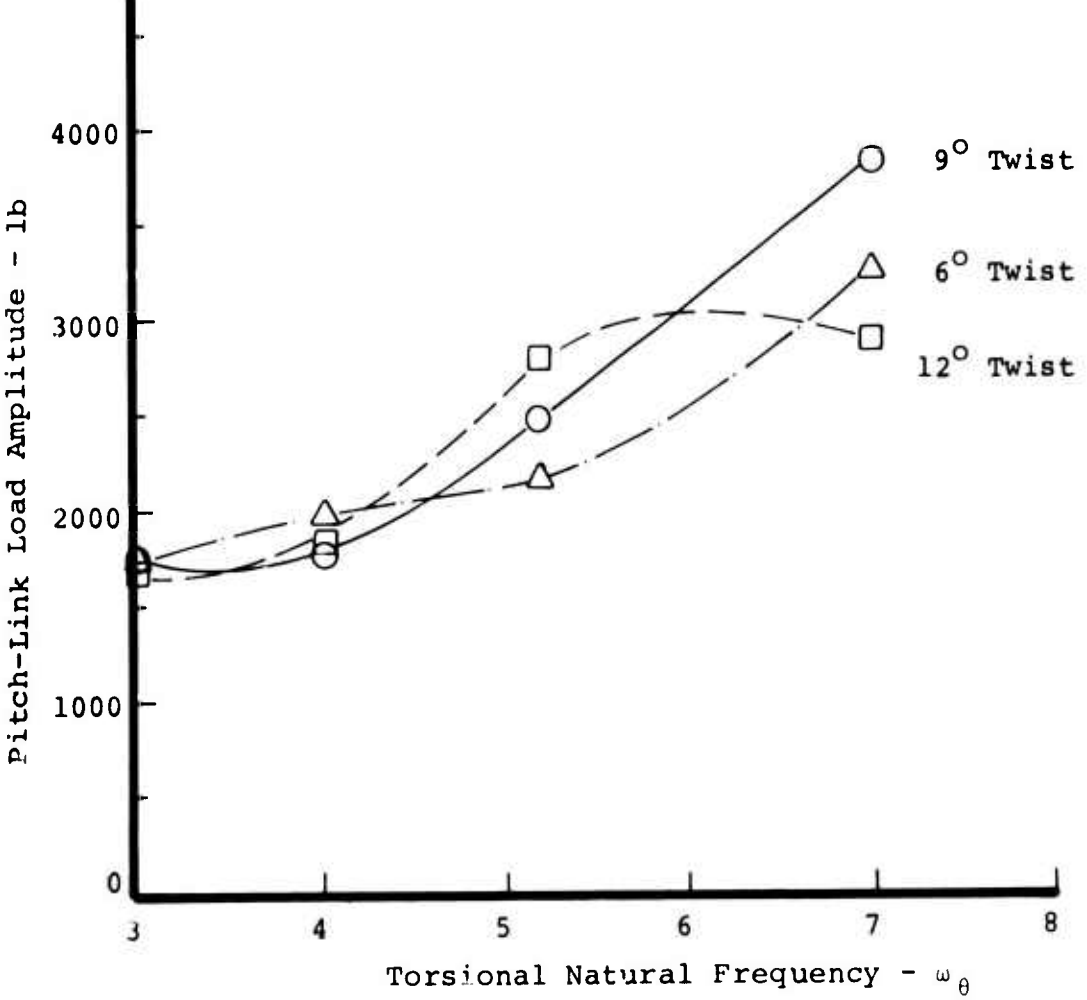

Figure 64. Variation of Pitch-Link Load Amplitude With Natural Frequency at 125 Knots and 0.115 Blade Loading for Blades of Various Twists.

In order to gain a better understanding of the effects of blade twist, additional flight conditions must be investigated, and the effects of blade twist on propulsive force and rotor power must be considered.

-Effect of Cyclic Pitch On Control Loads

One of the objectives of this study is to determine the effect of cyclic pitch on stall-induced control loads. Since stall is a function of the airfoil angle of attack, it is hoped that changes in cyclic pitch will result in a pitch-link load reduction. However, cyclic pitch changes by themselves are not meaningful since the rotor trim will not be maintained. If a cyclic pitch change reduces the control load along with a reduced propulsive force, the result is not useful since the rotor would not be able to overcome the fuselage drag, unless an auxiliary propulsive force is used.

Therefore, this study will consider two separate changes. First, the cyclic pitch will be independently varied plus and minus 2 degrees for both longitudinal and lateral cyclic. This will result in changes to both pitch-link load and rotor trim loads. Next, the rotor shaft tilt will be varied to bring the rotor propulsive force back to trim. The aim of this procedure is to determine if changes in cyclic pitch, with compensatory changes in shaft tilt to maintain the rotor trim, would reduce the pitch-link loads.

Figures 65 through 67 illustrate the variation of pitch-link load, propulsive force, side force, and rotor power for plus and minus 2-degree changes in longitudinal and lateral cyclic pitch at 150 knots for a blade loading of 0.115. No 3/rev blade results are shown, since this blade was divergent for all the cyclic pitch variations. The upper half of the figures illustrates the effect of lateral cyclic (θ_{1C}) for the 4/rev, 5.2/rev and 7/rev blades. Negative lateral cyclic always reduced the pitch-link loads, and positive lateral cyclic always increased the load. However, the maximum load reduction was only 185 pounds out of 2100 pounds for the 4/rev blade. In addition to reducing pitch-link loads, negative lateral cyclic pitch slightly reduces propulsive force and rotor power while causing a large change in side force. The side force change for the 5.2/rev blade is from 489 pounds to 1542 pounds, which is over 1000 pounds more side force than is needed for aircraft trim. Since longitudinal cyclic and rotor shaft tilt have little effect on side force, it would be necessary to introduce aircraft sideslip and steady roll angle to bring the aircraft back to trim. Therefore, since the pitch-link load reduction is small and since an extensive trim match investigation is beyond the scope of this study, changes in lateral cyclic will not be pursued further.

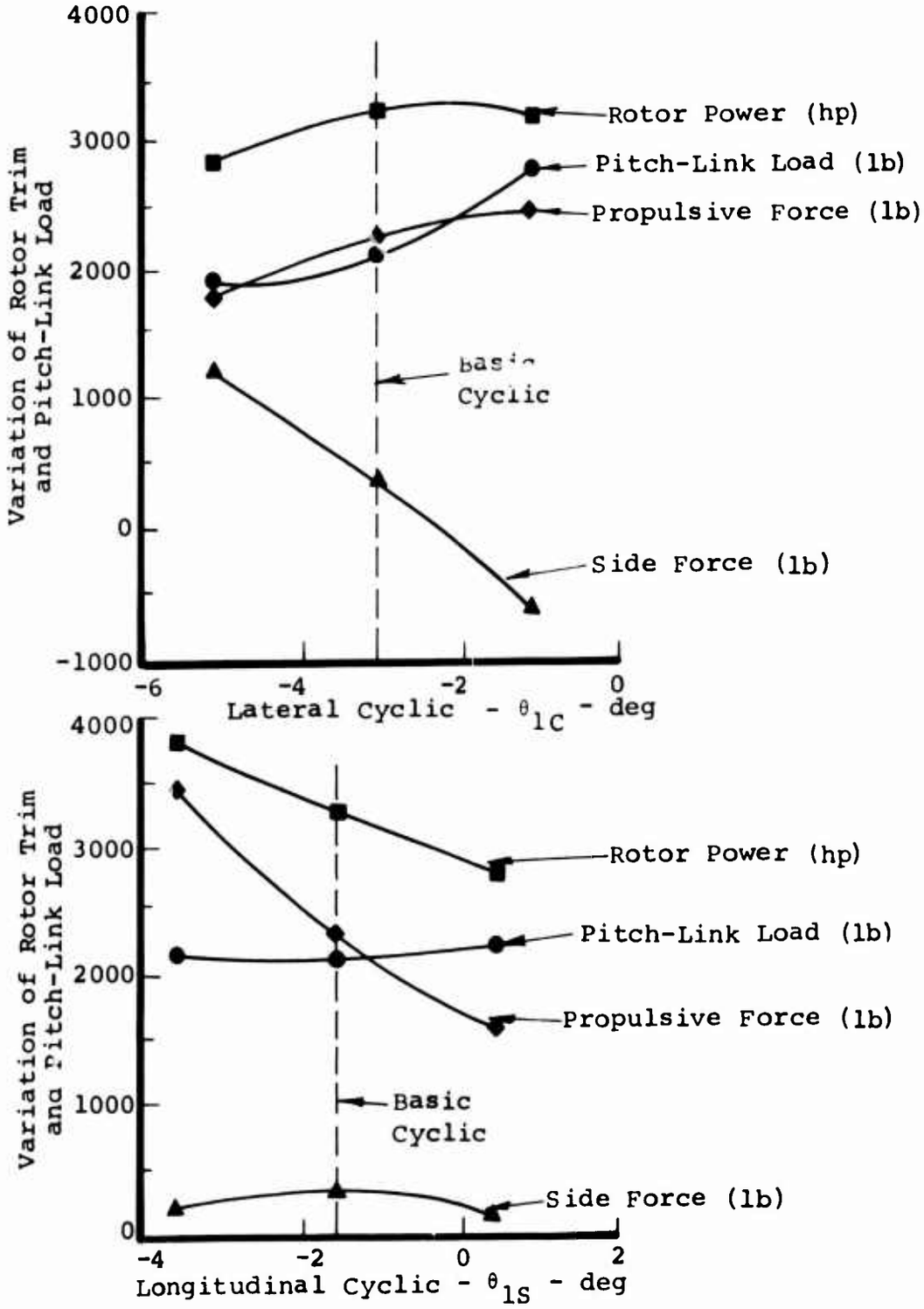

Figure 65. Effect of Cyclic Pitch Change for the 4/Rev Blade at 150 Knots for a Blade Loading of 0.115.

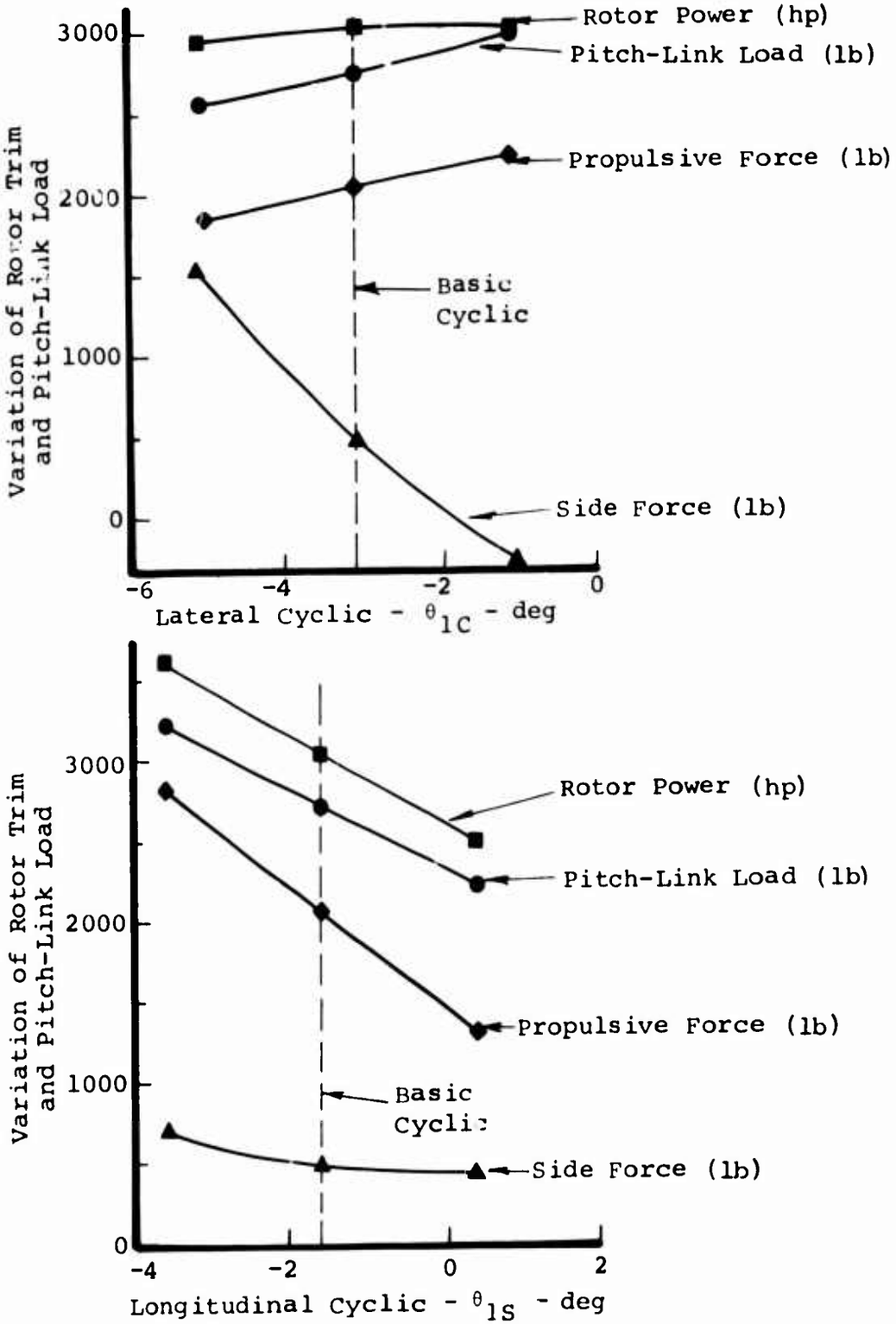

Figure 66. Effect of Cyclic Pitch Change for the 5.2/Rev Blade at 150 Knots for a Blade Loading of 0.115.

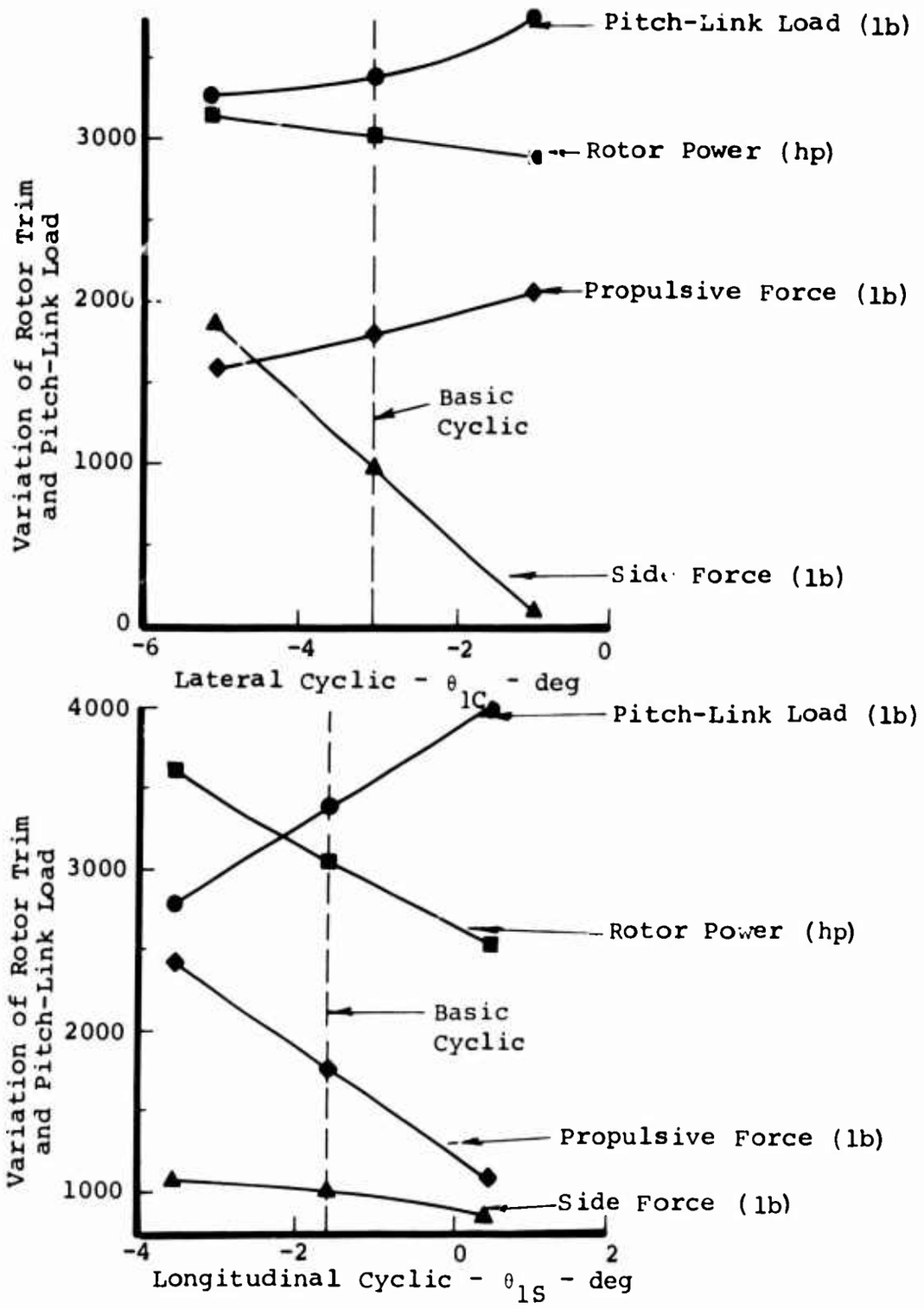

Figure 67. Effect of Cyclic Pitch Change for the 7/Rev Blade at 150 Knots for a Blade Loading of 0.115.

The bottom half of Figures 65 through 67 illustrate the variation of longitudinal cyclic (θ_{1c}). Changing the longitudinal cyclic pitch from -3.6 degrees to +0.4 degree (the basic trim is -1.6 degrees) produces little change for the 4/rev blade pitch-link load, reduces the 5.2/rev blade pitch-link load by 1000 pounds, and increases the pitch-link load by 1200 pounds for the 7/rev blade. For each blade, there is a correspondingly large reduction of propulsive force (over 1500 pounds for the 5.2/rev blade) and rotor power*, causing a significant change in the rotor trim. Therefore, the changes in pitch-link load are not meaningful, since the rotor is not trimmed and the results do not represent a single-main-rotor aircraft (unless an auxiliary propulsive system is used).

The 0.4-degree longitudinal cyclic pitch (i.e., a 2-degree increase over the basic cyclic pitch) was chosen to perform a propulsive force match by changing the rotor shaft tilt. This configuration was chosen since it produced a pitch-link load reduction for the basic blade (torsional frequency of 5.2/rev). The 2-degree decrease in longitudinal cyclic pitch produced a pitch-link load decrease for the 7/rev blade. Either cyclic change could have been used for the trim match, but the 2-degree increase was selected since it was hoped that this would reduce the basic blade loads.

Figure 68 shows the effect of reducing the rotor angle of attack from -11.5 degrees to -13.5 degrees by changing the rotor shaft tilt for a longitudinal cyclic of +0.4 degree. This change brings the propulsive force to within 250 pounds of the 2250 pounds required for trim. For all three blades, this revised cyclic pitch and shaft tilt increased the stall-induced pitch-link loads. The increase is 450 pounds for the 4/rev blade (a 21-percent increase), 300 pounds for the 5.2/rev blade (an 11-percent increase), and 450 pounds for the 7/rev blade (a 13-percent increase). Since increasing longitudinal cyclic by 2 degrees and reducing the shaft angle by 2 degrees increase the pitch-link load, it is possible that reducing the cyclic pitch by 2 degrees and increasing the shaft angle by 2 degrees may reduce the pitch-link load for all three blades.

In conclusion, this study shows that:

1) Lateral cyclic has a small effect on pitch-link load and propulsive force, but has a large effect on rotor side force.

---

*The observed reduction of rotor power along with a reduction in propulsive force reinforces the results obtained in the section on performance.

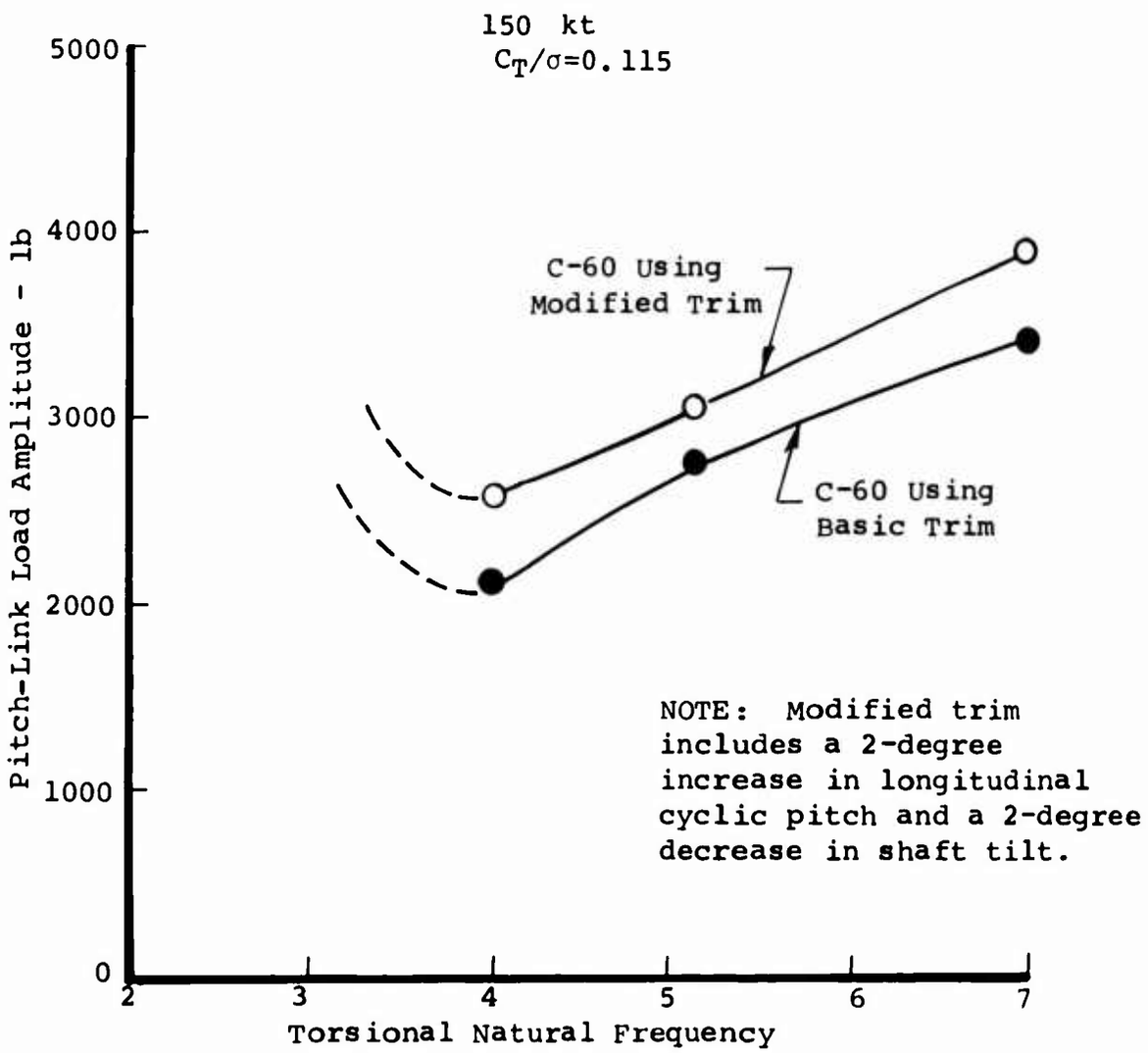

Figure 68. Effect of Changing Cyclic Pitch and Rotor Shaft Tilt on Pitch-Link Load for a Constant Propulsive Force.

2) Longitudinal cyclic has a large effect on pitch-link loads and rotor propulsive force.

3) Changing the rotor longitudinal cyclic pitch and shaft tilt while maintaining an approximate trim does change the stall pitch-link load. An expansion of this study may determine a new cyclic pitch-shaft tilt combination that will reduce the pitch-link loads.

CONTROL LOAD PREDICTION WITH A FULLY COUPLED ROTOR ANALYSIS

The section entitled EFFECTS OF TORSIONAL NATURAL FREQUENCY ON STALL-INDUCED DYNAMIC LOADS presented analytical trends of pitch-link load amplitude with blade torsional natural frequency for a wide range of flight conditions. Also presented were the effects of various blade and trim parameters on the relationship between control loads and torsional natural frequency.

These results were obtained by using the aeroelastic rotor analysis (program C-60). This program (described in Appendix I) is essentially a coupled flap-pitch dynamic response analysis linked to an airloads analysis by means of an iterative procedure. An approximation for the flap-lag-pitch coupling is provided in the program, but the lag degree of freedom is not fully coupled into the blade response calculations.

However, an approximate coupling of the lag blade response with the coupled flap-pitch blade response may not be adequate for obtaining stalled pitch-link loads*. A fully coupled flap-lag-pitch analysis would properly account for the torsional load due to inplane loads times flap deflection and vertical loads times the lag deflection.

A fully coupled flap-lag-pitch rotor analysis (program C-70) has been recently developed by the Boeing Vertol Company under contract with the Air Force (Reference 5) to model prop rotors. This program links the same aerodynamic loads analysis as used on program C-60 to a fully coupled blade response analysis.

---

*The section entitled CORRELATION OF MODEL TEST DATA showed that, when the complete effects of the lag degree of freedom were added to the last iteration control loads, a significant improvement in the correlation was realized, even though the program did not iterate on these effects.

This response analysis also accounts for variable shear center location, variable vertical neutral axis location, and large blade twist. However, providing full coupling greatly increased the program running time, so the running time of program C-70 is approximately five times that of program C-60. Due to the large running time, the C-70 program was not used to investigate the large number of flight conditions covered on the previous sections. However, it was planned to use the C-70 program to spot-check the C-60 results.

In order to establish the reliability of the C-70, a correlation was performed with the standard reference blade wind tunnel model data.

Figure 69 compares the measured data and the C-70 predictions of blade torsion amplitude for four different blade loadings at an airspeed of 133.6 knots. In general, for flight conditions below stall, the agreement between the measured data and the analytical results is fair. The worst agreement occurs at a blade loading of 0.07, where the C-70 analysis overpredicts the load by about 33 percent.

The analytical results for the substall conditions show a predominately 1/rev waveform which is typical of the unstalled model data.

The measured data shows that stall inception occurs at a blade loading of about 0.09. The C-70 analytical results are in excellent agreement with the model stall inception, whereas the C-60 program predicts inception prematurely.

Above stall, the C-70 analysis overpredicts by 400 percent. In order to determine the cause of the poor correlation, an extensive examination of the C-70 program was undertaken. This examination uncovered an error in the aeroelastic coupling matrix which provides iteration stability. Corrective action has been initiated. Once program checkout is complete, a correlation can again be attempted.

The C-70 analysis could not be used to confirm the C-60 results presented above due to the poor comparison obtained with the model test results. A modification of the C-70 program was beyond the scope of this study.

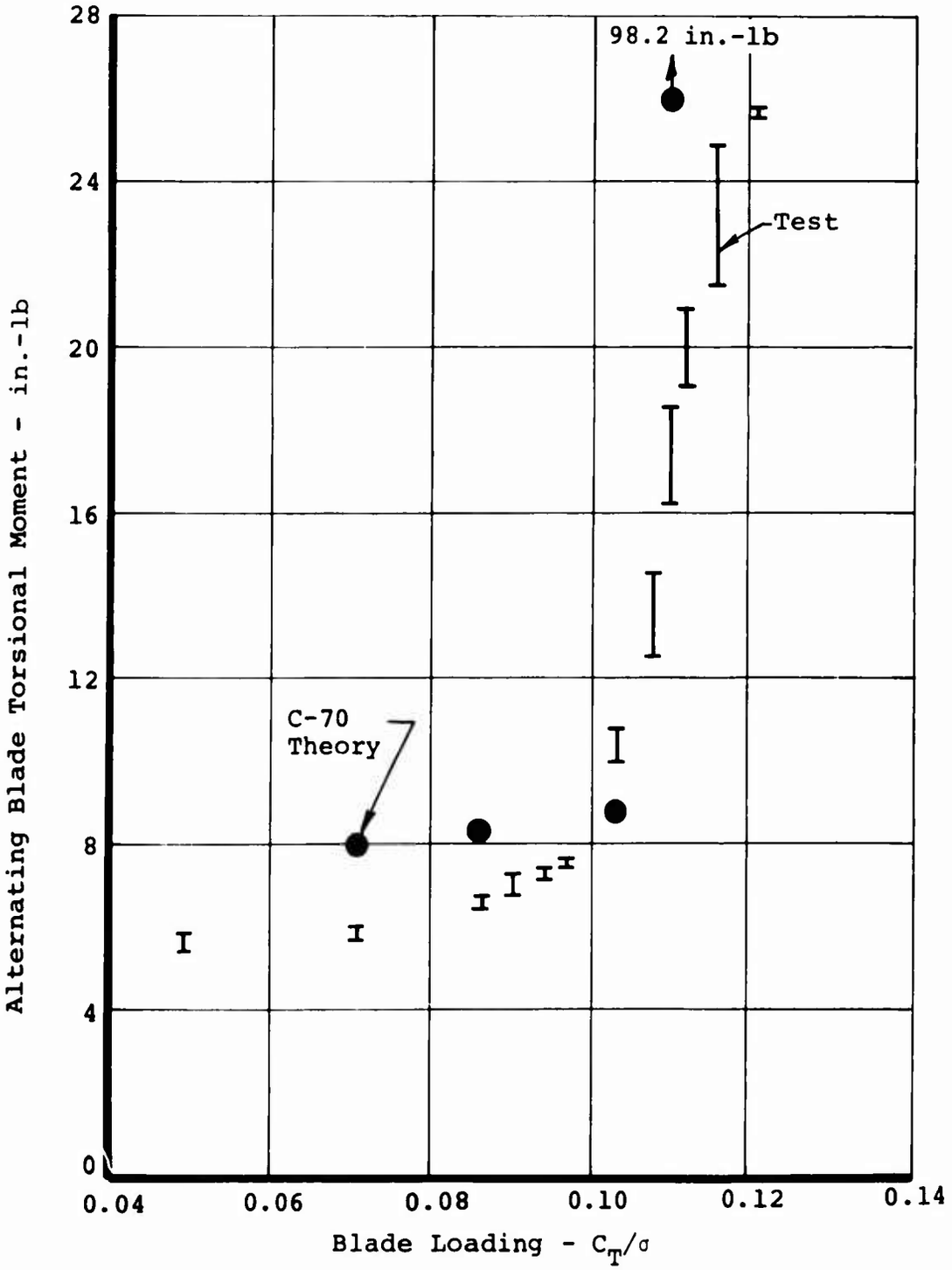

Figure 69. Comparison of Measured and Calculated Blade Torsion Amplitude for the Standard Reference Blade (Fully Coupled Analysis), V = 133.6 Knots .

CONCLUSIONS

For flight conditions at high blade loadings or airspeeds, the rotor control system experiences a rapid load growth resulting from stall-induced blade torsional moments. These loads frequently grow so large that the aircraft flight envelope is restricted before the aircraft power limit is reached. Limited analytical and experimental data show that changing the blade torsional properties can significantly reduce the large stall-induced control loads. The results of this study verify the control load reduction over a large flight region, indicating that a practical means for reducing stall-induced control loads is possible. The following conclusions can be drawn from this study.

1) The aeroelastic rotor analysis (program C-60) generally correlates well with model rotor torsional loads for blades with torsional natural frequencies of 3.1/rev, 4.25/rev, and 5.65/rev. The correlation includes both substall and stalled blade torsion loads for an advance ratio of 0.3. However, program deficiencies have been uncovered which require additional analytical development.

2) Torsional frequency is not a universal parameter that determines the magnitude of the stall-induced loads as indicated in Reference 1. At low airspeeds (125 knots), torsional frequency, regardless of whether it was obtained by varying blade torsional stiffness, control system stiffness or blade pitch inertia, is the major determinant of stall loads.

3) Changes in blade torsional properties can reduce the stall-induced pitch-link loads. These changes include torsional stiffness, control system spring rate, pitch inertia, and blade twist.

4) Reducing the blade torsional stiffness provides the largest reduction in stall-induced control loads. There is some indication that reduced torsional stiffness with a very stiff control system spring rate may reduce loads even more than a stiffness reduction with the nominal control system spring rate.

5) Reducing the CH-47C rotor blade torsional stiffness to one-half* produced a large stall-induced control load reduction at 125 knots and 150 knots for a wide range of blade loadings. At 175 knots, for reasonable rotor power, there is little control load difference between blades with 0.5, 1.0, and 3.3 times the blade torsional stiffness*. The net effect of reducing the stiffness by one-half is a large flight envelope increase for airspeeds up to 175 knots.

6) Reducing the CH-47C rotor blade torsional stiffness to one-quarter* its original value results in a blade that experiences advancing blade torsional divergence for the 150-knot and 175-knot flight conditions.

7) The rotor blade with the torsional stiffness increased by a factor of 3.3* has the smallest advancing blade load growth with airspeed. This is the highest stiffness for which an extensive investigation was performed. At very high airspeeds (175 knots and above) the advancing blade load growth becomes more important than the retreating blade stall spikes. In this environment the stiffest blade will probably provide the lowest torsional loads.

8) The fully coupled rotor analysis (program C-70) correlates well with substall model rotor torsional loads, but greatly overpredicts the stall-induced load. An error has been discovered in the dynamic/aerodynamic coupling matrix, and the analysis is not yet considered reliable.

The present analytical investigation established that a significant reduction of stall control loads is possible; what is needed now is extensive test verification, additional analytical investigation, and improved theoretical methods.

---

*

Torsional Stiffness Factor	Torsional Frequency
1.0	5.2/rev Basic CH-47C blade
0.5	4.0/rev
0.25	3.0/rev
3.3	7.0/rev

RECOMMENDATIONS

This study shows that the large stall-induced control loads can be reduced through blade design changes. Though these results are informative, much work remains before a real hardware payoff can be realized. Short-term efforts in the area of model test verification, additional analytical investigation, and improved theoretical methods are needed.

A meaningful wind tunnel test program is needed to validate the analytical load results. Using model blades with stiffness changes to provide torsional natural frequencies of 4.0/rev, 5.5/rev and 7/rev would probably provide the most useful results. Remote collective and cyclic pitch would be required to simulate trimmed rotor flight conditions so that the resulting control loads can be compared directly.

To more fully understand the influence of blade torsional properties on control loads, the following is recommended:

1. Investigate the mechanism that generates the large retreating blade stall-induced control loads and determine why a blade with large live twist* has the lowest load.

2. Examine the advancing blade load mechanism and determine the divergence boundary for blades with different torsional properties.

3. Continue the investigation of the effects of blade twist and cyclic pitch on control loads and initiate an investigation of the effects of center of gravity, pitch axis, and shear center location.

4. Determine the control load envelopes for other realistic rotors, including:

   The high-aspect-ratio Bell type rotor, which has a relatively high pitch inertia and a low torsional frequency.

   The large-aspect-ratio Sikorsky-type rotor, which has a relatively low pitch inertia and high torsional frequency.

   A Kaman-type aero tab controlled 'soft root' rotor.

   A hingeless rotor, to determine if articulated rotor results can be generalized to include a nonarticulated rotor.

*This blade has one-half the CH-47C blade's torsional stiffness and a 4/rev torsional frequency.

Improved analytical methods are needed to eliminate the deficiencies uncovered in the theory/test loads comparison, such as:

1. Completing the development of the coupled flap-lag-pitch rotor analysis.

2. Upgrading the unsteady aerodynamic theory by:

   Removing the deficiency in the blade plunging idealization

   Adding the effects of an oscillating tangential flow

   Continuing to refine the dynamic C_M overshoot term

   Determining the proper value for the pitching stall delay parameter for Mach numbers of 0.6 and above.

An upgraded analysis will not only provide more reliable control load results, but it would also result in the development of an available stepping stone toward understanding and eventually toward solving other rotor problems.

LITERATURE CITED

1. Tarzanin, F. J., Jr., and Gabel, R., BLADE TORSIONAL TUNING TO MANAGE ROTOR STALL FLUTTER, Presented at the AIAA 2nd Atmospheric Flight Mechanics Conference, AIAA Paper No. 72-958, September 1972.

2. Tarzanin, F. J., Jr., PREDICTION OF CONTROL LOADS DUE TO BLADE STALL, 27th Annual National V/STOL Forum of the AHS, Preprint No. 513, May 1971.

3. Theodorsen, T., GENERAL THEORY OF AERODYNAMIC INSTABILITY AND THE MECHANISM OF FLUTTER, NACA Report 496, National Advisory Committee for Aeronautics, Washington, D.C., 1935.

4. Carta, F. O., et al, ANALYTICAL STUDY OF HELICOPTER ROTOR STALL FLUTTER, 26th Annual Forum of the AHS, June 1970.

5. Tarzanin, F. J., Jr., et al, V/STOL DYNAMICS AND AERO-ELASTIC ROTOR-AIRFRAME TECHNOLOGY - VOLUME II, AFFDL-TR-72-40, September 1972.

6. Gormont, R. E., A MATHEMATICAL MODEL OF UNSTEADY AERO-DYNAMICS AND RADIAL FLOW FOR APPLICATION TO HELICOPTER ROTORS, USAAMRDL Technical Report 72-67, May 1973.

7. Yntema, R., and Gabel, R., HELICOPTER ROTOR HUB VIBRATORY FORCES SYSTEMIC VARIATION OF FLEXIBLE BLADE PARAMETERS, Boeing Vertol Company, R-244, May 1961.

8. Tarzanin, F. J., Jr., and Henderson, B. O., ROTOR ANALY-SIS PROGRAM D-82, Boeing Vertol Company, DYMR-5, September 1965.

9. Henderson, B. O., ROTOR LOAD CORRELATION REPORT, Boeing Vertol Company, DYMR-9, December 1965.

10. Tarzanin, F. J., Jr., and Thomas, E., AEROELASTIC ROTOR ANALYSIS D-94/95, Boeing Vertol Company, D8-0614, May 1967.

11. Gross, D., and Csoboth, F., TANDEM HELICOPTER ROTOR LOADS CORRELATION STUDY, Boeing Vertol Company, D8-1023, January 1968.

APPENDIX I

DESCRIPTION OF THE AEROELASTIC ROTOR ANALYSIS (PROGRAM C-60)

The aeroelastic rotor analysis (designated program C-60) calculates rotor blade flapwise, chordwise and torsional deflections and loads together with rotor performance, control system forces and vibratory hub loads. Articulated and hingeless rotors with from two to nine blades and low twist may be analyzed. The analysis is limited to calculations involving steady-state flight at constant rotor tip speeds. The blades may be of arbitary planform, twist and may contain up to 3 different airfoil sections.

The analysis considers coupled, flapwise-torsion deflections and uncoupled, chordwise deflections of the rotor blades. The blade is represented by 20 lumped masses, interconnected in series by elastic elements. Boundary conditions for either articulated or hingeless rotors are applied and the solution is obtained by expanding the variables in a 10-harmonic Fourier series.

Airload calculations include the effects of airfoil section geometry, compressibility, stall, three-dimensional flow, unsteady aerodynamics, and nonuniform inflow. Static airfoil tables are used to account for compressibility, static stall, and airfoil shape. The unsteady aerodynamic loads are calculated by modifying the static loads resulting from the airfoil tables to include Theordorsen's shed wake function, dynamic stall effects based on oscillating airfoil data, and yawed flow across the blade.

The nonuniform inflow calculations are based on a tip and root vortex trailed from each blade. Through an iterative technique, each trailed vortex is made compatible with the calculated blade lift distribution, and the lift distribution is compatible with the nonuniform downwash field. The vortex wake is assumed to be rigid and to drift relative to the hub with a constant resultant velocity composed of thrust-induced uniform downwash and the aircraft airspeed.

A flow diagram of this analysis is shown in Figure 70. The solutions for the nonlinear aerodynamic loads and the coupled flap-pitch blade response are performed in series, and up to ten iterations between the airloads and blade response are used to obtain the final solution. An iterative solution is used to account for the nonlinear coupling between the blade deflections and airloads that result from airfoil stall and compressibility. Iteration techniques are also used to obtain compatibility between the airloads, downwash, and vortex strength, and to obtain a match with a specified rotor thrust. A brief outline of the computer procedure is given below,

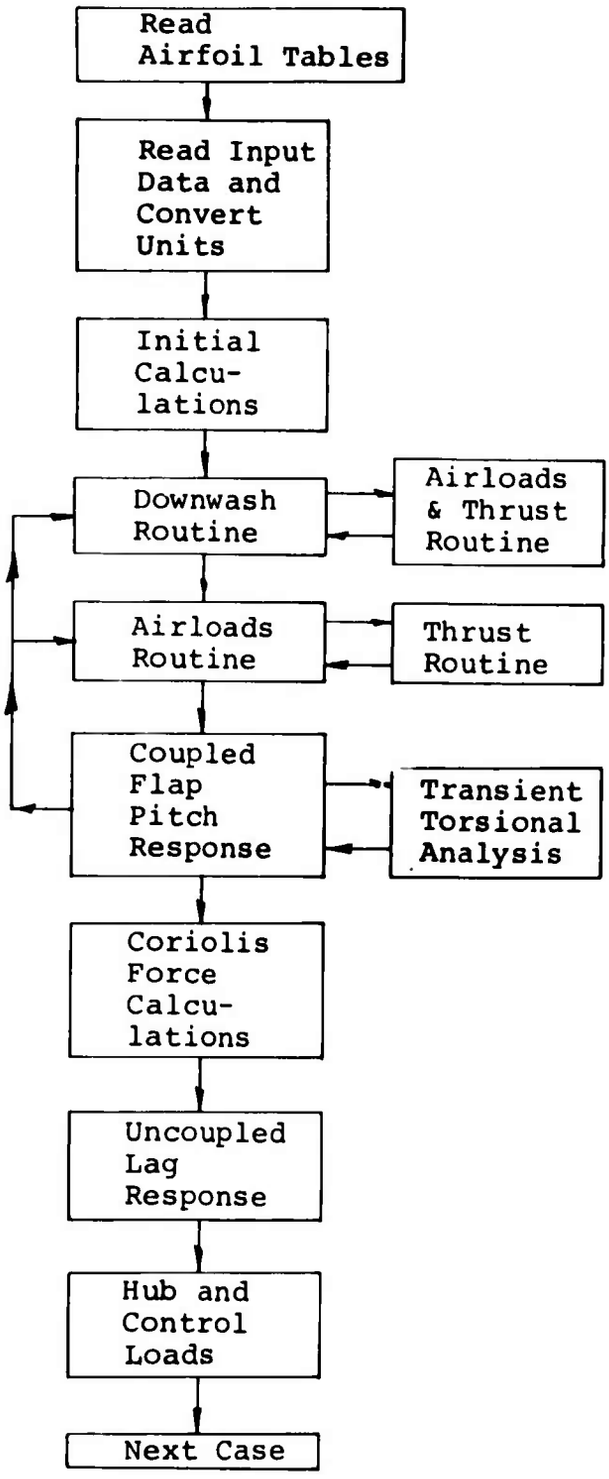

Figure 70. Program C-60 Flow Diagram.

followed by a description of the methodology used in this analysis.

The C-60 program is started by calculating initial deflections and defining boundary conditions from input (i.e., collective and cyclic pitch and root flap deflections). These inputs are either known (as in the case of a model test or where these quantities were measured in flight) or are obtained from an aerodynamic trim analysis. The Boeing program Y-92 calculates the rotor trim (i.e., aircraft angle of attack, thrust, collective pitch, cyclic pitch, and blade root flap angle) by considering aircraft gross weight, center of gravity, fuselage drag, rigid blade properties, quasistatic airfoil characteristics, nonuniform downwash, forward speed, and rotor speed to determine the airloads required to maintain the free-flight aircraft in equilibrium for a steady-state flight condition.

Next, the rotor-induced velocities are calculated to provide a downwash field for each blade. Uniform downwash is determined either from input or a simple calculation. If only uniform downwash is required, the program exits from the downwash routine and proceeds to the airload routine. If nonuniform downwash is required, a complex iteration loop is initiated. The downwash field resulting from this routine is used throughout the program with no updates or modifications.

For clarity, when calculating tandem-rotor downwash, the two rotors are designated as the "prime" rotor and the "other" rotors. If the program is calculating aft rotor loads of a tandem-rotor helicopter, the aft rotor is the prime rotor and the forward rotor is the other rotor. In the case of a single-rotor aircraft, the main rotor is always the prime rotor.

For a tandem-rotor helicopter, the program first calculates a compatible self-induced downwash for the other rotor. Then, the resulting vortex field of the other rotor is used to calculate the rotor interference downwash on the prime rotor. The prime rotor self-induced downwash is then calculated in the already defined rotor interference downwash field. The final prime rotor downwash is then the sum of the rotor interference downwash plus the self-induced downwash of the prime rotor. For a single-rotor aircraft, only the self-induced downwash is calculated.

Calculating the self-induced downwash requires an iteration between airloads, trailed vortex strength and downwash. This iteration is performed up to ten times to insure compatibility among these three quantities. Each time the partial airload routine is entered, an iteration between the thrust routine and airloads may be performed. This thrust routine iteration is performed when agreement with the thrust

defined by the trim program is desired throughout the analysis. To obtain this constant thrust, every time the airload routine is entered, an iteration process is performed on the airloads by altering the steady root collective pitch until a collective angle is found which corresponds to the required thrust. If no thrust match is required, the thrust routine iteration is not performed.

After the downwash field is calculated, the rigid blade deflections (initial deflections), nonuniform downwash, and nonlinear aerodynamic coefficients are then combined to calculate the airloads. Here again, a thrust routine iteration is provided to guarantee a thrust match if desired. Following the airload routine, the aerodynamic vertical force and pitching moment are harmonically analyzed and used as forcing functions to calculate the coupled flap-pitch dynamic response of the blade. Since the forcing loads are nonlinear functions of the forced response (due to stall and compressibility), iteration between aerodynamic loads and the blade dynamic response is required to provide feedback. To perform the iteration, the most recently calculated coupled flap-pitch deflections are substituted back into the aerodynamic analysis, the aerodynamic forcing functions are evaluated again, and the coupled flap-pitch response analysis is repeated. The iteration is continued until a specified number of iterations (usually ten) have been completed. The number of iterations specified should be sufficient to insure a converged solution.

After the coupled flap-pitch airload iteration is complete, the Coriolis force is calculated from the coupled flap-pitch deflections and added to the tangential aerodynamic forces for the lag forcing function. The uncoupled lag response is calculated in the same manner as the coupled flap-pitch response; however, no iterations are performed. The influence of lag deflections on airloads and the coupled flap-pitch response are assumed to be negligible.

Next, blade radial forces are calculated by considering blade shortening resulting from flap and lag deflections, pitch-link loads are calculated by determining the blade system pitching moment, and all loads are resolved from the rotor disc system into the blade system. Finally, fixed and rotating system hub and lower control loads are evaluated by combining the root shears and moments with the system geometry.

The program flow diagram shows that the aeroelastic rotor analysis is basically an aerodynamic analysis coupled by iteration to a dynamic analysis.

HISTORY OF DEVELOPMENT

This program has undergone continual modifications and improvements since its inception. The original analysis, which used ten mass and elastic bays, four harmonics of loads and deflections, uniform inflow, and linear aerodynamics, was developed by the Boeing Vertol Company's Dynamics Group for their study of helicopter rotor hub vibratory forces under Navy Bureau of Weapons Contract NOa (s) 60-6112c, May 1961. The program development and parameter study results are given in Reference 7. Following the completion of this contract, the analysis was expanded to include 15 mass and elastic bays, 10 harmonics of loads and deflections, and nonlinear aerodynamics, including stall and compressibility effects. As programmed on the IBM 650, the actual computing time of the expanded analysis was approximately 2 hours and required hand assembly of subprogram inputs. With the replacement of the IBM Model 650 computer by the faster computers and subsequent reprogramming into a continuous chain, the unit running time was reduced to approximately 10 minutes. Taking advantage of the faster computer, the Research and Development Group extended the rotor analysis to include special input formats, aerodynamic performance calculations, and an internal nonuniform downwash calculation. These improvements are reported in the program description and user's instructions (Reference 8, September 1965). Since downwash is a major source of higher harmonic rotor and hub loads, the development of an internal nonuniform downwash computation significantly improved rotor load prediction capability (Reference 9, December 1965).

In subsequent years, further improvements have been made in the thrust routine, pitch and elastic matrices, flap boundary conditions, and downwash representation. Special problems, such as mechanical flap-pitch coupling (δ_3), linear hub motion, and flap dampers, can now be analyzed. The engineer has the option to perform either a flexible- or a rigid-blade analysis. Either linear or nonlinear aerodynamics may be employed, and additional options are available to represent downwash. The program's aerodynamic theory was expanded to include an approximation for the unsteady shed wake of an oscillating airfoil, which significantly improved pitch-link load prediction capability. Any airfoil section may be used in the load calculations by inputting two-dimensional static airfoil data tables. Previously, only representative stall and compressibility effects were accounted for. In addition, blades with variable airfoil sections that change thickness ratio or camber with blade span can be accounted for by defining up to three airfoil sections along the blade and linearly interpolating between them. A description of the program with all the above changes has been documented in Reference 10, May 1967. A comparison of predicted loads with test is presented in Reference 5, January 1968.

Since 1967 the theory has been further improved to consider blade tab and trailing-edge bends, an increased number of mass stations (from 15 to 20) and aerodynamic stations (from 10 to 15), viscous damping in the pitch links, angular hub motion in the blade load calculations, rotors with from two to nine blades, and a three-point or four-point swashplate actuator system for the lower control load calculations. In addition, there were two major improvements: (1) the development of a nonuniform downwash theory that includes compatibility between vortex strength, downwash, and the airload distribution (August 1968); and (2) the inclusion of a nonlinear, unsteady aerodynamic theory (Reference 2, May 1971). The downwash modifications improved blade loads and probably hub loads. The new unsteady aerodynamics provided a signficant improvement in rotor performance prediction and can now predict the sharp increase in control loads that occur at the high C_T/σ or high airspeeds associated with blade stall (Figure 71).

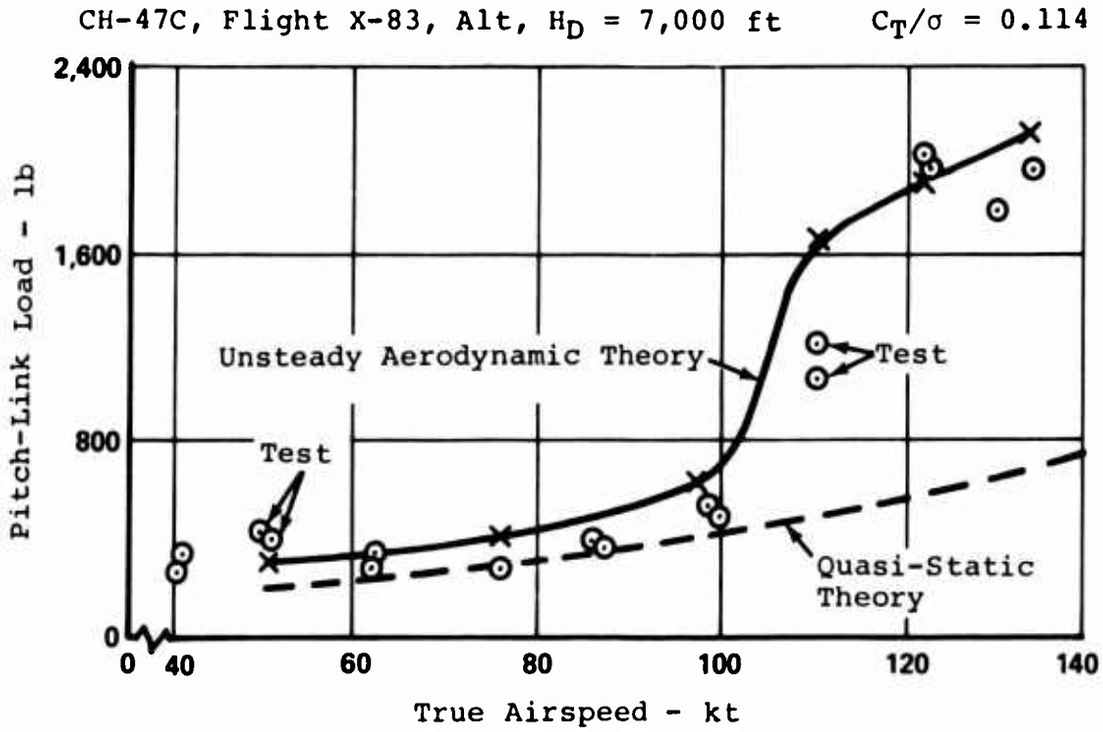

Figure 71. Comparison of Test and Analytical Pitch-Link Loads for an Airspeed Sweep.

APPENDIX II

WIND TUNNEL TEST PROGRAM (PROGRAM 089)

The Boeing Vertol Company 089 Wind Tunnel Test Program involved the measurement of blade and hub loads for three 3-bladed,6-foot-diameter model rotors at a $\mu = 0.3$ and a range of rotor thrust. Each of the three blade sets had NACA 23010 airfoil section with a constant 2.3-inch chord. The first set of blades had a torsional natural frequency of 4.25/rev and was constructed of fiberglass using conventional cross-ply torsion wrap. The second set of blades had mass properties similar to the first blade set, but had a torsional natural frequency of 3.1/rev. These blades were constructed with fiberglass using a uniply torsion wrap, which substantially reduced the blade torsional stiffness. The third set of blades had a torsional natural frequency of 5.65/rev and was constructed of morganite. Though the morganite blades were not significantly stiffer than the first set of blades, they had significantly lower torsional inertia, which accounts for the higher torsional natural frequency. The blades were connected to the hub without torsion bearings, and there were no connecting pitch links. This was done so that the blade torsional natural frequency would be known without concern for potential coupling with a dynamic control system. However, this resulted in the loss of cyclic pitch control and a requirement for manual setting of the blade collective.

Prior to each run, the collective pitch was set and the shaft incidence angle lowered to approximately 20 degrees into the wind. The rotor rpm was then brought up to the desired tip speed at an advance ratio (μ) of 0.3. In order to increase the rotor C_T/σ, the rotor shaft was slowly tilted toward the vertical.

TEST RESULTS

At a C_T/σ of approximately 0.1, the torsion loads began growing, indicating the development of stall flutter. It was intended that nondimensional propulsive force ($\bar{X}$) of about 0.2 would be obtained in the stall flutter regime, to represent actual flight conditions. This was to have been done by performing repeated shaft tilt sweeps at increasing collective pitch settings until the desired propulsive forces were obtained.

However, due to the lack of cyclic pitch, large blade flapping occurred at the high C_T/σ conditions and limited the collective settings through the generation of large chord bending loads and pounding of the up-flap stop. The result was that negative propulsive forces were obtained in much of the stall flutter region.

DATA SELECTED FOR CORRELATION

Table I lists the selected test points along with the wind tunnel operating conditions, trim data and measured loads.

Runs 317 (low-stiffness blade (GJ)), 306 (standard reference blade) and 323 (morganite blade) were selected because it was desired to correlate with rotors having similar propulsive force variations with thrust. From each of these runs, five test points were selected which covered the range of available C_T/σ and which provided at least one flight condition below stall, one condition in transition, and two stalled conditions.

Each blade on each rotor was instrumented to record blade torsion data. Due to gauge failures, however, only two gauges on the standard reference blades and only one gauge on the morganite blades were operational.

MODEL BLADES' PHYSICAL PROPERTIES

To adequately perform the theory/test comparison, the model blades' physical properties must be known accurately. However, at the time of the contract award, only theoretical distributions calculated from an idealized structure of the model blades were available. Therefore, to insure accuracy, direct measurements of the most significant blade physical properties were made to confirm the theoretical distributions.

Blade Weight

The experimental blade weight distribution was found by cutting a model blade into strips about 2 inches in length, weighing each strip, and calculating a weight per unit length. Figure 72 compares the theoretical and measured weight distributions for the standard reference blade. Since the two distributions agree within 10 percent of each other, the theoretical weight distribution was used. Since the cut-up standard reference blade was available, only the standard reference blade weight distribution was confirmed.

Blade Chordwise Center of Gravity

The distribution of blade chordwise center of gravity was not directly measured. Instead, a comparison was made of the measured center-of-gravity location of the entire blade and the theoretical center-of-gravity location obtained by integrating the theoretical center-of-gravity distribution.

The measured center-of-gravity location was obtained by placing each blade in a fixture of known geometry and center-of-gravity location and recording the change in readings on two balances. By summing moments, the location of the center of gravity could

TABLE I. SUMMARY OF SELECTED DATA

Test Point	μ	C_T/σ	α_s	$\bar{X}$	Alt. Blade Torsion	β_0	β_{1c}	β_{1s}
Low GJ Blade								
Run 317, ω_θ = 3.1/Rev,								
$\theta_{.75}$ = 16.5 Deg (Zero Thrust Collective as Reference)								
10	0.278	0.0889	-18.1	0.243	6.64	4.38	- 7.11	-0.007
12	0.281	0.095	-16.1	0.192	9.41	4.66	- 8.37	0.40
16	0.289	0.1123	- 9.15	0.037	15.67	5.16	-11.4	-1.46
17	0.291	0.1161	- 7.05	0.121	16.64	5.23	-11.77	1.72
18	0.292	0.1179	- 6.08	0.171	15.98	5.24	-12.0	1.77
Standard Reference Blade								
Run 306, ω_θ = 4.25/Rev,								
$\theta_{.75}$ = 15 Deg (Zero Thrust Collective as Reference)								
9	0.269	0.0711	-23.05	0.289	5.95	2.56	- 5.81	-0.9
10	0.275	0.0863	-19.99	0.267	6.73	3.21	- 6.61	-1.07
14	0.281	0.1027	-15.07	0.152	10.81	3.75	- 8.54	-1.13
16	0.285	0.1103	-11.92	0.037	18.56	4.04	-10.1	-0.97
19	0.291	0.1204	- 7.08	0.162	25.6	4.41	-11.5	-0.55
Morganite Blade								
Run 323, ω_θ = 5.65/Rev,								
$\theta_{.75}$ = 13.5 Deg (Zero Thrust Collective as Reference)								
5	0.276	0.0808	-19.31	0.244	6.05	4.5	- 7.32	-1.59
6	0.279	0.0885	-17.62	0.216	6.09	4.87	- 8.15	-1.75
7	0.282	0.0963	-15.66	0.177	8.24	5.15	- 9	-1.94
8	0.285	0.1035	-13.58	0.113	11.6	5.9	- 4.44	-2.06
11	0.292	0.1148	- 7.6	0.093	21.66	8.91	-12.54	-4.98

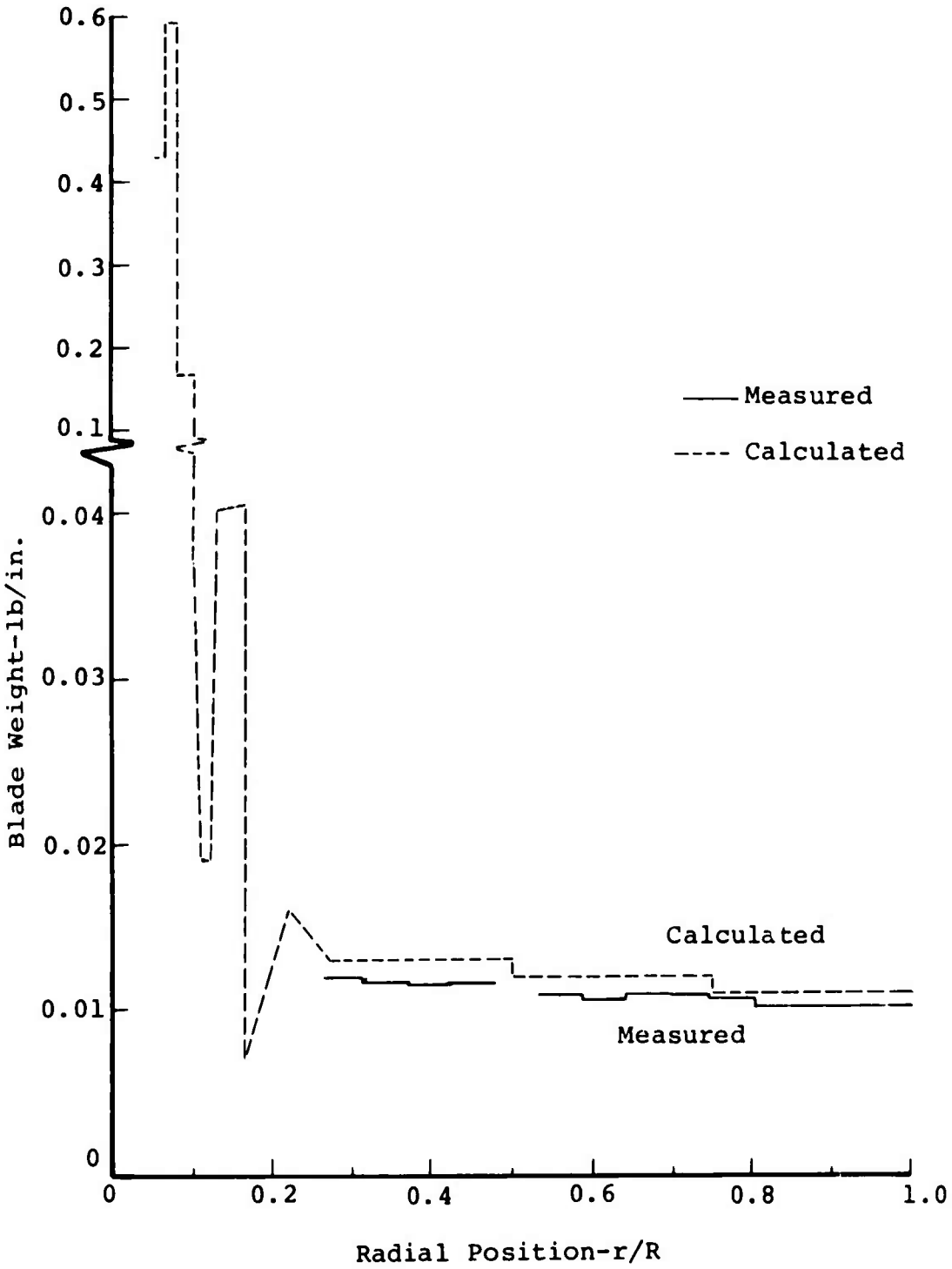

Figure 72. Comparison of Measured and Calculated Blade Weight Distributions.

be calculated.

The theoretical and measured center-of-gravity locations of each blade as a percentage of blade chord are shown below.

MEASURED AND THEORETICAL CHORDWISE CG LOCATIONS

Blade		%C (Aft of Leading Edge)
Low Stiffness	Test cg	24.84
	Analytical cg	24.68
Standard Reference	Test cg	24.98
	Analytical cg	24.67
Morganite	Test cg	26.53
	Analytical cg	24.36

As shown, the theoretical center-of-gravity location compares very favorably with measured values; therefore, the theoretical distributions were accepted as correct.

Blade Pitch Inertia

The blade pitch inertia distribution was not directly measured, and so a direct verification of the theoretical pitch inertia was not possible. An indirect verification was made, however, by comparing the measured total blade pitch inertia with the theoretical total pitch inertia obtained by integrating the distribution.

The total blade pitch inertia was measured as follows:

A steel rod of known cross section and length (and, hence, pitch inertia, $I_{\theta rod}$) was allowed to oscillate in torsion on the end of a wire. The frequency of vibration, $\omega_{\theta rod}$, was measured, and the torsional stiffness of the wire, $K_{\theta wire}$, was calculated using the relation

$$\omega_{\theta rod} = \frac{K_{\theta wire}}{I_{\theta rod}}$$

Then, each of the model blades, together with the root end hardware, was suspended from the wire and allowed to vibrate about the pitch axis. From the measured natural frequency, $I_{\theta blade}$ was calculated using

$$\omega_{\theta blade} = \frac{K_{\theta wire}}{I_{\theta blade}}$$

Measured and theoretical values are compared below:

COMPARISON OF MEASURED AND THEORETICAL BLADE PITCH INERTIA

Blade		Total Pitch Inertia
Low Stiffness	Measured	0.0004650
	Theoretical	0.0004892
Standard Reference	Measured	0.0004767
	Theoretical	0.0004903
Morganite	Measured	0.0003818
	Theoretical	0.0003839

Torsional Stiffness

The theoretical torsional stiffness was checked by comparing it to the measured stiffness over two blade sections (i.e., from 21 percent to 50 percent span and 50 percent to 90 percent span). The experimental values were obtained by applying a known torsional load, T, and then measuring the angular deflection, $\Delta\theta$, over the given span. The torsional stiffness, GJ, could then be calculated from the relation

$$\Delta\theta = \frac{T\ell}{GJ}$$

where ℓ is the span length.

Figure 73 compares the theoretical and measured torsional stiffness distribution for each blade and shows that, although the shape of the theoretical distribution agrees well with the experimental values, it is consistently too low. In order to improve the agreement of magnitudes, the theoretical distribution was increased by 25 percent for all three blades over the outboard 75 percent of the blade.

Flap Stiffness

Measurements of flapwise stiffness were made over the 30 percent to 70 percent radial position for each model blade. The procedure used was to apply a known load, P, and to measure the deflection, δ, over the span. The flapwise stiffness, EI, could then be calculated using the relation

$$\delta = \frac{P\ell^3}{EI_\beta}$$

where ℓ is the span length.

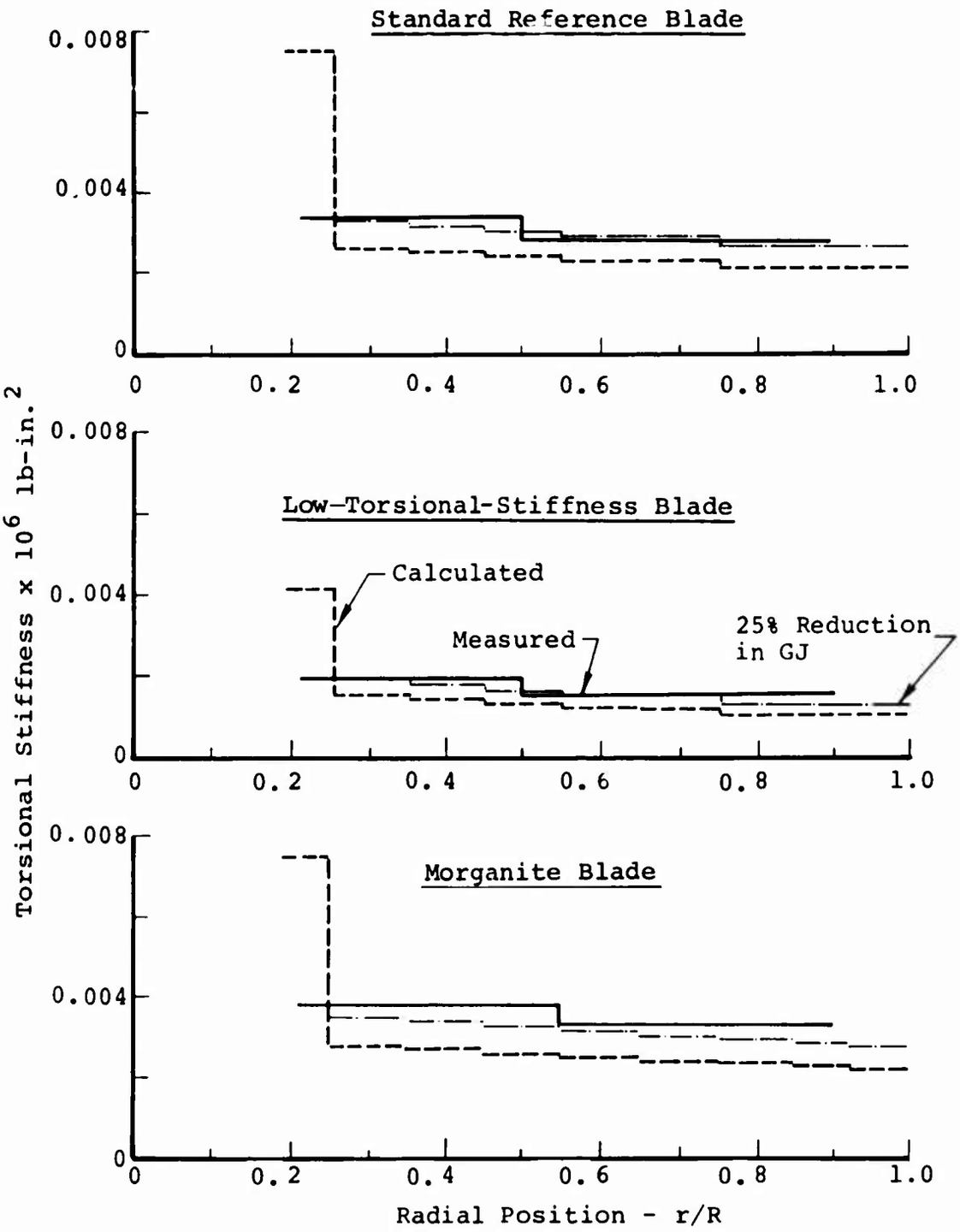

Figure 73. Comparison of Measured and Calculated Torsional Stiffness.

The measured and theoretical flapwise stiffnesses between the 30 percent and 70 percent radial position are compared below:

COMPARISON OF MEASURED AND THEORETICAL FLAPWISE STIFFNESSES

Blade		Flapwise Stiffness (0.3 to 0.7 r/R) $lb/in.^2$
Low Stiffness	Measured	3135
	Theoretical	2926
Standard Reference	Measured	3099
	Theoretical	2975
Morganite	Measured	4843
	Theoretical	4660

Since the agreement is good, the theoretical flapwise stiffness distribution was accepted as correct.

Chordwise Stiffness

Since no measurements of chordwise stiffness were made, the theoretical chordwise stiffness distribution was used.

Shear Center

Measurements of shear center location were made for each of the model blades by applying a static load and measuring the angular deformation over a span. The chordwise position of the load was varied until no angular deformation occurred. This, by definition, is the shear center location.

Measurements were made for each model blade over the 0.21 to 0.5 r/R and 0.5 to 0.9 r/R spans. The results are summarized below:

MEASURED CHORDWISE SHEAR CENTER LOCATION

Blade	Chordwise Position -%C 0.21-0.5 r/R	0.5-0.9 r/R
Low Stiffness	22.0	26.0
Standard Reference	30.2	31.0
Morganite	18.0	25.5

A theoretical calculation for shear center location was not available but it was estimated to be at 25 percent. Since the measured values showed significant scatter, their validity

was in doubt, and the estimated shear center of 25 percent was used for the load calculations.

Blade Twist

At the time of manufacture, it was intended that each blade have a nominal 9-degree linear twist distribution. Measurements, however, indicate that each set of blades had a different twist (see below). Since two sets of measurements made 20 months apart compare very favorably, it was concluded that the measured twist is correct and that the difference between the actual and the 9-degree intended twist resulted from blade warping after removal from the molds. For simplicity, the most recently measured blade twists were used for the analytical calculations.

SUMMARY OF BLADE TWIST MEASUREMENTS

Blade	Measured 3/71	Measured 11/72
Low Stiffness		
S/N 210	9.7	
211	10.3	
212	11.5	
213	10.0	
Average	10.4	10.4
Standard Reference		
S/N 121	7.48	
122	7.68	
123	7.76	
124	7.39	
Average	7.55	7.7
Morganite		
S/N 154	11.07	
155	10.87	
156	10.86	
157	10.3	
Average	10.77	10.5

Root Torsional Spring

The pitch arm and housing for the model blades were replaced by an adjustable root torsion spring. This device was intended to provide a means for changing the blade torsional frequency over a wide range. However, the device did not work properly during the test, and no significant frequency variations were obtained.

After the rotor test, the root torsional spring was measured, and a stiffness of 1850 inches/pound/radians was obtained.

In order to provide a double check of the root torsional spring, blade torsional stiffness, and pitch inertia, a natural frequency analysis was run using all the blade properties obtained above. These calculated torsional frequencies were compared with torsional frequencies obtained as part of the rotor test, by tweaking the blade manually and determining the frequency from the recorded free-vibration torsional loads. The results of this comparison are shown in Figure 74.

This figure shows that the predicted and test torsional natural frequencies agree very well for the morganite and low-stiffness blades. However, the measured frequency is significantly larger than the calculated frequency for the standard reference blade. Since the frequency correlation with two of the blades was very good and the blade physical properties were all obtained with the same approach, it is doubtful that there could be an error in the blade properties large enough to explain the large frequency discrepancy of the standard reference blade.

Later discussion with test personnel revealed that the root torsional spring joints were filled with an epoxy prior to the wind tunnel test to minimize assembly slop. The standard reference blade was run first, and, before the rotor was turned on, the torsional frequency was measured with the tweak test. During the standard reference blade test, it was noticed that the epoxy was broken; hence, the torsional frequency of all subsequent blades was obtained without the epoxy inoperative. Therefore, it is reasonable to assume that the standard reference blade frequency was measured high, since the epoxy stiffened the spring. After discussing the problem with the test personnel, it was concluded that the epoxy is very brittle and probably broke very early in the test. Since the standard reference blade run selected for correlation was near the end of the test runs, the epoxy was surely broken; and the measured root end stiffness of 1850 inch-pounds/radian is the proper value to use for all the blades.

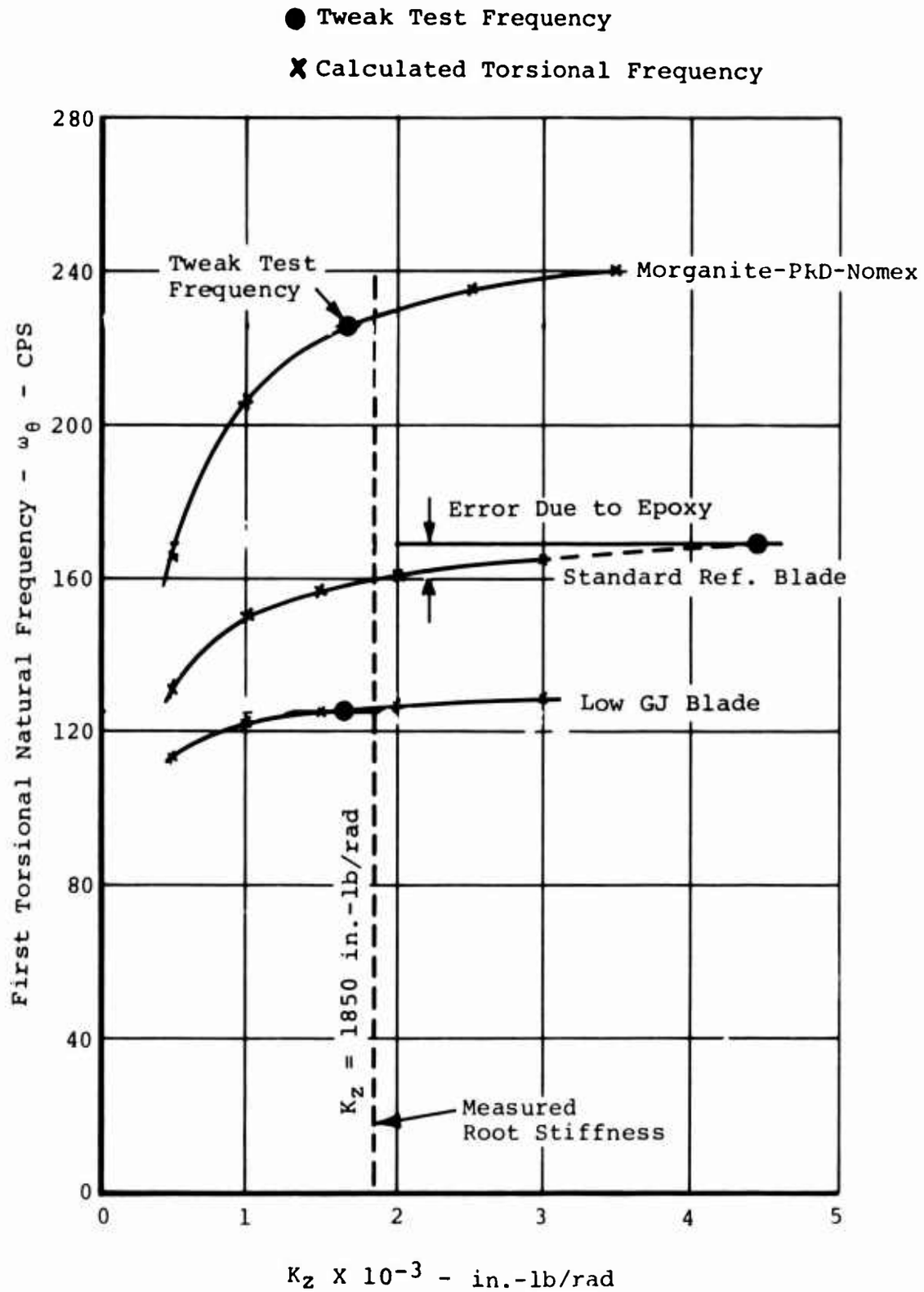

Figure 74. Comparison of Tweak Test and Analytical Blade Torsional Natural Frequencies.

APPENDIX III
DETAIL PHYSICAL PROPERTIES OF THE CH-47C ROTOR

The CH-47C rotor system consists of three 30-foot-radius blades mounted on an articulated rotor hub which is inclined 9 degrees into the wind.

Each blade has a constant chord of 25.25 inches: a pitch axis located at 19.5 percent chord with a blade cut out at 19.5 percent span. The airfoil section is a cambered Vertol 23010-1.58 with a -9.137 linear twist distribution.

Table II presents a tabulation of blade physical properties versus radial position. (Radial position, r/R, is expressed as a nondimensional fraction where 1.0 corresponds to the blade tip and 0 denotes the rotor center. (A repeated radial position in the tabulation denotes a step in the value of the blade property at that point.) The tabulated properties include blade weight; chordwise center-of-gravity location; pitch inertia; and flap, lag, and torsional stiffness. Blade weight and pitch inertia are presented on a per-inch basis.

Figure 75 illustrates the root end geometry. The figure shows that the blade pitch axis is offset from the center of rotation by 1.58 inches. The flap and lag hinges are located at the 0.022 r/R and 0.082 r/R radial positions, respectively; and the lag damper rate is 70,000 inch-pound-seconds/radian. The pitch bearing is located between the two hinges. The line of action of the pitch link is located 10.25 inches from the pitch axis on the leading-edge side of the blade spar, and the pitch link has a nominal stiffness of 11,850 pounds/inch.

TABLE II. CH-47C BLADE PHYSICAL PROPERTIES

Radial Position, r/R (non-dim)*	Running Weight (lb/in)	Radial Position, r/R (non-dim)*	Chordwise cg (in. aft of leading edge)	Radial Position, r/R (non-dim)*	Pitch Inertia X 10^{-2} ($lb/sec^2/in$)	Radial Position, r/R (non-dim)*	Flap Stiffness, (EI) X (10^6) (lb/in^2)	Radial Position, r/R (non-dim)*	Lag Stiffness, (EI) X (10^6) (lb/in^2)	Radial Position, r/R (non-dim)*	Torsional Stiffness, (GJ) X (10^6) (lb/in^2)
0.022	8.01	0.082	4.93	0.022	18.87	0.022	1159.0	0.082	365.0	0.022	202.0
0.025	8.01	0.165	4.93	0.043	18.87	0.082	1159.0	0.125	365.0	0.125	202.0
0.025	6.24	0.192	4.77	0.043	15.84	0.082	364.0	0.125	270.0	0.165	190.0
0.05	6.24	0.192	7.22	0.092	15.84	0.125	364.0	0.187	463.0	0.1875	95.0
0.05	9.25	0.267	7.41	0.092	6.96	0.125	265.0	0.267	1524.0	0.294	82.1
0.075	9.25	0.267	6.71	0.125	6.96	0.135	300.0	0.295	1500.0	0.339	65.2
0.075	5.01	0.283	6.75	0.125	1.35	0.187	79.2	0.342	1615.0	0.342	75.2
0.1	5.01	0.342	5.7	0.14	1.553	0.342	70.3	0.381	1606.0	0.381	60.0
0.1	3.37	0.342	6.2	0.192	1.377	0.381	59.2	0.519	1606.0	0.519	60.0
0.125	3.37	0.355	6.0	0.192	10.48	0.519	59.2	0.537	1546.0	0.537	49.5
0.125	0.84	0.381	6.1	0.267	10.3	0.537	50.9	0.672	1546.0	1.0	49.5
0.192	0.84	0.519	6.1	0.267	7.4	0.96	50.9	0.672	1965.0		
0.192	1.085	0.537	6.26	0.342	7.97	0.96	55.1	0.761	1965.0		
0.267	0.99	0.672	6.26	0.381	7.61	1.0	55.1	0.761	1546.0		
0.267	0.92	0.672	6.55	0.519	7.61			0.96	1546.0		
0.342	1.012	0.761	6.55	0.537	7.48			0.96	1603.0		
0.342	0.9	0.761	6.26	0.672	7.48			1.0	1603.0		
0.381	0.85	0.96	6.26	0.672	8.75						
0.519	0.85	0.96	6.04	0.761	8.75						
0.537	0.76	0.979	6.04	0.761	7.48						
0.672	0.76	0.979	4.58	0.96	7.61						
0.672	0.772	1.0	4.58	0.979	7.61						
0.761	0.772			0.979	11.34						
0.761	0.76			1.0	11.34						
0.96	0.76										
0.96	0.78										
0.967	0.78										
0.967	0.83										
0.979	0.83										
0.979	1.008										
1.0	1.008										

*nondimensional

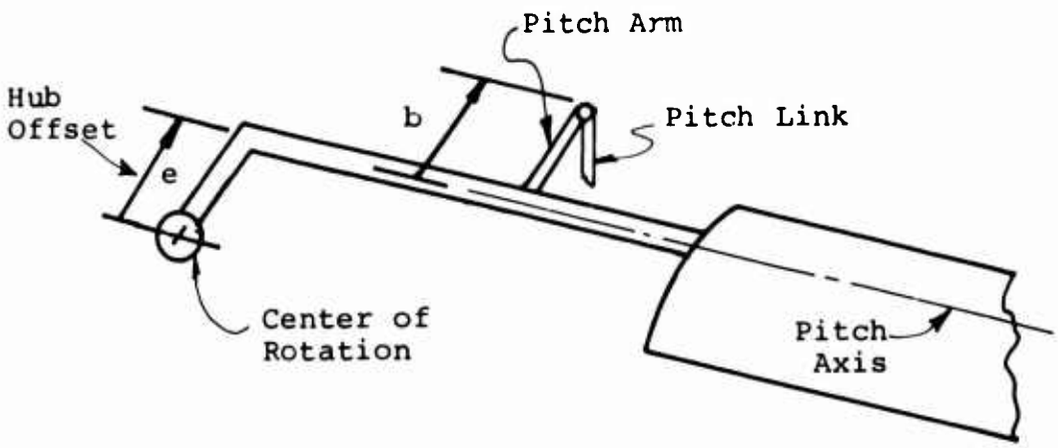

Figure 75. CH-47C Blade Root Geometry.

APPENDIX IV
EFFECT ON DYNAMIC C_M OVERSHOOT ON MODEL ROTOR CORRELATION

During the model rotor correlation, a term was added to the unsteady aerodynamic equations to account for the dynamic change of the aerodynamic center of pressure. Correlation of the resulting modified analysis with the model data provided excellent agreement with the standard reference blade alternating torsional load. The correlation was so good that additional theory/test comparisons were made with the low-stiffness blade and the morganite blade.

Figures 76, 77, and 78 illustrate the variation of alternating torsional moment with blade loading for the standard reference, low stiffness, and morganite blades. For all three blades, the theory/test correlation of stall inception and load growth rate is good. For deep stall, the standard reference blade load agreement is good; however, the low-stiffness blade underpredicts by 19 percent and the morganite blade underpredicts by 42 percent. Therefore, though there are many excellent features of this theory, it is unable to properly predict the deep stall loads.

Since the primary objective of this study is to determine means of reducing the stall-induced loads, it is clear that this modified analysis cannot be used for the study. However, these results merit development.

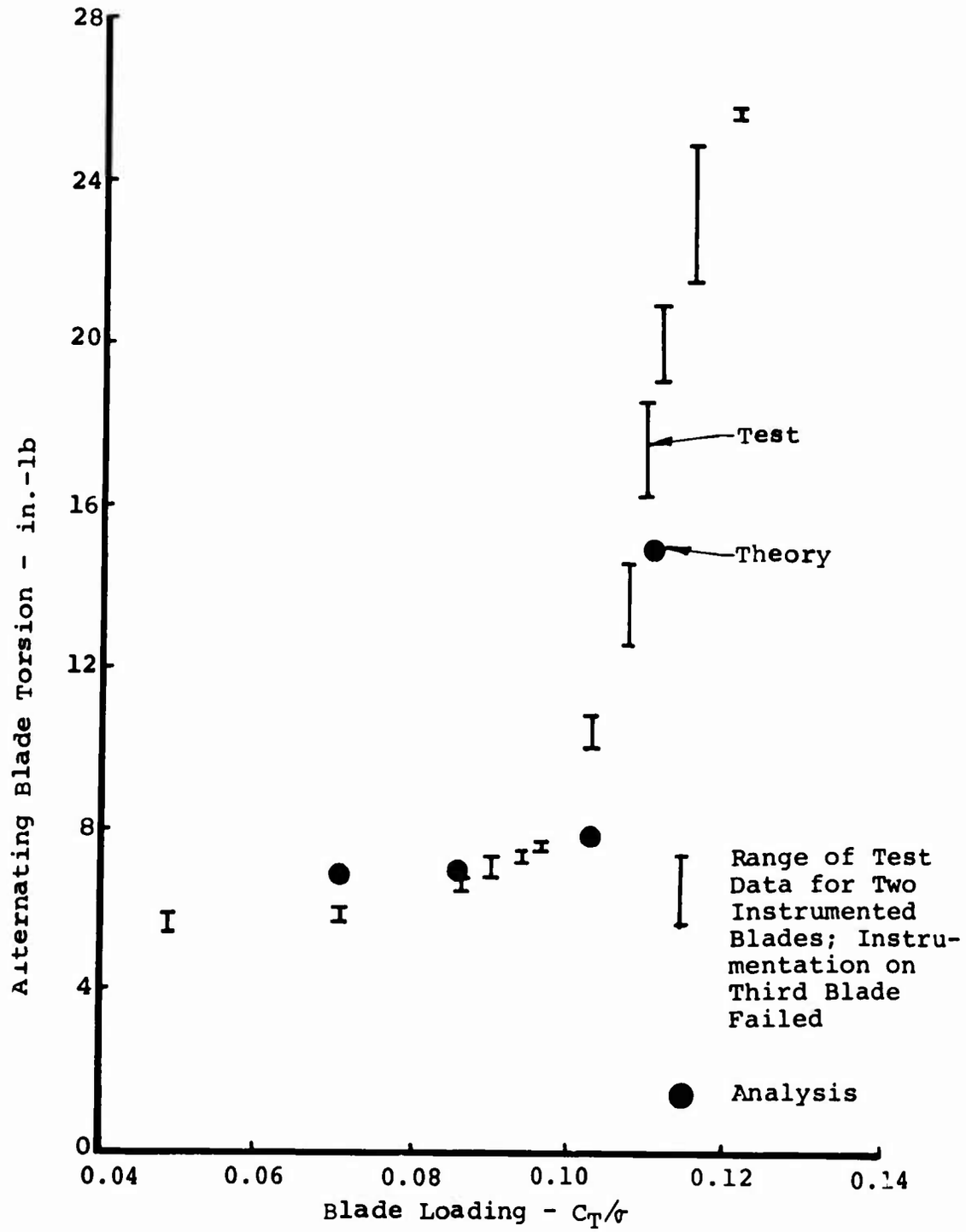

Figure 76. Standard Reference Blade, Run 306 C_T/σ Versus Blade Alternating Torsion C-60 Theory With Static C_M Dynamic Overshoot in the Unsteady Aero Equations.

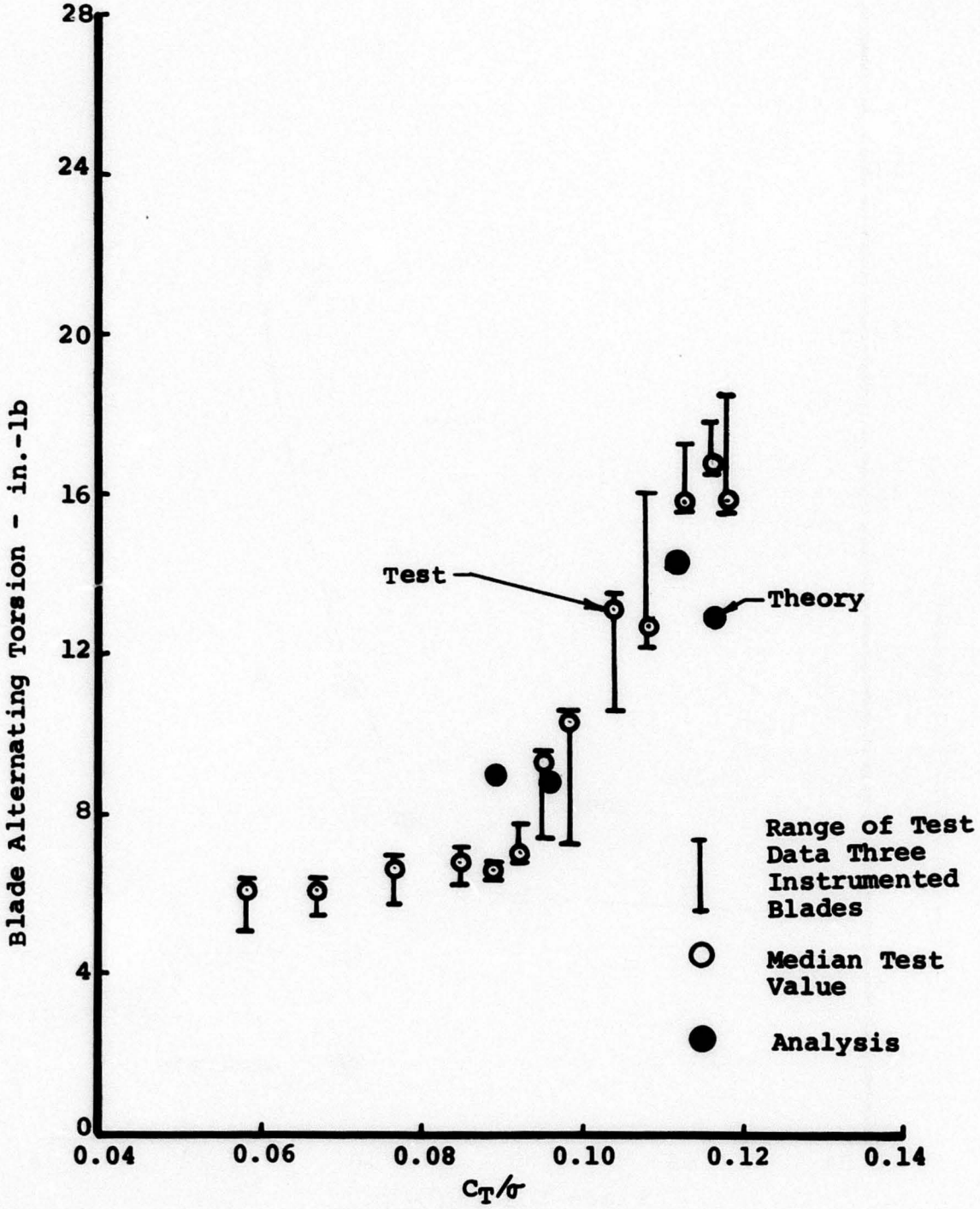

Figure 77. Low-Stiffness Blade, Run 317
C_T/σ Versus Blade Alternating Torsion
C-60 Theory With Static C_M Dynamic Overshoot
in the Unsteady Aero Equations.

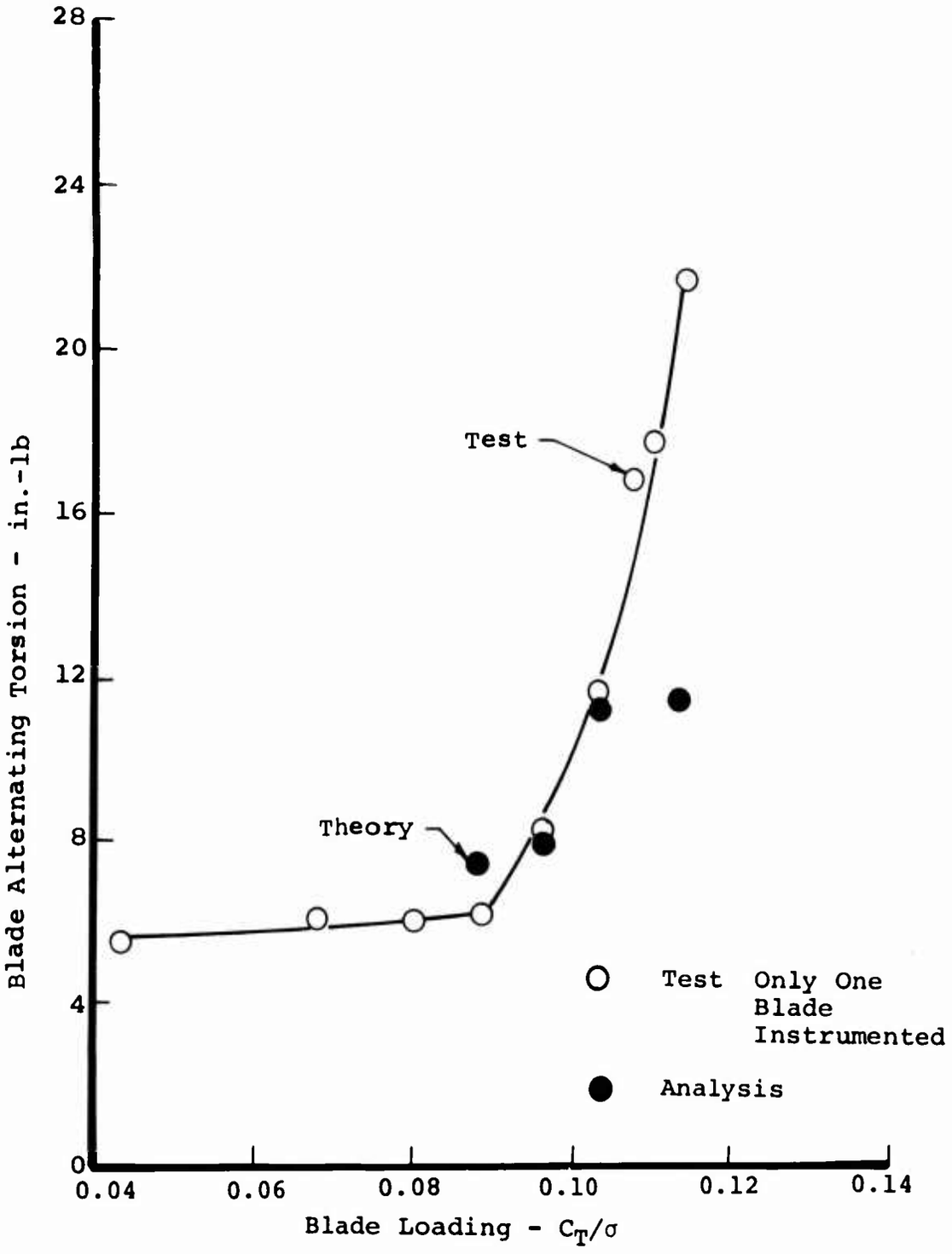

Figure 78. Morganite Blade, Run 323
C_T/σ Versus Blade Alternating Torsion
C-60 Theory With Static C_M Dynamic Overshoot
in the Unsteady Aero Equations.